Dissertation
submitted to the
Combined Faculties for the Natural Sciences and for Mathematics
of the Ruperto-Carola University of Heidelberg, Germany
for the degree of
Doctor of Natural Sciences

presented by
Diplom-Phys. Christian Buck
born in Riedlingen
oral examination: 5 May 2004

Development of
metal loaded liquid scintillators for future detectors
to investigate neutrino properties

Referees: Prof. Dr. W. Hampel
Prof. Dr. W. Krätschmer

Entwicklung von metallbeladenen Flüssigszintillatoren für zukünftige Detektoren zur Untersuchung von Neutrinoeigenschaften

Mehrere zukünftige Neutrinoexperimente erfordern zum Neutrinonachweis metallbeladene Flüssigszintillatoren. Die Herausforderung in der Entwicklung eines solchen Szintillators liegt darin, große Mengen des betreffenden Metalls in einem organischen Flüssigszintillator zu lösen, ohne dabei die optischen Eigenschaften zu beeinträchtigen. Ein vielversprechender neuer Ansatz liegt in der Verwendung von Metall-β-Diketonen. Im Unterschied zu vorherigen Ansätzen, die zu instabilen metallbeladenen Szintillatoren führten, wird Langzeitstabilität der optischen und chemischen Eigenschaften erwartet.

Es wird eine Methode zur Herstellung eines Szintillators mit hoher In-Beladung für ein zukünftiges Echtzeit Experiment, das das niederenergetische Sonnenneutrinospektrum über Reaktionen durch den geladenen Strom nachweisen soll, untersucht. Diese Entwicklung beinhaltet die Synthese und Reinigung von hochreinem In(Acetylaceton)$_3$, die optische Charakterisierung der Szintillatorkomponenten, die theoretische Modellierung und die Optimierung der Szintillatorzusammensetzung sowie Messungen in einem Prototyp Detektor. Der verwendete Ansatz wird durch die erwartete Stabilität und Reinheit, die beide zu den grundlegenden Anforderungen an den metallbeladenen Szintillator gehören, motiviert.

Die selbe Methode wird verwendet, um einen Gd-beladenen Szintillator für ein zukünftiges Reaktorneutrinoexperiment, das sich die Messung von Mischungsparametern bei Neutrinooszillationen zum Ziel gesetzt hat, zu entwickeln. Eine weitere Anwendung dieses Ansatzes könnte schließlich die Herstellung eines Nd-beladenen Flüssigszintillators für ein zukünftiges Experiment zur Suche nach dem neutrinolosen doppelten β-Zerfall sein.

Development of metal loaded liquid scintillators for future detectors to investigate neutrino properties

Several future neutrino experiments call for metal loaded liquid scintillators for neutrino detection. The challenge in the development of such scintillators is how to dissolve large amounts of the metal in an organic liquid scintillator without degrading the optical properties. A promising new approach is the use of metal β-diketonates. Different to earlier approaches which resulted in non-stable metal loaded scintillators, long term stability of optical and chemical properties is expected.

A method to develop a highly In-loaded liquid scintillator for a future real-time experiment that measures the low energy solar neutrino spectrum via the charged current interaction is investigated. This research includes the synthesis and purification of pure In(acetylacetone)$_3$, optical characterization of scintillator components, theoretical modeling, optimization of the scintillator composition and measurements in a prototype detector. The approach used is motivated by the expected stability and purity which are both basic requirements on such a metal loaded scintillator.

The same method is used for the investigation of a Gd-loaded scintillator for a reactor neutrino experiment that aims to measure neutrino mixing parameters. Finally, a further application of this approach could be the fabrication of a Nd-loaded liquid scintillator for a future experiment searching for neutrinoless double β-decay.

Contents

1 Neutrino experiments using liquid scintillators **1**
- 1.1 Solar neutrinos . . . 2
  - 1.1.1 Status . . . 2
  - 1.1.2 Target candidates for real time experiments at low energies . . . 5
  - 1.1.3 The LENS project . . . 7
  - 1.1.4 Detector design . . . 10
  - 1.1.5 The Borexino-Experiment . . . 11
- 1.2 Reactor anti-neutrinos . . . 14
  - 1.2.1 Status . . . 14
  - 1.2.2 Future experiments . . . 16
- 1.3 Neutrinoless $\beta\beta$-decay . . . 17
- 1.4 Conclusion . . . 18

2 Energy transfer in scintillators **19**
- 2.1 Fluorescence und phosphorescence . . . 19
- 2.2 Energy transfer between isolated molecules . . . 20
- 2.3 Energy transfer in organic liquid scintillators . . . 23

3 Development of an In-loaded liquid scintillator **25**
- 3.1 The β-diketone system . . . 26
  - 3.1.1 β-diketones . . . 26
  - 3.1.2 $In(acac)_3$ synthesis . . . 27
  - 3.1.3 $In(acac)_3$ purification . . . 30
  - 3.1.4 Solubility . . . 35
  - 3.1.5 Chemical stability . . . 40
  - 3.1.6 The fluor . . . 40
- 3.2 Carboxylates . . . 41
  - 3.2.1 The Ytterbium system . . . 42
  - 3.2.2 The Indium system . . . 43

4 Optical properties of the In-loaded scintillator **47**
- 4.1 Absorption measurements . . . 47
  - 4.1.1 Measuring apparatus and definitions . . . 47
  - 4.1.2 Sample preparation . . . 48
  - 4.1.3 Results . . . 49
- 4.2 BPO purification tests . . . 53

4.2.1 Recrystallization . . . 53
4.2.2 Washing . . . 53
4.2.3 Column purification . . . 54
4.2.4 Water extraction . . . 54
4.2.5 Conclusion . . . 54
4.3 Fluorescence measurements . . . 55
4.3.1 The fluorimeter . . . 55
4.3.2 Emission spectra of the basic ingredients . . . 56
4.3.3 The effect of bis-MSB . . . 58
4.3.4 Maximization of energy transfer to the fluor . . . 60
4.3.5 Reemission of BPO and bis-MSB . . . 62
4.4 Light yield under irradiation with a γ-source . . . 63
4.4.1 Experimental setup . . . 63
4.4.2 Standards . . . 67
4.4.3 Fluor variation . . . 67
4.4.4 Light yield at varying fluor concentrations . . . 69
4.4.5 Light yield at varying In-concentrations . . . 70
4.5 Comparison with theory . . . 71
4.5.1 In-free scintillator . . . 71
4.5.2 In-loaded scintillator . . . 73
4.5.3 Critical transfer distances and critical concentrations . . . 75
4.6 Long term stability of the optical properties . . . 76

5 Prototype measurements 79
5.1 Background measurements in the LLBF . . . 79
5.1.1 Radon . . . 79
5.1.2 Background measurement using a Ge-detector . . . 81
5.1.3 Background measurement using a liquid scintillator . . . 82
5.2 Optical properties in long quartz cells . . . 86
5.2.1 Light transport in a long cell . . . 86
5.2.2 Measurements in a 1 cm wide and 1 m long cell . . . 87
5.2.3 Measurements in a LENS-like cell . . . 89
5.3 Underground measurement of In-loaded cells in the LLBF . . . 91
5.3.1 Scintillator preparation . . . 93
5.3.2 Cell loading . . . 94
5.3.3 Results . . . 95

6 Rare earth acetylacetones in liquid scintillators 97
6.1 Physical and chemical properties of rare earth acetylacetones . . . 97
6.2 Gd-loaded scintillator for a reactor neutrino experiment . . . 98
6.2.1 Synthesis and dehydration of $Gd(acac)_3 \cdot nH_2O$ . . . 98
6.2.2 Solvent selection . . . 102
6.2.3 A Gd carboxylate system . . . 103
6.2.4 Attenuation lengths . . . 104
6.2.5 Light yields of Gd-loaded scintillators . . . 105
6.2.6 Stability . . . 107
6.3 Nd-loaded scintillator for a $\beta\beta$-decay experiment . . . 107

7 ^{222}Rn background in solar neutrino experiments **109**
7.1 ^{222}Rn emanation measurements in Borexino 109
7.1.1 Scintillator purification systems in Borexino 109
7.1.2 Measurements and results 110
7.2 ^{222}Rn background in LENS 113

Summary **115**

Bibliography **119**

Acknowledgements **123**

List of Tables

1.1 Predicted and measured neutrino flux 5
1.2 Target candidates for real time experiments at low energies 6
1.3 Simulation of the background in a LENS detector 11

3.1 List of some selected β-diketones 27
3.2 Properties of some selected solvents 38
3.3 Solubility of In-β-diketones in various solvents 39
3.4 Solubility of fluors in anisole 40
3.5 pK_a values and solubility in water for some carboxylic acids 41
3.6 Light yield measurements for In-carboxylate scintillators 45

4.1 Light yield measurements at varying fluors 68
4.2 Light yield measurements at 1 wt. % In-loading and varying PPO concentrations 69
4.3 Critical PPO-concentrations in various models 72
4.4 R_0 for anisole and several components 75
4.5 R_0 for bis-MSB and fluors 76
4.6 Light yield stability of an In-loaded scintillator 76

5.1 Count rate in the LLBF Ge measurement at selected energies 83
5.2 Attenuation lengths measured in a 1 m cell at varying bis-MSB concentrations 88
5.3 Contribution of single components to attenuation length 90
5.4 Scintillator performance in a LENS-like cell 91
5.5 Scintillator properties in prototype detector 96

6.1 Melting points of the rare earth acetylacetonates 98
6.2 Solubility of $Gd(acac)_3 \cdot nH_2O$ in various solvents 102

7.1 Rn-emanation of purification Skids components 111

List of Figures

1.1 pp–cycle . . . 3
1.2 CNO–cycle . . . 3
1.3 The solar neutrino spectrum . . . 4
1.4 Term scheme of the ^{115}In-system . . . 9
1.5 Bremsstrahlung background in an In-detector . . . 10
1.6 The Borexino detector . . . 13

2.1 Term scheme for explanation of fluorescent and phosphorescent radiation . . . 20

3.1 Tautomerism of β-diketones . . . 26
3.2 Solvent extraction and synthesis of $In(acac)_3$ . . . 29
3.3 Structure of the $In(acac)_3$ molecule . . . 30
3.4 Absorption of $Fe(acac)_3$ at 440 nm at varying concentrations . . . 32
3.5 Absorption spectrum of sublimed and unsublimed $Fe(acac)_3$-doped $In(acac)_3$ 34
3.6 Absorption spectra of purified $In(acac)_3$ samples . . . 34
3.7 Calibration curve in a atomic absorption measurement . . . 37
3.8 Stability region for a Yb carboxylate system . . . 43
3.9 Stability region for an In carboxylate system . . . 44

4.1 Absorption spectrum of $In(acac)_3$ . . . 50
4.2 Molar extinction coefficient for BPO, PPO and bis-MSB . . . 50
4.3 Attenuation length for main components . . . 51
4.4 BPO and $In(acac)_3$ absorbance . . . 52
4.5 BPO purification tests . . . 53
4.6 Geometries used for the fluorescence measurements . . . 55
4.7 Absorption and emission spectrum of anisole . . . 57
4.8 Non-radiative energy transfer from BPO to bis-MSB . . . 59
4.9 Radiative energy transfer from BPO to bis-MSB . . . 59
4.10 Emission spectra using various fluors . . . 60
4.11 Emission spectra of a 5 wt.% In-scintillator excited at 271 nm and 320 nm . 61
4.12 Emission spectra of BPO at varying excitation energies . . . 63
4.13 Emission spectra of bis-MSB at varying excitation energies . . . 64
4.14 Drawing of the light yield setup . . . 65
4.15 Electronics for light yield measurements . . . 65
4.16 Compton spectra of BC-505 and a 7 wt.% loaded In-LS . . . 66
4.17 Light yield of 4.1 wt.% In-scintillator a as a function of PPO . . . 70
4.18 Light yield as a function of the In-concentration . . . 71

4.19 Light yield curves at varying PPO-concentrations without In 72
4.20 Light yield curves at varying PPO-concentrations including self-quenching . 73
4.21 Light yield as a function of BPO 74
4.22 Stability test of the attenuation length of several In-loaded solutions 77

5.1 Sketch of the LLBF shielding 80
5.2 Rn–activity in the LLBF 80
5.3 Background spectrum inside LLBF 82
5.4 Attenuation length PXE scintillator before and after column purification . . 85
5.5 Background spectrum inside LLBF measured with a PXE based scintillator . 86
5.6 Attenuation length in a 1 m long LENS-like cell. 92
5.7 Absorbance of BPO master solution before and after water extraction 93
5.8 Configuration of the prototype array 95

6.1 Absorption peaks of diluted metal acetylacetones 99
6.2 Molar extinction coefficient of $Nd(acac)_3 \cdot nH_2O$ 99
6.3 Dehydration of $Gd(acac)_3 \cdot 3H_2O$. 101
6.4 Chemical compatibility test of acrylic samples with PXE 103
6.5 Light yield at varying dodecane concentration 104
6.6 Attenuation length of $Gd(acac)_3H_2O$ at scintillator emission 105
6.7 Light yield of Gd-scintillator for varying PPO-conc. (solvent PXE) 106
6.8 Light yield of Gd-scintillator for varying PPO-conc. (solvent PXE/dodecane) 107
6.9 Stability test of Gd-loaded scintillator 108

7.1 Diagram of a heat exchanger in the purification Skids 112

Chapter 1

Neutrino experiments using liquid scintillators

In 1930 Pauli introduced a particle to explain the continuous electron energy distribution in nuclear beta-decay. In 1933 Fermi developed the first weak-interaction theory and named this particle neutrino. Neutrinos have no electric charge, their mass and magnetic moments are small and they do not participate in the strong interaction making the detection of these particles difficult. Measurements of the decay width of the Z boson have shown that just three neutrinos with mass below $M_Z/2$ participate in the weak interactions: ν_e, ν_μ and ν_τ. The neutrino mass properties are of great relevance for the understanding of particle physics as well as for cosmology and astrophysics.

Several attempts were done to measure the neutrino mass. Direct measurements of the neutrino mass by the investigation of the endpoint energy of the electron in β-decay have been performed. However, these measurements lack at present the required sensitivity and have only been able to set a limit [WEI03]. Indirect methods as the search for neutrino oscillations are also pursued. If neutrinos are massive particles then the flavour eigenstates $|\nu_l>$ could be a linear superposition of the mass eigenstates $|\nu_i>$:

$$|\nu_l>=\sum_{i=1}^{3} U_{li}|\nu_i> \qquad\qquad (l=e,\mu,\tau) \tag{1.1}$$

where the coefficients U_{li} form a unitary 3×3 mixing matrix. When the neutrino propagates the mass states evolve differently with time resulting in a changing mix of mass eigenstates. Therefore, the detected neutrino types appear to oscillate among the neutrino flavors. The mixing matrix can be parameterized in terms of three angles $\Theta_1=\Theta_{13}$, $\Theta_2=\Theta_{23}$, $\Theta_3=\Theta_{12}$ and the CP violating phase δ:

$$\begin{pmatrix} \nu_e \\ \nu_\mu \\ \nu_\tau \end{pmatrix} = \begin{pmatrix} c_1c_3 & c_1s_3 & s_1e^{-i\delta} \\ -c_2s_3-s_1s_2c_3e^{i\delta} & c_2c_3-s_1s_2s_3e^{i\delta} & c_1s_2 \\ s_2s_3-s_1c_2c_3e^{i\delta} & -s_2c_3-s_1c_2s_3e^{i\delta} & c_1c_2 \end{pmatrix} \begin{pmatrix} \nu_1 \\ \nu_2 \\ \nu_3 \end{pmatrix} \tag{1.2}$$

where $c_1=\cos\Theta_1$, $s_1=\sin\Theta_1$, etc.

Under the simplified assumptions that only two neutrino flavors mix and that there are no matter effects the probability of conversion into the other flavour eigenstate after the

pathlength L is

$$P = \sin^2 2\Theta \sin^2 \left(\frac{\Delta m^2 L}{4E_\nu} \right) \tag{1.3}$$

When neutrinos travel through dense matter additional effects can result in a change of the oscillation process. This so-called MSW-effect [WOL78, MIK85] is associated with the fact that electron neutrinos can forward scatter on electrons by charged current and neutral current interactions while other flavours interact with electrons via neutral current interactions only.

Several neutrino sources such as the Sun, nuclear reactors, and neutrinos from the decay of pions created by cosmic rays in the atmosphere, have been used to search for neutrino oscillations. For each source direct or indirect evidence for flavour conversion was observed. Another possibility to find the neutrino mass is the search for neutrinoless $\beta\beta$-decay which only occurs if the neutrino is a massive Majorana particle. In the following the present status of solar neutrino, reactor neutrino and $\beta\beta$-decay physics as well as future experiments in these fields that plan to use metal loaded liquid scintillators are described. The main requirements for the scintillator are similar in all the experiments. A way to produce a scintillator suitable for low background neutrino experiments has therefore been investigated in this thesis.

1.1 Solar neutrinos

1.1.1 Status

One of the main sources of neutrinos that can be detected on the earth is the Sun. Energy is produced in the Sun through the reaction

$$4p \rightarrow {}^4\mathrm{He}^{++} + 2e^+ + 2\nu_e + 24.7 \text{ MeV} \tag{1.4}$$

via the pp–cycle (see Fig 1.1) and the CNO-cycle (see Fig 1.2). The solar neutrino flux on the earth is predicted by the Standard Solar Model (SSM) [BAH01]. In the model a total neutrino flux on earth of $6.5 \cdot 10^{10}$ cm^{-2}s^{-1} is expected produced mainly by the pp-reaction. The solar neutrino spectrum according to the SSM is shown in Fig. 1.3. The energy range of the spectrum is between 0 and 18 MeV whereas most of the flux is at energies below 1 MeV. The flux of the low energetic pp-neutrinos is known with the highest accuracy of approximately 1 %.

After 35 years of solar neutrino detection the so-called 'solar neutrino problem' is now solved. The long history of solar neutrino experiments started in 1968 with the experiment of R. Davis (Nobel prize 2002) in the Homestake mine [DAV68, CLE98]. In this radiochemical measurement ^{37}Cl isotopes were transformed by an inverse β-decay into the radioactive ^{37}Ar isotope ($T_{1/2}$=35 d). The Ar atoms produced are extracted out of a large tank containing 615 t of perchlorethylene (C_2Cl_4) and detected in miniaturized proportional counters. The experiment measured only 1/3 of the predicted solar ν_e signal (see Table 1.1) above a threshold of 0.814 MeV. For many years there were numerous attempts to explain this deficit either by changes in the SSM or by new ν physics. Nowadays the SSM is confirmed by helioseismology [BAH97] and other experiments proved that the deficit can only be explained by neutrino physics.

In 1966 Kuzmin proposed ^{71}Ga which is transformed by ν capture into ^{71}Ge ($T_{1/2}$=11.4 d) as a target for solar neutrinos. This target has the advantage of a lower energy threshold (233 keV) allowing the detection of the neutrinos from the fundamental pp-reaction.

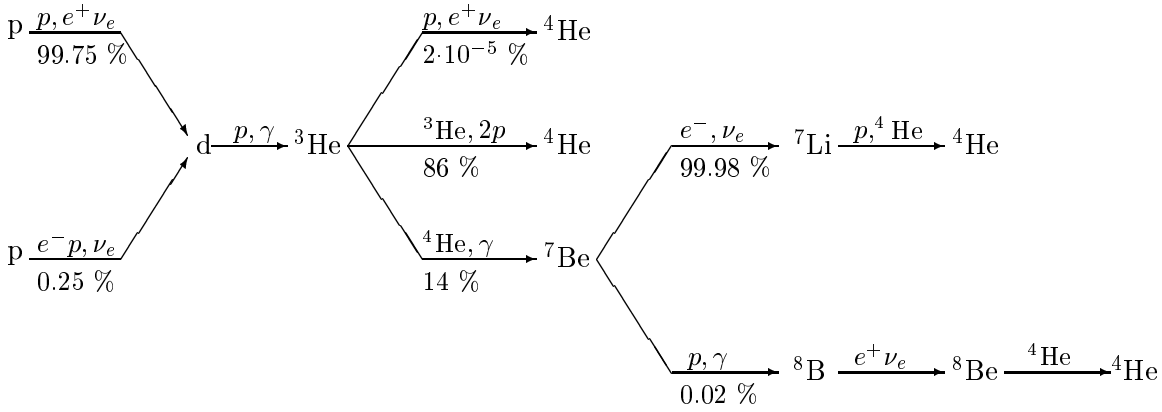

Figure 1.1: *The pp–cycle.*

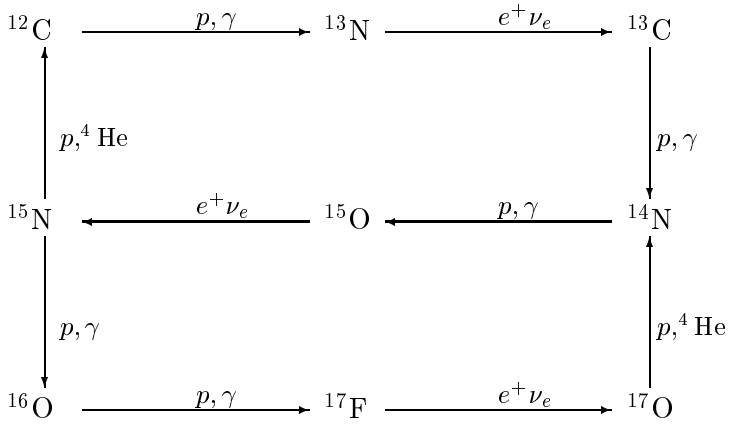

Figure 1.2: *The CNO–cycle.*

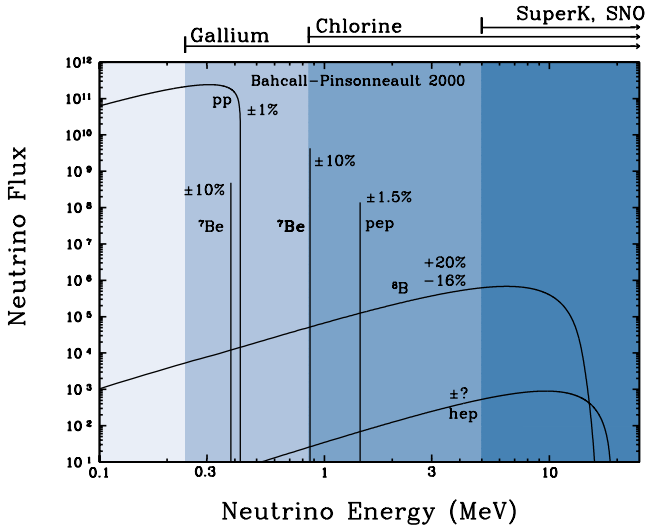

Figure 1.3: *The solar neutrino spectrum as expected by the standard solar model. The energy threshold for neutrino detection by several experiments is given.*

The radiochemical experiment was started approximately 20 years after Kuzmins proposal by two collaborations: GALLEX [GAL99] (now GNO [GNO00]) and SAGE [SAG03]. The GALLEX/GNO experiment is located in the Gran Sasso underground laboratory in Italy. A technique similar to the Chlorine experiment was used to detect the neutrinos. Every month, a tank of approximately 100 t of $GaCl_3$ in HCl-solution containing 30 t of natural Ga was exposed to neutrinos. The Ge was then extracted in form of $GeCl_4$, converted into German gas (GH_4) and filled into miniaturized proportional counters. For calibration purposes an artificial ^{51}Cr source was used with a flux approximately 10 times bigger than the solar neutrino flux. The efficiency was found to be consistent with unity. A further efficiency test was performed by inserting a known amount of ^{71}As ($T_{1/2}$=2.7 d) which decays into ^{71}Ge in the solution. This test demonstrated that the recovery efficiency is (100 ± 1) %. The SAGE experiment operates in the Baksan underground laboratory in Russia and uses metallic gallium which is a liquid at about 30°C. This experiment was also successfully calibrated with a ^{51}Cr source. Both experiments confirmed the solar neutrino deficit and gave consistent results. The outcome of these experiments made it hard to explain the deficit by changes in the SSM.

A real-time experiment based on direct detection of neutrinos via elastic scattering on electrons was started in Japan. The electron scattering reaction is sensitive to all neutrino flavours, but has larger cross sections for $\nu_e - e^-$ scattering than for $\nu_{\mu,\tau} - e^-$ scattering. The water Cherenkov detector used in Kamiokande started in 1983 as detector to study the proton decay [KAM96]. In 1986 the detector was improved allowing the detection of the solar neutrino energy spectrum above 7 MeV, atmospheric neutrinos and neutrinos originating from the supernova in 1987. This detector offered the opportunity to reconstruct the direction of the neutrino. By this directional information an excess of events from the Sun could be observed confirming the solar origin of the neutrinos. The next generation experiment Superkamiokande [SUP01] consisted of 50 kt of water of which 22 kt served as 'fiducial volume'. The target mass was observed by 11500 PMTs (20 inch diameter) giving a coverage of 40 %. This experiment proved that atmospheric ν_μ neutrinos oscillate [SUP00] and determined the

experiment	exp. flux	theory [BAH01]
Homestake	2.56 ± 0.23 SNU [CLE98]	$7.6^{+1.3}_{-1.1}$ SNU
Kamiokande	$2.80 \pm 0.19 \pm 0.33 \cdot 10^6$ cm^{-2}s^{-1} [KAM96]	$5.05^{+1.01}_{-0.81} \cdot 10^6$ cm^{-2}s^{-1}
Superkamiokande	$2.35 \pm 0.02 \pm 0.08 \cdot 10^6$ cm^{-2}s^{-1} [SUP02]	
GALLEX + GNO	$69.3 \pm 4.1 \pm 3.6$ SNU [BEL03]	128^{+9}_{-7} SNU
SAGE	$70.9^{+5.3}_{-5.2}$ SNU [SAG03]	
SNO (ES)	$2.39 \pm 0.03 \pm 0.08 \cdot 10^6$ cm^{-2}s^{-1} [SNO03]	$5.05^{+1.01}_{-0.81} \cdot 10^6$ cm^{-2}s^{-1}
SNO (CC)	$1.75 \pm 0.07 \pm 0.12 \cdot 10^6$ cm^{-2}s^{-1} [SNO03]	
SNO (NC)	$5.09 \pm 0.44 \pm 0.45 \cdot 10^6$ cm^{-2}s^{-1} [SNO03]	

Table 1.1: *In the Table the solar neutrino flux on the earth predicted by the SSM and measured in the experiments is listed. 1 SNU (Solar Neutrino Unit) corresponds to 1 neutrino interaction/10^{36} target atoms.*

relevant oscillation parameters: $\sin^2 2\Theta > 0.92$ and $1.6 \cdot 10^{-3}$ eV$^2 < \Delta m^2_{atm} < 3.9 \cdot 10^{-3}$ eV^2. The energy threshold for solar neutrino detection was lowered to 5 MeV which allows mainly the detection of ^{8}B neutrinos whose flux predictions have large errors. After 1496 days of data collection Superkamiokande measured less than half of the expected neutrino flux under the assumption that there are no neutrino oscillations. The combination of all mentioned solar neutrino results narrowed the allowed space for the mixing parameters Δm^2_{ij} and Θ_{ij}.

The solar neutrino experiments described above measured the disappearance of solar electron neutrinos and gave therefore only indirect hints for neutrino oscillation. The SNO experiment placed in a mine in Canada is also a real-time Cherenkov detector containing 1 kt of heavy water (D_2O) in an acrylic vessel [SNO03]. The coverage of the 10000 PMTs is 31 %. There are mainly three reactions for neutrino detection:

$$\text{electron scattering(ES)} \qquad \nu_l + e^- \rightarrow \nu_l + e^- \tag{1.5}$$

$$\text{charged current reaction(CC)} \qquad \nu_e + d \rightarrow e^- + p + p \tag{1.6}$$

$$\text{neutral current reaction(NC)} \qquad \nu_l + d \rightarrow \nu_l + p + n \tag{1.7}$$

The flux measured with the electron scattering reaction is consistent with the Superkamiokande result. Whereas in the charged current reaction only 1/3 of the solar neutrino signal that would be expected without oscillation is measured, in the neutral current reaction a number consistent with the standard solar model is measured above the energy threshold of 2.2 MeV. This result clearly demonstrated independent from solar model calculations, that there is a conversion from the initial ν_e to other active ν.

1.1.2 Target candidates for real time experiments at low energies

After the results and discoveries of the recent neutrino experiments the goal of upcoming solar neutrino experiments is to measure neutrino oscillation parameters with high accuracy and to determine the low energy neutrino fluxes of the primary pp-, pep- and ^{7}Be-branches.

At energies below 1 MeV the Cherenkov photon yield is insufficient to perform spectroscopic measurements. Therefore scintillation techniques will be used for future low-energy neutrino experiments. One possibility to detect low energy neutrinos is with a scintillator using $\nu_e - e^-$ scattering. This technique requires very high purity levels of the detector materials. The ES reaction is mainly sensitive to ν_e, but also to other neutrino flavours.

Another possibility is to make use of the charged current inverse electron-capture reaction

$$\nu_e + (A, Z) \rightarrow e^- + (A, Z+1) \tag{1.8}$$

which is only sensitive to electron neutrinos. The high radioactive background in the energy region of the prompt electron requires a specific signature to the neutrino event. Therefore the transition should populate an unstable state of the daughter nuclei, which decays into the ground state after a sufficient time period to separate the prompt electron event from the delayed electromagnetic radiation. The characteristic coincidence between the prompt and the delayed event can then be used for efficient background reduction. The interaction rates depend on the nuclear structure of the isotope under consideration and its relative abundance.

Isotope	$T_{1/2}$	Abund.	Progeny	Q [keV]	E^* [keV]	$T^*_{1/2}$
^{115}In $(9/2^+)$	$4.4 \cdot 10^{14}$ a	95.7%	^{115}Sn $(7/2^+)$	114	$116 + 498$	3.26 μs
^{176}Yb (0^+)	stable	12.7%	^{176}Lu (1^+)	301	72	35 ns
^{160}Gd (0^+)	stable	21.9%	^{160}Tb (1^+)	244	$75 + 64$	$6 + 60$ ns
^{82}Se (0^+)	$1 \cdot 10^{20}$ a	9.4%	^{82}Br (1^+)	173	29	7 ns
^{100}Mo (0^+)	$1 \cdot 10^{19}$ a	9.6%	^{100}Tc (1^+)	168	3202 (β)	15.8 s
^{71}Ga $(3/2^-)$	stable	39.9%	^{71}Ge $(1/2^-)$	404	175	79 ns
^{137}Ba $(3/2^+)$	stable	11.2%	^{137}La $(5/2^+)$	611	11	89 ns
^{123}Sb $(7/2^+)$	stable	42.7%	^{123}Te $(7/2^+)$	541	$330 + 159$	31 ns
^{159}Tb $(3/2^+)$	stable	100%	^{159}Dy $(5/2^+)$	543	$177 + 121 + 56$	9 ns

Table 1.2: *Target candidates for real time experiments at low energies. The de-excitation energies (E^*) and half-lifes ($T^*_{1/2}$) of the isomeric states are given.*

A list of candidates for CC real-time solar neutrino detection at low energies is shown in Table 1.2. The first candidate of that type was proposed in 1976 by R. Raghavan [RAG76]. He proposed the use of ^{115}In which in principle allows the detection of pp-neutrinos due to its low Q-value of 114 keV. The most challenging issue for this target is its radioactivity. ^{115}In decays with a half life of $4.4 \cdot 10^{14}$ a into the ground state of ^{115}Sn with a beta endpoint energy of 499 keV which is in the energy range of the delayed γ-cascade.

In 1997 new candidates were proposed by R. Raghavan [RAG97] and pursued for neutrino detection by the international LENS Collaboration [LEN99] that attempts to measure low energy solar neutrinos. These were the long-lived isotopes ^{176}Yb, ^{160}Gd and ^{82}Se. All of them are $\beta\beta$-decay unstable and have Q-values which would allow the detection of pp-neutrinos.

The most promising candidate of these isotopes is ^{176}Yb with a Q-value of 301 keV. The excited state of the daughter nucleus ^{176}Lu decays under emission of a 72 keV gamma with a half-life of 35 ns. The pp-neutrino signal could be mimicked by the isotopes ^{235}U and ^{169}Yb. The latter isotope is produced by neutron capture on ^{168}Yb (natural abundance 0.13 %) and has a half-life of 32 days. The main background sources for ^{7}Be neutrinos in a ^{176}Yb detector

would probably be of instrumental nature and due to ^{176}Lu. This isotope with a natural abundance of 2.6 % could mimic the neutrino tag and is hard to separate from the Yb.

One of the other target candidates, ^{160}Gd, is transformed into ^{160}Tb and has a Q-value of 244 keV. The daughter isotope ^{160}Tb has several excited states which can be populated with rather high probability in the neutrino reaction. This makes a calibration and the determination of the cross section for the inverse electron capture for this system complicated. Another challenging task in this system is the radioactive isotope ^{152}Gd (natural abundance 0.2%) that decays under emission of an 2.14 MeV α-particle.

The neutrino reacts with the last of the three candidates that were originally proposed for LENS, ^{82}Se, to an excited state of ^{82}Br. The experimental challenge of this target is the short half-life of less than 10 ns and the low energy of the delayed gamma (29 keV). All of these three target isotopes proposed were found to be technically difficult.

The MOON Collaboration [MOO00] proposed the use of ^{100}Mo for solar neutrino detection. It has a low threshold of 168 keV. In this case the neutrino signature consists of a prompt electron followed by the delayed β-decay of the unstable daughter nucleus ^{100}Tc with an endpoint energy of 3.4 MeV. The disadvantage of this target is the long half-life of ^{100}Tc of 15.8 s.

In the search for new target candidates for CC real time solar neutrino detection at low energies several aspects have to be considered. First of all the target nucleus should be stable. The Q-value should be below 0.4 MeV for pp-neutrino and below 0.8 MeV for ^{7}Be-neutrino detection. The daughter nucleus should have an excited isomeric state or an unstable ground state that is populated with high probability in the neutrino reaction. To obtain small ft–values resulting in higher transition probabilities, the change in the total angular momentum should not be larger than 1. The isomeric state of the daughter nucleus should decay under emission of electromagnetic radiation. The life time of the excited state should be long enough to obtain a feasible separation of the prompt and the delayed event ($>$ 10 ns). On the other a much longer life time increases the background e.g. by random coincidences. The energy of the delayed event should not be far below 100 keV. Finally, the relative abundance of the isotope should be as high as possible.

One isotope that fulfills the above requirements is ^{71}Ga. This system has an isomeric state with a Q-value of 404 keV. However, in more than 95% of the transitions, the ground state of ^{71}Ge is populated. As part of this thesis the table of isotopes was checked for new isotopes that also satisfy the needs for a candidate target. During the comprehensive study of the nuclei some additional target candidate isotopes were found: ^{137}Ba, ^{123}Sb and ^{159}Tb. They can, however, only be used in a detector for ^{7}Be-neutrinos since their Q-values are all above 500 keV. Therefore they are not further investigated. The LENS Collaboration considers ^{176}Yb and ^{115}In as the best candidates for a low energy solar neutrino experiment.

1.1.3 The LENS project

Motivation

LENS (Low Energy Neutrino Spectroscopy) is a R&D phase project that aims to measure low energy ($<$ 1 MeV) solar electron neutrinos via the charged current interaction. At the beginning of the project the main goals of the experiment were to prove that the origin of the solar neutrino deficit are neutrino oscillations and to pin down the region of the neutrino oscillation mixing parameters. With the recent results from the SNO experiment and the

reactor neutrino experiment KamLAND [KAM03] the scientific goal of future solar neutrino experiments has shifted to an accurate determination of neutrino mixing parameters and to astrophysical questions. A real-time measurement of the low energy solar neutrino spectrum is of relevance for the following topics:

- **Astrophysis:** A measurement of the individual solar fluxes in LENS provides a fundamental test of the reaction details of the SSM. With a high precision measurement the uncertainties in the predictions of the ^{7}Be (10 % uncertainty in SSM) and CNO-fluxes (CNO-cycle contributes 0–8 % to energy production in solar core) can be improved. A better knowledge of the ^{7}Be neutrino flux can also indirectly improve the current accuracy of the pp-flux predictions which is known with a precision of 1 %. By a comparison of the neutrino luminosity vs. the photon luminosity a hidden source of energy in the Sun could be found. Furthermore, in case that the neutrino has a sufficiently large magnetic moment, solar magnetic fields can be probed.

- **High precision parameter determination:** While reactor neutrino experiments have a better sensitivity on Δm^2 solar neutrino experiments offer better sensitivity on the mixing angle Θ_{12}. To improve the accuracy on Θ_{12} with LENS a precision measurement of the pp-flux is needed.

- **Sub-dominant processes:** The solar neutrino data are currently explained by a 2 neutrino oscillation analysis. In a 3 neutrino mixing analysis LENS can set stronger limits on the admixture with the third mass eigenstate (Θ_{13}). Other sub-dominant effects as admixtures of sterile neutrinos can also be investigated with LENS.

- **Redundancy:** LENS could specifically prove the current favorite solution for the mixing parameters, the so-called LMA MSW-solution. The 'survival probability' for electron neutrinos $P(\nu_e \rightarrow \nu_e)$ is energy dependent. In the LMA parameter region $P(\nu_e \rightarrow \nu_e)$ is driven at low energies (pp-neutrinos) by vacuum oscillation whereas at higher energies (^{8}B-neutrinos) matter effects in the Sun start to dominate in the conversion mechanism. Therefore a measurement of the pp-neutrino reduction factor combined with the measured reduction factors at higher energies would be a clear evidence for the LMA solution. If the LENS result would not support the LMA solution this could be a hint for CPT violation or other exotic scenarios.

In order to contribute significantly to the topics mentioned above a high precision in the measurement of the pp-flux of at least 3 % has to be achieved.

Neutrino detection in LENS

The neutrino detection in LENS is based on inverse electron capture of a target atom to an isomeric state of the progenitor, followed by one or more delayed gammas. The prompt electron carries the information on the neutrino energy. The delayed gammas provide a characteristic tag allowing effective background rejection. As mentioned in the previous section several targets such as ^{176}Yb, ^{160}Gd and ^{82}Se were originally proposed for neutrino detection. Finally the collaboration focused on ^{115}In as a target. The term scheme of this system is shown in Fig. 1.4. The neutrino tag consists of a prompt electron, followed by an electromagnetic cascade of a 115 keV event (conversion electron or γ) and a 497 keV γ. The half life of the excited ^{115}Sn state is 3.26 μs. Assuming the oscillation parameters of the LMA-solution,

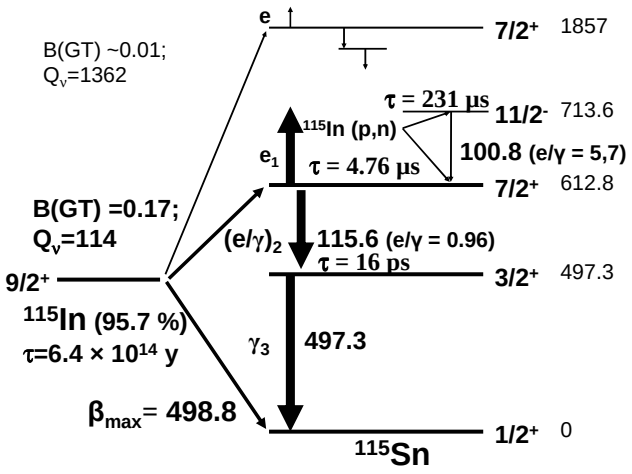

Figure 1.4: *Term scheme of the ^{115}In-system. Energies are given in keV.*

an interaction rate of 57 events/(t·y) for pp-neutrinos and 14 events/(t·y) for ^{7}Be-neutrinos is expected. Due to the low count rates, the experiment requires a target mass of 10 t to 100 t and has to run for several years to obtain high precision results. Therefore long term stability of the detector performance is essential. The challenge of the In-target is the β^--decay of ^{115}In into the ground state of ^{115}Sn, with a specific activity of 0.26 Bq per gram of indium.

LENS would be based on a modular design with cells filled with an In-loaded liquid scintillator. A liquid scintillator detector has the advantage as compared to solid scintillators that it can be constructed cheaply on large scales. In such a modular detector a neutrino event can be identified by a space-time coincidence. First, there is a delayed time coincidence between the prompt electron and the delayed γ-cascade with a time window of 10 μs. The prompt electron and the low energy γ or conversion electron should be in spatial coincidence in a primary 'microcell'. The higher energy γ would be detected in a bigger 'macrocell' around the microcell. Energy cuts for the first e^-/γ as well as for the second γ have to be applied. Despite the specific neutrino signature, the background from In β-decay is still one of the most critical issues.

Background

There are essentially three main background sources: random coincidences, electromagnetic cascades of impurities and background involving Bremsstrahlung. The scintillator quality has a big influence on the signal to noise ratio for all these background sources. To avoid background due to random triple coincidences of three In-β-decays one can select events where the high energy γ triggers at least two cells. The background due to random coincidences of four In-decays determins the granularity of the detector. To overcome this kind of background the number of cells has to be in the range of 10^4 for a detector with several tons of indium.

Another background source is due to β-γ cascades in the decay chains of Th and U. More serious is the background due to random coincidences between an In-β-decay in the energy window of the prompt event combined with a γ of some radioactive impurity in the detector. It was shown in several experiments [LOW02, KAM03] that there are liquid scintillator solvents with a sufficient radiopurity for the needs of a LENS detector, but a method has to be found

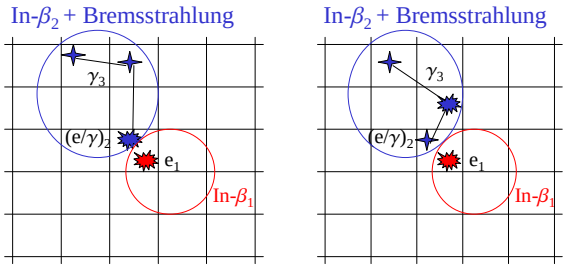

Figure 1.5: *Background events due to an In-decay in the microcell mimicing the prompt signal (In-β_1) followed by a second In-decay producing Bremsstrahlung mimicing the delayed event.*

to keep the purity level when the Indium is loaded.

The most challenging background is due to an In β-decay followed by another In-decay within 10 μs producing a Bremsstrahlung-γ. This kind of background is shown in Fig. 1.5. The second In-decay could deposit some energy in the microcell and the Bremsstrahlung photon could exit the microcell to mimic the second γ. Although the endpoint energy of the β-spectrum is below the energy required to mimic the γ-cascade of the tag, there is a probability that such an event contributes to the background because of the finite energy resolution of the detector. For this reason the role of scintillator performance is important in such an experiment. This is especially because a high energy resolution requires a high light yield of the scintillator to reduce this kind of background. Not only the Bremsstrahlung above 400 keV ('hard BS'), but also low energy Bremsstrahlung ('soft BS') is crucial. The γ-cascade can be mimicked by an energy deposition of a β-decay in a cell around the microcell and some soft photons detected in neighboring cells. The 116 keV candidate originates from one of the soft photons whereas the 497 keV γ can be faked by the electron plus another soft photon. The signal to noise ratio for this kind of background depends on the detector geometry and is therefore reported in the following section.

1.1.4 Detector design

In a homogeneous detector design (all the cells are In-loaded and of the same size) the signal would be dominated by the Bremsstrahlung (BS) background. In order to suppress the BS background a hybrid design should be adopted. In this design the In-loaded cells are surrounded by In-free cells and the background due to soft BS is efficiently reduced. The In-free cells also have the advantage of a higher energy resolution. This helps to reduce the background due to hard BS.

Simulations were performed to estimate the efficiency and the background for both detector designs [JPM02, JPM03]. In these simulations the cells have a length of 3 m and an In-free buffer of 50 cm is inserted between the cells and the multipliers. The In-loading was assumed to be 80 g/l, the effective attenuation length in the cell 2.9 m, the light yield 6000 photons/MeV and the total target mass 4 t. The results are shown in Table 1.3. In a

homogeneous pp-neutrino detector with a cell size of 4 cm×4 cm×3 m and 310 photoelectrons (pe) per MeV the signal to noise ratio (S/N) would be 0.062 at an efficiency of 21 %. With a higher light yield (410 pe/MeV) the S/N is increased by approximately a factor 5. The 410 pe/MeV correspond approximately to 50 % of the signal obtained in a typical In-free scintillator. Another possibility is to increase the ratio by a harder energy cut. In this way the background can be reduced by a factor of three with the prize of a lower efficiency of 11.5 %. In a ^{7}Be-detector the S/N ratio would be well above 1 at an efficiency of approximately 50 %. For a pp-neutrino detector the hybrid design is needed. Various cell sizes were tested in the simulations. Using a size of 10 cm×10 cm×3 m for the In-loaded cells and a thickness of 20 cm In-free scintillator the efficiency for pp-neutrino detection (310 photoelectrons/MeV) would be 20 % at a S/N ratio of 1.7 (noise due to Bremsstrahlung only). It should be mentioned that the assumptions on the scintillator properties are quite challenging.

design	cell size	efficiency	S/N
homogeneous (pp)	$4 \times 4 \times 300$ cm^3	21 %	0.062
homogeneous (^{7}Be)	$4 \times 4 \times 300$ cm^3	48.5 %	6
hybrid (pp)	$10 \times 10 \times 300$ cm^3	20 %	1.7

Table 1.3: *In the Table the efficiency for neutrino detection and the noise to signal ratio (S/N) for different detector designs is given [JPM02][JPM03]. In the simulation was assumed that the number of photoelectrons per MeV is 310, the attenuation length is 2.9 m and the In-loading 8 %.*

Another critical background is the background created by an In-decay combined with a γ of a ^{40}K–decay within 10 μs. A main source for this isotope is the glass in the PMTs. Monte Carlo simulations have shown that a buffer of 100 cm length is still not sufficient at a potassium contamination of 50 ppm in the PMT glass. To reduce this background to justifiable amounts longer or denser buffers have to be used or the potassium contamination has to be reduced. Another option is to use an active instead of a passive buffer.

Due to the high granularity required in an In-detector a large number of cells and PMTs are needed. Therefore the costs of the experiment are rather high. To reduce the costs, high In-loading in the scintillator is mandatory. Another possibility to reduce the costs is to increase the cell length. This would lower the number of PMTs, but needs very long transmission lengths in the In-loaded scintillator. In conclusion, excellent scintillator performance is the key to a successful measurement of low energy solar neutrinos.

1.1.5 The Borexino-Experiment

Borexino is an upcoming real-time experiment for solar neutrino detection at low energies [BOR02]. It would be complementary to a charge current experiment, since it detects neutrinos via $\nu - e^-$ scattering which has a NC contribution, and is therefore sensitive to all known neutrino flavors. In combination with a high precision CC experiment at the same energy one could estimate the contribution of the non-electron neutrino flavors and with it the total solar neutrino flux as the SNO Collaboration has done for the high energy part in the solar neutrino spectrum. Borexino is designed to measure basically the monoenergetic line at of the ^{7}Be reaction in the pp-cycle at 0.862 MeV (see Fig. 1.3). These neutrinos create a

Compton-like spectrum with a maximum energy of 0.665 MeV. The signal window is between 0.25 and 0.8 MeV. Since Borexino detects scattered electrons without any distinct signature, purity levels in the scintillator and detector materials of previously undetected magnitudes are required. Further physics goals include the detection of pep and CNO neutrinos, neutrinos from supernovae, antineutrinos from distant nuclear reactors and antineutrinos from geophysical sources.

The Borexino detector is built in Hall C of the underground laboratories of Gran Sasso (LNGS) in Italy. The rock shielding of 3500 m w.e. suppresses the muon flux by six orders of magnitude to 1.1 $m^{-2}h^{-1}$. The detector uses a graded shielding structure where the materials closer to the target have the higher purity levels. The inner part consists of 300 t of liquid scintillator (1,2,4-trimethylbenzene, known as pseudocumene or PC, mixed with 1.5 g/l PPO as fluor) enclosed in a UV-transparent nylon balloon. The central 100 t are used as a fiducial volume for the data analysis. Outside this inner vessel (IV) will be 1000 t of pure PC as a buffer inside a stainless steel sphere (SSS) of 13.7 m diameter. There are 2200 8" photo multiplier tubes (PMTs) observing the inner vessel. Most of the PMTs are equipped with light concentrators increasing the coverage to 30 %. To avoid scintillation light in the buffer liquid, a light quencher (DMP) is added. It is planned to have an additional Nylon vessel between the SSS and the IV as a barrier against Radon emitted by the PMT material and the wall of the SSS. The SSS itself is enclosed in a cylindrical tank, 18 m in height and in diameter. The volume between the tank and the SSS will be filled with pure water, as a buffer against external radiation as well as a muon veto. There are 208 outward looking PMTs on the SSS detecting the Cherenkov light created by the muons in the water. This shielding should allow to detect the approximately 30 neutrino events per day expected by the SSM and the predictions of the LMA solution.

To identify some of the background events in Borexino pulse shape discrimination (PSD) of α-particles and delayed coincidences (DC) of correlated decays of impurity activities are used. The α-particles emitted in the ^{238}U and ^{232}Th-chain have energies from 4 MeV to 9 MeV. The scintillation light produced is quenched by factors of 10 to 15 relative to β or γ-signals, so that they appear in the neutrino signal window. This quenching mechanism also results in characteristically long scintillation times. The different pulse shapes of α and β-particles can be used to tag α-events with 90 % to 99 % efficiency depending on the scintillator composition and the α-energy. Some of the daughters in the U and Th decay chains decay in a time correlated coincidence which can be tagged. The efficiency of these methods are investigated in a Borexino prototype detector.

The requirements on the scintillator purity are unique and were never measured before. Therefore a prototype detector, the so-called Counting Test Facility (CTF) had to be built to measure the purity levels of the scintillator. The heart of this detector is a Nylon vessel with 4.8 m^3 of liquid scintillator surrounded by water as a buffer. The detector is inside a cylindrical tank with a diameter of 11 m and a height of 10 m. Around the Nylon vessel is a structure of 100 PMTs. Since the second measuring period of the CTF it is equipped with an additional radon barrier, a muon veto and a liquid handling system.

The CTF has been used to measure the radiocontamination in scintillators based on PC and PXE [LOW02]. The $^{14}C/^{12}C$ ratio was measured to be $(1.94 \pm 0.09) \cdot 10^{-18}$ in PC and $(11.74 \pm 0.03) \cdot 10^{-18}$ in PXE. The equivalent rates of the radioactive isotopes ^{238}U and ^{232}Th have also been measured via the delayed coincidences of the Bi-Po decays. The relevant isotopes of Bi and Po are daughter nuclei of the Rn-chain. It should be noted that ^{222}Rn is not necessarily in equilibrium with the U-activity. The measured ^{222}Rn-activity expressed

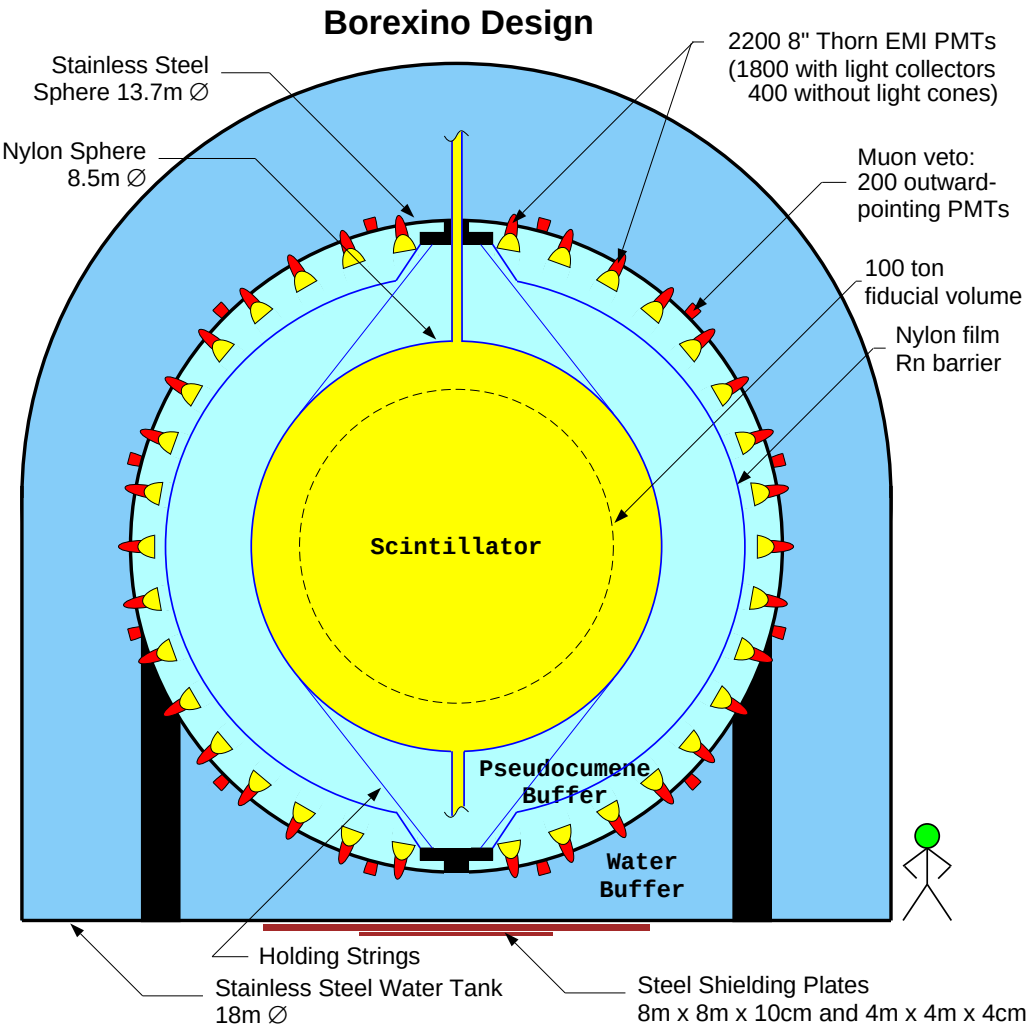

Figure 1.6: *Schematic view of the Borexino detector.*

as ^{238}U equivalent was $(3.5 \pm 1.3) \cdot 10^{-16}$ g/g in PC and $(7.3 \pm 2.4) \cdot 10^{-16}$ g/g in PXE. The altered detector performance makes a comparison of the ^{238}U-activity in PC and PXE difficult. For ^{232}Th the values are $4.4^{+1.5}_{-1.0} \cdot 10^{-16}$ g/g in PC and $(4.0 \pm 4.4) \cdot 10^{-16}$ g/g in PXE. Lower limits were obtained for PXE by direct measurements using neutron activation analysis. The design specifications for the allowed U and Th concentrations are 10^{-16} g/g and for the allowed ^{14}C/^{12}C ratio 10^{-18}.

One of the most dangerous background sources in Borexino are the radioactive isotopes of the noble gases, especially the omnipresent ^{222}Rn which is a member of the ^{238}U-chain. It has a half-life of 3.8 days and a high mobility. Rn emanates from the detector materials in contact with the scintillator, and dissolves in the liquid. The Rn itself would decay within a few weeks, but there is the long-living isotope ^{210}Pb in the decay chain with a half-life of approximately 22.3 a. Therefore Rn-emanation from all detector components have to be checked to verify their purity.

1.2 Reactor anti-neutrinos

The source of the first experimentally measured neutrinos by F. Reines and C. Cowan in 1956 was a nuclear reactor [REI59]. Since that time several experiments used nuclear reactors as an intense neutrino source to investigate neutrino properties. Nuclear reactors produce electron antineutrinos in the β-decay of the neutron-rich fission fragments. Contributions of other neutrino types in the flux can be neglected. The detection of the antineutrinos is based on the inverse β-decay:

$$\bar{\nu}_e + p \rightarrow e^+ + n \tag{1.9}$$

The measured kinetic energy of the e^+ allows the reconstruction of the $\bar{\nu}$ energy. The threshold in this reaction is 1.8 MeV.

1.2.1 Status

From the recent reactor neutrino experiments important information on the mixing parameters in neutrino oscillations could be obtained. Since the energy of reactor neutrinos is in the MeV range they do not have enough energy to produce muons or taus. Therefore reactor experiments can only measure the disappearance of electron antineutrinos. The experiments Chooz [CHO99] and Palo Verde [PAL01] having baselines between source and detector in the 1 km range set the current upper limit for one of the elements in the neutrino mixing matrix, U_{e3}. The Japanese reactor experiment KamLAND [KAM03] confirmed the LMA-solution in the mixing parameter space already favored by a global fit of all solar neutrino experiments. In this experiment the combined flux of several reactors at distances in the 100 km range is measured. These experiments will now be separately described.

Chooz

The Chooz detector was placed about 1 km from the neutrino source in an underground lab (300 m w.e. overburden) to reduce the muon flux by approximately a factor of 300. The muons produce fast neutrons in the detector material which constitute one of the main backgrounds in such an experiment. The power plant in Chooz consists of two twin pressurized water

reactors (total thermal power 8.5 GW). The detector is mounted in a 5.5 m high cylindrical tank which is 5.5 m in diameter. This steel vessel is surrounded by 75 cm low-radioactivity sand and covered by 14 cm of cast iron to protect the detector from natural radioactivity of the surrounding rocks.

The central part of the detector is a transparent plexiglass container filled with 5 t of a 0.09 % Gd-loaded paraffinic liquid scintillator. ^{157}Gd and ^{155}Gd both have a high thermal neutron capture cross section combined with a high energy (approximately 8 MeV) of gammas emitted in the reaction:

$$n + Gd \rightarrow Gd^* \rightarrow Gd + \sum_i \gamma_i \tag{1.10}$$

The use of Gd allows for an efficient background reduction since natural radioactivity has energies mainly below 3 MeV. The neutrino signal consists of a delayed coincidence between the prompt positron signal in the neutrino reaction followed by the the γ-ray emission after the neutron capture. At the chosen Gd-concentration the neutron capture time is 30.5 μs. The inner plexiglass container is surrounded by 17 t of an undoped liquid scintillator in a plastic structure that supports 192 inward-looking PMTs. This region acts as a buffer from the PMT radioactivity and provides containment of the γ-rays from the neutron capture. Optically separated from this volume are another 90 t of undoped scintillator used as additional shielding and as a muon veto (24 PMTs).

When the reactor is running at full power the measured neutrino signal is (24.7 ± 0.7) events per day. The ratio R between measured and expected flux was determined to be $(1.01 \pm 0.028(stat) \pm 0.027(syst))$. In the two-neutrino mixing analysis of the Chooz data the limit for $\sin^2\Theta$ which is a function of Δm^2 was calculated to be < 0.09 for $\Delta m^2_{atm} > 1.5 \cdot 10^{-3}$. No evidence for neutrino oscillation in the $\bar{\nu}_e$ disappearance mode was found for maximum mixing and $\Delta m^2 > 7 \cdot 10^{-4}$ (90 % CL) [CHO99]. In a three neutrino mixing analysis an upper limit for $|U_{e3}|^2$ of $1.7 \cdot 10^{-2}$ was found for $\Delta m^2_{atm} = 2.5 \cdot 10^{-3}$ eV^2 (90 % CL) [BIL02]. Up to now the Chooz-experiment gives the best upper limit on $|U_{e3}|^2$.

The first Gd-loaded scintillator used in the Chooz experiment needed to be replaced after 4 months due to a chemical instability. A modification of the scintillator composition improved the stability. However, the detector still varied its response due to a decrease in the transparency of the Gd-loaded scintillator whereas the light production of the scintillator was stable. The light at the PMTs exponentially decreased with a time constant of approximately 750 d. Therefore, one of the limitations of the Chooz experiments was the stability of the liquid scintillator.

Palo Verde

The 3-reactor plant of Palo Verde with a distance of 750 m to 890 m from the detector has a total thermal power of 11.6 GW. The Palo Verde detector was placed in an underground bunker (32 m w.e. overburden). At this depth the muon flux is reduced only by a factor of five. Due to the many neutrons produced by the muons a segmented detector was needed to obtain a sufficient background reduction. In this design a $\bar{\nu}$ event is detected by the triple coincidence of the positron ionization, the annihilation γ's of the positrons which are generally detected in different cells and the delayed γ shower after the neutron capture. The fiducial mass of the detector was 12 t and consisted of 66 acrylic tanks filled with 0.1 % Gd-loaded scintillator. Each cell was 9 m long with a (12.7×25.4) cm^2 cross-section and equipped with

two 5" PMTs at each end. The array of scintillator cells was surrounded by a water shielding and a muon veto. The still high background due to cosmic rays was reduced by making use of the conventional reactor-on and reactor-off cycles. In the Palo Verde experiment the ratio of observed interaction rate to the one expected is $(1.01 \pm 0.024(stat) \pm 0.053(syst))$.

As scintillator solvent a mixture of mineral oil and pseudocumene (PC) was chosen in the Palo Verde experiment [PAL99]. The solution was optimized at 60 % oil by volume as this is the minimum oil concentration necessary that the liquid does not harm the acrylic cells. Since the fully blended scintillator was even unstable during the truck transport in a steel drum, the PC based Gd-loaded 'concentrate' prepared by the Bicron company was shipped separately from the mineral oil to the detector site. There the liquids were mixed in steel drums. The handling of the scintillator had to be done in a very careful way to avoid precipitation or destabilization of the Gd compound. Despite all efforts to keep the scintillator stable there was still a loss of transparency of about 2 cm/day at the scintillator emission around 440 nm.

KamLAND

KamLAND is located at the site of Kamiokande with an average rock overburden of 2700 m w.e. The neutrino target consists of 1000 t of liquid scintillator contained in a 13-m-diameter nylon balloon. The scintillator solvent here is 80 % dodecane and 20 % PC. In KamLAND it was chosen not to load the scintillator with Gd. They achieved a scintillator purity that allows to measure the delayed coincidence of the e^+ and the 2.2 MeV γ-ray from the neutron capture on a proton. The mean neutron capture time without Gd is about 180 μs. A nonscintillating buffer between the balloon and an 18-m-diameter spherical stainless steel containment serves as a shielding from external radiation. An array of 1879 PMTs is mounted on the inner surface of the steel vessel. The neutrino target has a 30 % photocathode coverage. The space between the steel sphere and the cylindrical rock cavity is filled with 3.2 kton of water and used as Cherenkov detector in order to veto incoming muons.

The long distance from the detector to the nuclear reactors of typically 180 km enables KamLAND to address the oscillation solution already favored by the solar neutrino experiments. The ratio of the observed reactor $\bar{\nu}_e$ events to that expected without neutrino oscillation was found to be:

$$R = 0.611 \pm 0.085(stat) \pm 0.041(syst) \tag{1.11}$$

The probability that this result is consistent with the no disappearance hypothesis is less than 0.05 %. The shape of the spectrum is consistent with the expected distortion from neutrino oscillations as well as with the no-oscillation shape. This ratio R is consistent with the LMA-solution and excludes under the assumption of CPT invariance all other solutions that were allowed by the solar neutrino data. Assuming two neutrino mixing the best fit to the KamLAND data in the physical region suggests $\sin^2 2\Theta_{12} = 1.0$ and $\Delta m^2 = 6.9 \cdot 10^{-5}$ eV^2 compared to the best fit LMA-values of $\sin^2 2\Theta_{12} = 0.833$ and $\Delta m^2 = 5.5 \cdot 10^{-5}$ eV^2.

1.2.2 Future experiments

The aim of a future reactor neutrino experiment will be to measure Θ_{13} via the energy dependent $\bar{\nu}_e$ disappearance. A vanishing Θ_{13} would imply that no CP violation is observable in the lepton sector and ν_e could be simply expressed by a linear superposition of ν_1 and ν_2

while ν_μ and ν_τ become superpositions of ν_3 and the orthogonal combination of ν_1 and ν_2. The best current upper limit on Θ_{13} comes from the Chooz experiment.

To improve this limit or to actually measure a non zero Θ_{13} the statistical and systematic error has to be reduced in a new reactor experiment. To reduce the systematic error it is planned to have two identical detectors containing 10 t to 20 t of Gd-loaded liquid scintillators at different distances from the reactor core. Several reactor sites in Brazil, China, Europe, Japan, Russia and the US are under study for such an experiment. One of the most promising sites is the Chooz reactor in France. At this place the experience and the already existing infrastructure of the original Chooz experiment could be used in a future experiment called 'Double Chooz'. The underground neutrino laboratory of the first experiment would be used for the far detector (1.05 km baseline) whereas the near detector would be at a distance of 100 m to 200 m from the two reactor cores. From simulations one expects a sensitivity of $\sin^2 2\Theta < 0.03$ (90% CL) in the Double Chooz experiment after three years of operation. After the experiences in Chooz and Palo Verde one of the main challenges in such an experiment is to produce a Gd-loaded scintillator that is stable in time and has a long attenuation length.

1.3 Neutrinoless $\beta\beta$-decay

Double beta decay (DBD) is a rare nuclear transition in which the charge of two isobaric nuclei changes by two units. Two electrons and two $\bar{\nu}_e$ are emitted at the same time.

$$ {}^{A}_{Z}X_N \rightarrow {}^{A}_{Z+2}X_{N-2} + 2e^- + 2\bar{\nu}_e \tag{1.12} $$

As in the single β-decay there is a continuous spectrum for the sum of the electron energies. In the lepton number violating neutrinoless DBD the electron spectrum would be a monoenergetic line at the transition energy. The detection of the neutrinoless DBD would imply that the neutrino is a Majorana and not a Dirac particle since the antineutrino emitted in the first vertex has to be absorbed at the second vertex as a neutrino. This process also requires a change in the helicity of the neutrino which is only possible for massive particles. The solar, reactor and atmospheric neutrino experiments have shown that neutrinos have a mass. However, in these experiments only squared mass differences can be measured. A DBD experiment allows the determination of the absolute neutrino mass scale. Future DBD experiments can probe part of the parameter range predicted by other experiments.

The main challenge in DBD experiments based on the direct observation of the two electrons emitted in the decay is a low background in the energy window of the electrons at large target masses. It is advantageous to have a good energy resolution in the detector, since it decreases the width of the signal energy window. The best limit on neutrinoless DBD has been obtained by the Heidelberg-Moscow experiment on ^{76}Ge (transition energy 2039 keV). The use of germanium has the advantage that it can be used as detector with very good energy resolution. The lower limit for the half-life of neutrinoless DBD $T^{0\nu}_{1/2}$ given by the collaboration is $1.9 \cdot 10^{25}$ y corresponding to an upper limit on the effective neutrino mass of 0.35 eV (90% CL) [HMO01]. Some members of the Collaboration reported evidence for neutrinoless DBD with $T^{0\nu}_{1/2} = 0.8 - 18.3 \cdot 10^{25}$ y corresponding to an effective neutrino mass range of $0.11 - 0.56$ eV (best value 0.39 eV) [KLA01]. This number has to be confirmed or disproved by a next generation of experiments [CRE03].

A very attractive isotope for a future DBD experiment is the isotope ^{150}Nd (natural abundance 5.6 %, $T^{2\nu}_{1/2} = 1.9 \cdot 10^{19}$ a). It has the advantage of a high Q-value (3.37 MeV)

which implies high probability of neutrinoless DBD due to the higher phase space integral. Also the background due to natural radioactivity is low in the energy region above 3 MeV. We currently study the feasibility to load a Borexino type detector with a Nd-loaded liquid scintillator. This demonstrates the wide range application of metal loaded scintillators in neutrino physics.

1.4 Conclusion

Projects in low energy solar neutrino physics, in future reactor neutrino experiments and in $\beta\beta$-decay experiments ask for metal loaded liquid scintillators with a high light yield to enhance the energy resolution, high transparency of several meters in the wavelength region of the scintillator emission and radiopurity. Furthermore a basic requirement in all the experiments is long term stability of the scintillator which is mandatory for a stable detector performance over the long time period of several years that is necessary to get high statistics.

In this thesis a method will be presented to produce metal loaded liquid scintillators that basically meet all these requirements. In Chapter 2 a theoretical background of the energy transfer processes in a scintillator system will be given which is of relevance to find the optimized composition of the metal loaded scintillator. Chapter 3 describes the synthesis and purification of an In-β-diketone complex that can be dissolved in organic liquid scintillators. In Chapter 4 the optical properties of an In-loaded scintillator that could be used in a solar neutrino detector are reported. Experimental results of measurements in a prototype cell and in an underground prototype detector are presented in Chapter 5. The performance of a Gd-loaded scintillator for a future reactor neutrino experiment and first tests on a Nd-system for $\beta\beta$-decay measurements are presented in Chapter 6. In the last chapter the topic of Rn-background is addressed which is of relevance for all the experiments described above.

Chapter 2

Energy transfer in scintillators

The understanding of the energy transfer processes between the various scintillator components is essential towards the development of a useful scintillator system. In this chapter, the basic principles of energy transfer from an excited donor to an acceptor in the ground state and their fluorescence behavior is discussed. The equations introduced here motivate the fluor and solvent variations presented in the experimental chapters.

2.1 Fluorescence und phosphorescence

This section deals with the basics of the fluorescence and phosphorescence of aromatic molecules. The responsible processes of absorption and emission are shown in Fig. 2.1. There the energy levels of the electronic states (several eV difference) and vibrational states (difference in the range of 0.1 eV) are plotted. The energy difference in the rotational levels is one or two orders of magnitude smaller than that of the vibrational states and can therefore be ignored.

Fluorescence radiation is created in the transition of an electron between the two singlet states of the lowest levels S_0 and S_1 (having total angular momentum J= 0). In the absorption of a photon or other electromagnetic interaction, the ground state electrons of a molecule can be lifted up into excited vibrational states of a higher electronic state. In this event, for the case of liquids and solids the electron rapidly looses energy in collisions and populates a vibrational ground state of the first excited electronic state (S_1). The order of magnitude for the time scale of these relaxation processes is 10^{-12} s. If the electron stays in that state for more than about 10^{-9} s without loosing its energy by other processes, the emission of fluorescence radiation occurs in the transition $S_1 \rightarrow S_0$. Since the excitation is usually from the vibrational ground state of S_0 to an excited state of S_1 and the decay is usually from the vibrational ground state of S_1 to an excited vibrational state of S_0, the emission spectrum is shifted to longer wavelengths compared to the absorption spectrum (the Stokes shift).

There is some probability that a transition from the singlet state S_1 to the lowest triplet state T_1 (total angular momentum 1) can occur. These states are metastable with a mean lifetime up to several seconds. In the transition $T_1 \rightarrow S_0$ so-called phosphorescence radiation is emitted. This radiation is found at longer wavelengths compared to fluorescence radiation, because the lowest triplet T_1 is below S_1.

In some rare cases the ground state of a molecule is in a triplet state and excited triplet states are populated in the excitation process. They decay again into the ground state under the emission of fluorescence radiation. Therefore fluorescence means in general the emission

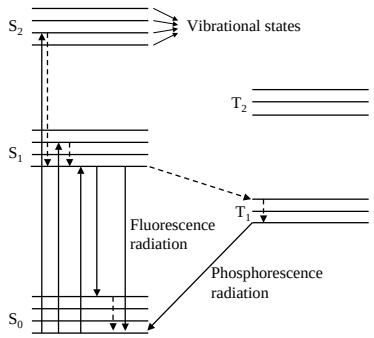

Figure 2.1: *This diagram exemplarily depicts the energy levels of the singlet (S) and triplet (T) states with the corresponding vibrational levels. In addition, the transitions leading to fluorescence or phosphorescence radiation are plotted (solid arrows). Dashed arrows indicate radiationless transitions.*

of a photon in the transition of states with the same multiplicity. On the other hand phosphorescence means photon emission in transitions between states with different multiplicity.

2.2 Energy transfer between isolated molecules

The subject of energy transfer between a donor molecule D in an excited electronic state and an acceptor molecule A is of interest in several fields in science, especially for the understanding of many biological processes. The first observation of non-radiative energy transfer was made by Cario and Franck [CAR23] between mercury and thallium atoms in their experiments on sensitized fluorescence in the vapour phase.

In a scintillator system, the molecules of the scintillator base are excited by ionizing particles and part of the absorbed energy is transferred into electromagnetic radiation, typically in the UV-region. The emission spectra are generally the same for excitation by photons or excitation by high energy α-, β- or γ particles. After the excitation by the incident radiation the molecules may be excited to highly excited electron levels and atomic vibrations, but in a short time (10^{-12} s) most excited molecules are converted to the first excited state.

Often, a scintillator needs more than one fluorescent component. The energy shift between the absorption and emission spectrum is not sufficient in most cases for the fluorescent radiation to leave the medium without reabsorption. For this reason scintillator systems typically consist of at least two components. One fluorescent molecule – often the solvent itself in liquid scintillators – is used in high concentrations. The main part of incoming radiation is absorbed by that molecule and the energy then transferred as effectively as possible to another fluorescent molecule, called the *fluor*. The fluor emits at longer wavelengths and is usually present in lower concentrations. Moreover the fluor typically has a large Stokes shift that the effect of self-absorption is minimized.

The energy can be transferred from D to A in several ways. There is the trivial process of energy transfer by photon emission of the excited D and photon absorption of A. In the systems described below this kind of transfer is negligible, because most of the energy transfer processes in scintillators are non-radiative. At close distances the excited molecules or atoms can transfer there excitation energy e.g. by collisions with their partners. The energy can also be transferred radiationless over distances much longer than the dimension of the molecules involved. This kind of transfer dominates in most scintillator systems and is specified below.

One of the first theories describing the energy transfer between D and A with distance R was formulated by Perrin [PER24]. In this model the energy is always transferred if R is smaller than a critical distance R_0. The efficiency η for energy transfer depends on the acceptor concentration by

$$\eta = 1 - e^{-\frac{c}{c_0}} \tag{2.1}$$

Here c is the concentration of A (in the case of a scintillator of the fluor) and c_0 is known as the critical concentration. The definition of c_0 can be different in the various models and needs to be specified when a particular model is used. Typically the concentration c_0 corresponds, on average, to one acceptor molecule in a sphere of radius R_0. In the kinetic approach of Stern–Volmer [STE19] the efficiency η can be expressed by:

$$\eta = \frac{1}{1 + \frac{c_0}{c}} \tag{2.2}$$

Förster worked on a detailed quantum mechanical treatment of the energy transfer between a donor and an acceptor [FOR48]. His model is based on the assumptions that D and A are both diluted in an inert medium being transparent in the wavelength region of interest and that the distances between the molecules are large compared to their dimensions. He explains the radiationless energy transfer by interaction of the electrical dipole fields of D and A. This interaction energy has a $1/R^3$ dependency. The transition probability is proportional to the square of the interaction energy leading to a $1/R^6$ dependency. In this model one can derive the equation [FOR59]

$$\eta = \sqrt{\pi} \cdot x \cdot exp(x^2)[1 - erf(x)] \tag{2.3}$$

where $x = \frac{1}{2}\sqrt{\pi}\frac{c}{c_0}$ and the error function is defined by $erf(x) := \frac{2}{\sqrt{\pi}} \int_0^x e^{-u^2} du$.

A critical transfer distance R_0 can be defined by the distance where the probability for spontaneous decay of the excited D equals the probability for energy transfer to A in the case of an isolated donor-acceptor pair. According to Försters theory R_0 can be calculated using the experimentally determined absorption (by A) and emission (by D) spectra through use of the equation

$$R_0^6 = \frac{K \cdot \kappa^2 \cdot Q}{n^4} \cdot J \tag{2.4}$$

where

$$J = \int \frac{f_D(\nu)}{\nu^4} \epsilon_A(\nu) d\nu \tag{2.5}$$

is the energy (frequency ν) weighted absorption-emission overlap and

$$K = \frac{9000 \cdot ln(10)}{128 \cdot \pi^5 \cdot N_A} \tag{2.6}$$

contains various constants. Here κ^2 is an orientation factor with possible values between 0 and 4. At a random orientation of the dipoles to each other the value is $\frac{2}{3}$. Furthermore Q is the quantum yield of D, n the refraction index of the solvent, ν the wavenumber, $f_D(\nu)$ the emission spectrum of D normalized to one, $\epsilon_A(\nu)$ the molar extinction coefficient of A and N_A the Avogadro Number.

The equations show that a large overlap between the spectra $f_D(\nu)$ and $\epsilon_A(\nu)$ lead to a large R_0 implying an efficient transfer rate (typical values of R_0 are between 1 nm and 10 nm). R_0 corresponds to the critical concentration c_0 by

$$c_0 = \frac{3}{4\pi R_0^3 N_A} \tag{2.7}$$

Note that at this concentration η is approximately 0.7.

There can be a temperature dependency in the amount of overlap between the absorption and emission spectra. Both functions, $f_D(\nu)$ and $\epsilon_A(\nu)$, broaden with temperature. If they overlap perfectly at all temperatures the transfer probability will decrease with increasing temperature. On the other hand, if their centers are well separated, the broadening will increase the overlap and hence the transfer probability. It is also possible, in some cases, that there is a shift of the center of one of the functions which may increase or decrease the overlap integral.

The seminal theory of Förster was extended a few years later by Dexter [DEX53]. In Dexters model not only the resonant energy transfer between allowed transition is described, but also the energy transfer due to interactions between e.g. dipole and quadrupole fields. For a dipole-quadrupole transition, the transition probability is proportional to $1/R^8$. Additionally, Dexter included energy transfer due to the exchange interaction in the model. The energy transfer via the exchange interaction needs some overlap of the electronic orbitals of both A and D. This occurs at short distances only. Non-radiative energy transfer by the exchange interaction starts to dominate at distances R below 1 nm. Here, the transition probability is proportional to $exp(-2R/L)$, where L is a positive constant. The exponential dependence reflects the fact that the overlap depends on the radial behavior of molecular orbitals where 'tails' have the $exp(-R/L)$ behavior, in the model. Again the transfer rate depends directly on the overlap between $f_D(\nu)$ and $\epsilon_A(\nu)$. Dexter specially investigated systems where D and A are situated inside crystals. Due to the dipole-dipole interaction, acceptors can be excited on approximately 10^3 to 10^4 lattice points around the excited donor and have successful energy transfer. In the dipole-quadrupole interaction this number drops down to approximately 10^2 and in the exchange interaction only about 30 lattice points can be reached [1].

In some systems deviations from these models are observed experimentally in the early stages of the donor lifetime. One possible explanation could be in some cases that the positioning of donors and acceptors is not random in the material. A more generalized equation for the non-radiative energy transfer then results, as described in references [ROT88] and [ROT89] (derived in the context of co-doped fluorescing crystals but generally applicable). A

[1] Calculations of the yield and decay time of the donor luminescence (derived for rigid solution) as functions of the acceptor concentrations using Dexters model can be found in reference [INO65].

second possible explanation for deviations from the Förster Dexter equations could be that an additional mechanism exists for rapid short range transfer. In reference [HAR91] a physical mechanism based on dynamical symmetry arguments is presented which can account for a fast transfer in the local donor region.

2.3 Energy transfer in organic liquid scintillators

The energy transfer parameters are best determined in dilute solutions when the donor and acceptor concentrations are low and when there is no interaction between like molecules or between the solutes and the solvents. In organic liquid scintillators the donors are often the solvent itself and therefore present in high concentrations. In such a system multiple processes can be at play which are not discussed in the models presented up to now.

Kallmann et al. [KAL59] developed a model that includes such effects. This model can be applied in our case of an organic liquid scintillator where the solvent takes the role of the donors and the fluor is the acceptor. The model distinguishes three different processes being responsible for the energy transfer between D and A

- An excited solvent molecule D^* moves through the solvent by diffusion until it is close enough to an acceptor to transfer its energy. This kind of transfer does not occur in solids (material diffusion transfer).
- The excitation energy can be transferred between several neighboring donors until it is in the vicinity of an acceptor (migration transfer).
- The energy of the solvent molecule may be transferred in a single step by one of the interactions described above without diffusion or migration of excitation energy (single step transfer).

Process two is assumed to be the dominant processes for energy transfer in an organic liquid scintillator. The equations used up to now do not apply in this case. They are important for determining the parameters and then using these parameters in more complicated expressions. Because the material diffusion transfer does not occur in solids it is expected that the energy transfer from the excited solvent to an acceptor is smaller in rigid media compared to a liquid scintillator. Due to the favourable energy transfer in liquids lower fluor concentrations should be needed in a liquid scintillator. Besides the fluor, there can be acceptor molecules which are non-fluorescent and do not contribute to the production of scintillation light. Often these light quenching molecules are impurities in the scintillator, but sometimes the scintillator is doped with these 'Quenchers', on purpose at high concentrations. Quenching is also found to be higher in a liquid compared to a solid at the same quencher concentration [KAL59] due to the more effective energy transfer.

The excited solvent molecule D^* in a scintillator has in principle two possibilities of de-excitation. First the energy can be transferred to the environment without excitation of an acceptor ('Quenching', probability $P1$), e.g. by internal conversion of the electronic excitation energy into oscillation energy of the atomic constituents of the molecule. The probability of quenching due to this internal conversion becomes higher with increasing temperature. Second, the energy can be transferred from D^* to A. The transfer rate of this process is proportional to the concentration c of A (Probability $P2 \cdot c$). The probability that D^* decays by the emission of a real photon to the ground state and this photon escapes from the solution,

is negligible in most systems (the principle of the following argumentation would not change if this effect would be included). For the number n_A of excited acceptor molecules A* then applies:

$$n_A \propto \frac{P2 \cdot c}{P1 + P2 \cdot c} \tag{2.8}$$

The A* ideally emit a photon (Probability $P3$). However the A* can be quenched in some way ($P4$). A special kind of quenching is the self-quenching which can occur at very high concentrations. It was first observed by Walter in 1888 who proposed aggregation as the cause of the quenching [WAL88]. The mechanisms of self-quenching are still not entirely understood. In this context the creation of double molecules (dimerization) and energy transfer to non-fluorescent dimers could be of importance. Another possibility are collisional quenching interactions between fluor monomers. Probably self-quenching is a combination of the two effects. It is not observed in solids. The self-quenching of A* is assumed to be proportional to c ($P5 \cdot c$). Including these processes in the model we get for the light intensity I of an organic liquid scintillator the following dependency on the fluor concentration c:

$$I(c) \propto \frac{P3}{P3 + P4 + P5 \cdot c} \cdot n_A \propto \left(\frac{P2 \cdot c}{P1 + P2 \cdot c}\right) \cdot \left(\frac{P3}{P3 + P4 + P5 \cdot c}\right) \tag{2.9}$$

$$\Rightarrow I(c) = \frac{P \cdot c}{(Q + c) \cdot (R + c)} \tag{2.10}$$

with the constants P, Q und R. This equation predicts a linear increase of the light intensity at low fluor concentrations. At higher concentrations I approaches a maximum. In an extreme case the maximum is reached when all the energy of the excited donors is transferred to the fluor. This part of the curve is represented by the $(Q + c)$ term in the denominator. The self–quenching of the fluor leads at high concentrations to a decrease of I. The strength of this effect depends on the $(R + c)$ term in the equation. In practice one finds usually a steep increase at low concentrations which ends at a c level of a few g/l. Around the maximum there is a broad plateau. At concentrations of much more than 10 g/l I typically decreases again due to the self-quenching .

The model does not include direct light excitation of the fluor by the primary radiation. Under the assumption that the additional contribution to the light intensity by this effect is proportional to c one can add a correction term $S \cdot c$ to the above equation. Doing so one obtains an extended Kallmann model:

$$I(c) = \frac{P \cdot c}{(Q + c) \cdot (R + c)} + S \cdot c \tag{2.11}$$

In Chapter 4 the experimental data of the light yields for some scintillator systems at varying fluor (acceptor) concentrations are presented. There, some of the equations above are fitted to the experimental data points. From these fits parameters such as the critical concentration c_0 can be derived.

Chapter 3

Development of an In-loaded liquid scintillator

One of the big challenges in a solar neutrino experiment as LENS is how to put the target material into the liquid scintillator. The demands of a low energy indium based solar neutrino detector call for a scintillator having a metal loading in the 5 wt.% to 8 wt.% range, a large light output and a long attenuation length (several meters) at the emission wavelength of the scintillator (typically at 430 nm). Furthermore long term stability over years and radiopurity of the scintillator are crucial.

Several studies of In-loaded liquids have been published. L. Pfeiffer [PFE78] used phenethyl alcohol ($C_6H_5C_2H_4OH$) as scintillator solvent. This solvent has a high solubility for indium trifluoroacetate allowing an In-loading up to 80 g/l. This scintillator was reported to be limited in light attenuation. The basic formulation of this system was duplicated and improved by Payne and Booth [PAY90]. Essentially they reduced the amount of phenylethanol to the minimum amount that is needed to keep the In compound in solution. As bulk scintillating material a xylene based solvent with significant higher light yield was used. Their 5 % In-loaded scintillator had an effective attenuation length of only 54 cm measured in a 1 m long quartz cell. The attenuation length of a 10 % In version was furthermore published to be 45 cm.

A new way to dissolve indium in a scintillator was found by Suzuki et al. [SUZ90]. They used an organic scintillator with a surfactant (surface active agent) which has both hydrophilic (polar) and hydrophobic (nonpolar) chemical groups. This 'emulsive' scintillator enables polar indium compounds to be mixed into nonpolar organic scintillators. The scintillator was made by mixing $InCl_3 \cdot 4H_2O$ (In trichloride tetrahydrate) with a commercially available xylene based liquid scintillator. The maximum In loading in this system is 7.5 wt.%. An attenuation length of more than 150 cm and an energy resolution of 11.7 % for 477 keV electrons was measured in a 1 m long test cell with a diameter of 5 cm. Still, all these scintillators are not suitable to the above mentioned needs of the LENS project.

One new approach to develop an In loaded scintillator is to dissolve a metal-β-diketone (e.g. $In(acac)_3$) in the scintillator solvent. This method is based on the suggestion of F.X. Hartmann which first was presented in [FEI01]. In this chapter the investigation of the synthesis and purification of pure $In(acac)_3$ is described along with solubility studies of In-β-diketones in several solvents. These topics are also summarized in [BUC03]. An alternate approach to develop an In loaded scintillator based on carboxylate systems are also pursued extensively

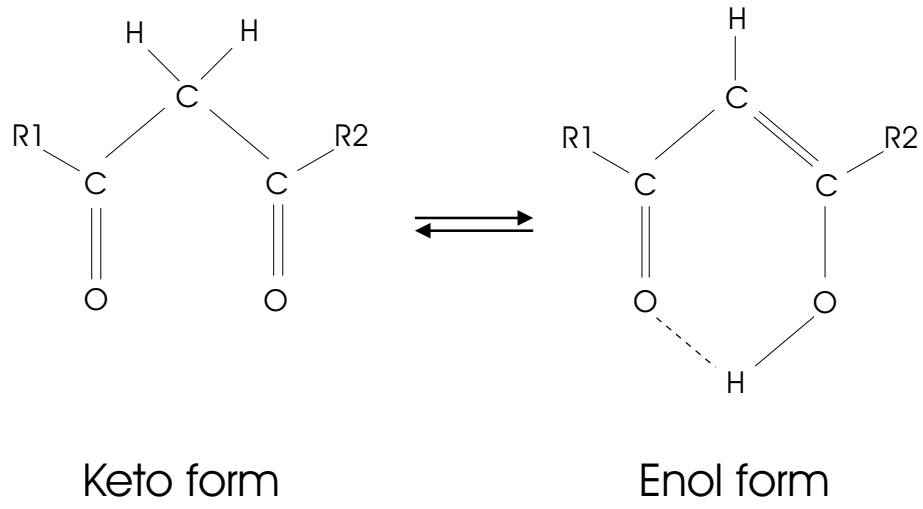

Figure 3.1: *The figure shows the two forms (tautomers) of β-diketones. These tautomers exist in equilibrium with each other.*

by several groups inside the LENS collaboration. In the second part of this chapter this carboxylate system is briefly discussed.

3.1 The β-diketone system

3.1.1 β-diketones

The β-diketone molecule has a section R1–(C=O)–CH_2–(C=O)–R2 consisting of two ketones (C=O) that 'sandwich' a methylene carbon atom; R1 and R2 are carbon-based side chains. In Table 3.1 a number of selected β-diketones is listed having various substituents. β-Diketones are capable of keto–enol tauterism (see Fig. 3.1). A hydrogen atom of the CH_2 group is activated by the C=O groups, and a conjugate system can arise by a prototropic shift. The enol content of Hacac is 81% [MEH78]. Most other β-diketones in Table 3.1 have enol contents of 90 % to 100 %. A large number of β-diketones form metal complexes. The enolic hydrogen atom of the β-diketone can be replaced by a metal cation to produce a six-membered chelate ring.

Stability and volatility of the metal β-diketones is particularly noteworthy. Stability is important for the construction of large scale detector systems, while volatility is important for the purification steps. Generally the volatility increases with a decrease in the radius of the central metal atom. In most complexes volatility and thermal stability are increased when fluorine substituents are present in the ligand shell [MEH78]. For example, the *fod* chelates of rare-earths are known to have very high volatilities.

The key stabilizing feature affording the utility of β-diketonate metal complexes is the strong chemical bond of the β-diketone anions to the centrally chelated metal ion due to resonance stabilization of the delocalized negative electric charge of the β-diketone anion. It is this feature that traps the metal, not only in an organic soluble structure, but in a compound sufficiently stable that it can be heated without decomposition to permit purification steps using sublimation.

R1	R2	Name	Abbr. anion	Boil. pt. [°C/mm Hg]
CH_3	CH_3	Acetylacetone (Pentane-2,4-dione)	acac	140
CH_3	C_6H_5	Benzoylacetone (1-Phenylbutane-1,3-dione)	bzac	261
C_6H_5	C_6H_5	Dibenzoylmethane (1,3-Diphenylpropane-1,3-dione)	dbzm	220/18
$(CH_3)_3C$	$(CH_3)_3C$	Dipivaloylmethane (2,2,6,6-Tetramethylheptane-3,5-dione)	dpm	215
CF_3	CH_3	Trifluoroacetylacetone (1,1,1-Trifluoropentane-2,4-dione)	tfac	107
CF_3	CF_3	Hexafluoroacetylacetone (1,1,1,5,5,5-Hexafluoropentane-2,4-dione)	hfac	70
$CF_3CF_2CF_2$	$(CH)_3C$	Heptafluorodimethyloctanedione (1,1,1,2,2,3,3-Heptafluoro-7,7-dimethyloctane-4,6-dione)	fod	33/207

Table 3.1: *List of some selected β-diketones (general form R1COCH$_2$COR2) [MEH78]. The abbreviations of the anions and the boiling points are given.*

3.1.2 In(acac)$_3$ synthesis

A number of complexes of indium were synthesized using β-diketones: acetylacetone (Hacac), dibenzoylmethane (Hdbzm) and dipivaloylmethane (Hdpm also sometimes called Hthd). Of the various β-diketonate forms of indium In(acac)$_3$ was selected because of its simplicity and low molecular weight. Namely, for a given weight loading of indium into the scintillator mixture, the lower the molecular weight of the compound, the higher the weight of the other useful light-emitting components of the scintillator.

The molecule is formed through the reaction of In^{+3} with Hacac through a sequence of steps focused on achieving optical clarity. All newly purchased materials obtained were of a yellow tone. As will be described below it was found that the yellow color is due to impurities in the In(acac)$_3$ material. Consequently, part of the chemical research dealt with the resolution of some subtle impurity issues. The procedure summarized below succeeds in eliminating all of the yellowing impurities.

The chemicals used below are all reagent grade – for the case of the indium non-reagent grade sources were used. Indium is purchased as $InCl_3$ which is dissolved in $\sim$ 100 ml water (0.2 mol, scalable). The pH-value of this solution is between 1.8 and 2. The first hydrolysis constant of indium is measured to be in the range of $pK_{h1} \sim 1.5$, thus only at high acidity (pH < 1) the indium is largely In^{3+} (as opposed to partially hydrolyzed species). After the addition of 0.75 mol of Hacac (Merck, 99.5 %) to the mixture, the pH drops further to ~ 0.6. The solubility of Hacac in water is 16.6 wt.% and the solubility of water in Hacac 4.5 wt.% [RID86]. At the concentrations used only part of the Hacac dissolves in the water and a two-phase system of an aqueous and an organic phase is created.

The indium material is transferred from the aqueous into the organic phase using solvent extraction. 1,2-Dichlorobenzene is added to the water solution and the pH is adjusted upwards

using a NaOH solution (10 %) until pH ~ 7 is reached. The base concentration and volumes are selected to avoid hydrolysis as much as possible. Nonetheless, some hydrolysis does occur and these products are subsequently removed later in the procedure. The solubility of the $In(acac)_3$ molecule produced is high in the dichlorobenzene and low in the aqueous phase. Therefore the $In(acac)_3$ concentration in the water can be neglected.

The simplified reactions that take place in the synthesis are given below, along with the symbols for their equilibrium constants:

$$3\,\mathrm{Hacac_{org}} \longleftrightarrow 3\,\mathrm{Hacac_{aq}} \qquad \mathrm{K_s^3} \qquad (3.1)$$

$$3\,\mathrm{Hacac_{aq}} \longleftrightarrow 3\,\mathrm{acac^-_{aq}} + 3\,\mathrm{H^+_{aq}} \qquad \mathrm{K_a^3} \qquad (3.2)$$

$$\mathrm{In^{3+}_{aq}} + 3\,\mathrm{acac^-_{aq}} \longleftrightarrow \mathrm{In(acac)_{3,org}} \qquad \mathrm{K_r} \qquad (3.3)$$

$$\mathrm{In^{3+}_{aq}} + 3\,\mathrm{Hacac_{org}} \longleftrightarrow \mathrm{In(acac)_{3,org}} + 3\,\mathrm{H^+_{aq}} \qquad \mathrm{K_{net}} \qquad (3.4)$$

These equations describe the two phase system, aqueous (aq) and organic (org) along with the four equilibrium constants as defined: solubility (K_s), acid (K_a), reaction or 'stability' (K_r) and the net reaction (K_{net}). With pure Hacac the extraction equilibrium is reached in some seconds. When solutions of Hacac in organic solvents are used, the extraction rate is smaller. The overall equilibrium constant K_{net} of the above reaction is defined by:

$$\mathrm{K_{net}} = \mathrm{K_s^3} \cdot \mathrm{K_a^3} \cdot \mathrm{K_r} = \frac{[\mathrm{In(acac)_3}][\mathrm{H^+}]^3}{[\mathrm{In^{3+}}][\mathrm{Hacac}]^3} \qquad (3.5)$$

From this equation it can be seen that for a constant Hacac concentration the distribution ratio of the indium between the two phases is a function of pH alone. The pK values are ([STA64] and references therein):

$$pK_s = 0.77 \qquad (3.6)$$

$$pK_a = 8.95 \qquad (3.7)$$

$$pK_r = -21.06 \qquad (3.8)$$

$$pK_{net} = 8.1 \qquad (3.9)$$

where pK_r is deduced by balance.

The specific numerical values above are for the case of a benzene solvent (characteristic of the scintillator solvents of interest). For the case of extraction into the dichlorobenzene, which is used in the synthesis, there arise some differences in the above values. Thus the ratio of the concentration of indium in the organic dichlorobenzene phase to that in the aqueous phase was measured as a function of pH in order to obtain the needed data for the pK value. The concentrations of indium in the two phases were measured using atomic absorption spectroscopy (AAS). For these purposes, the indium in the organic phase is determined by adding a quantitatively derived aliquot of the organic fraction to an aqueous 3 M HCl-solution in a ratio of 1:1000.

In Fig. 3.2 the experimental data are shown illustrating the transfer of indium into the dichlorobenzene as a function of pH. In this case the organic phase consisted of 60 ml dichlorobenzene and 35 ml Hacac. This corresponds to an Hacac concentration of 3.7 M. The volume of the organic phase V_{org} and the volume of the aqueous phase V_{aq} were approximately the same. The volume of the aqueous phase was 100 ml in the beginning and

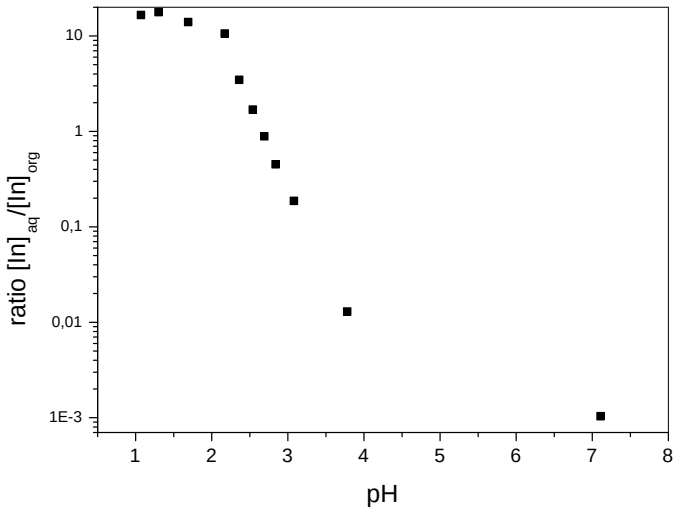

Figure 3.2: *Solvent extraction and synthesis of In(acac)$_3$. The ratio of the In-concentration in the aqueous phase to the In-concentration in the organic phase is shown as a function of the pH of the aqueous phase as measured using AAS. The experimental errors are comparable to the symbol sizes.*

increased with the addition of the NaOH solution. From the measured values, the $pH_{1/2}$ was determined to be equal to 2.6. At $pH_{1/2}$ the indium is equally partitioned between the organic and the aqueous layer. The ratio between the total amount of indium in the organic phase y to the indium amount in the aqueous phase x obeys the equation

$$\frac{y}{x} = \frac{V_{org}}{V_{aq}} \cdot \frac{[In(acac)_3]_{org}}{[In]_{aq}} = \frac{V_{org}}{V_{aq}} \cdot K_{net} \cdot \frac{[Hacac]^3}{[H^+]^3} \tag{3.10}$$

At $pH_{1/2}$ the ratio y/x equals unity and the constant K_{net} can be calculated by

$$K_{net} = \frac{V_{aq}}{V_{org}} \cdot \frac{[H^+]^3}{[Hacac]^3} \tag{3.11}$$

For pK_{net} one gets from that equation

$$pK_{net} = -\log_{10}(\frac{V_{aq}}{V_{org}}) + 3pH_{1/2} + 3\log_{10}([Hacac]) \tag{3.12}$$

Using this equation and under the approximation that $V_{org} \approx V_{aq}$ one can calculate pK_{net} for our system to be 9.5. This value implies a $pH_{1/2}$ of 3.2 in a system having equal volumes of an organic (1.0 M Hacac in dichlorobenzene) and aqueous layer ($pK_{net} = -3pH_{1/2}$ in this case). If the V_{org} dominates over V_{aq} or the Hacac concentration is high the extraction curve of the system is shifted to the acid side. These effects can be used to avoid the formation of complexes of the type $In(acac)_n(OH)_m$ at high pH-values where hydrolysis takes place. In systems with trivalent metal ions a ratio V_{aq}:V_{org} of e.g. 1:10 results in a shift of the $pH_{1/2}$

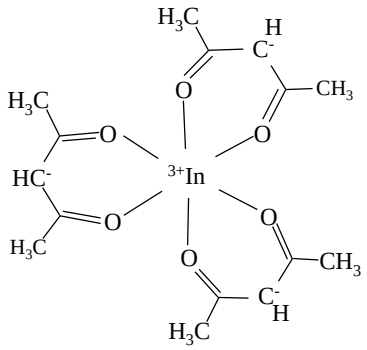

Figure 3.3: *Structure of the In(acac)$_3$ molecule.*

by 0.33 to the acidic side. A change in the Hacac concentration by a factor 10 corresponds to a pH shift of one in the extraction curve.

After approximately one day during which some hydrolysis byproducts collect in a thin layer between the aqueous and the organic phase, the dichlorobenzene layer containing the indium is separated from the aqueous layer. This layer, containing the In(acac)$_3$ is then transferred to a rotary evaporator[1] where the solvent is removed at 25 mbar and a temperature of 90° C. The resulting white crystals, which remain behind after removal of the solvent are mixed with 200 ml of 2-propanol and put into an ultrasonic bath for 15 minutes. The solubility of In(acac)$_3$ in 2-propanol is much lower than in dichlorobenzene. Then, the solution is filtered through the use of a vacuum filtration apparatus fitted with a 0.45 μm regenerated cellulose (RC) filter paper. Finally, the material is dried for one day in an oven at 80 °C. The overall yield is $\sim$ 90 % up to this step of the procedure.

The crystal structure of the white powder thus produced was investigated by X-ray powder diffraction measurements performed at the University of Heidelberg. This X-ray spectrum was compared to theoretical predictions and with a commercially available sample. The measurements confirm the production of In(acac)$_3$ in accordance with the procedure presented here. In metal complexes of stoichiometry M(acac)$_3$, the MO$_6$ array is octahedral. In Fig. 3.3 is shown a 2-dimensional picture of the In(acac)$_3$ molecule.

3.1.3 In(acac)$_3$ purification

Impurities in the components involved in its preparation

The three main reagents are pre-purified in order to remove organic contaminations (in the Hacac and in the dichlorobenzene) and if necessary iron (in the indium starting material). Both types of contaminations lead to optical absorbance problems.

[1] A rotary evaporator is a distillation unit incorporating a evaporation flask that rotates in a heated oil bath.

The Hacac, as purchased, is too impure to yield optically useful materials. A procedure was developed that yields sufficiently pure Hacac through use of a rotary evaporator operating at 60°C and a vapor pressure of 60 mbar to distill the Hacac liquid. In the case that the Hacac contains acetic acid, it can be pre-purified using the solvent extraction method of reference [STE53] with benzene substituted by chloroform as the extracting solvent. For acetic acid removal, one extracts a mixture of Hacac and solvent (in a ration of 1 to 4 by volume) into equal volumes of water three times to clean off any dissolved acetic acid. It was found that the presence of acetic acid in the Hacac does not deteriorate the optical transparency of the final material. For this reason this purification step was skipped.

The dichlorobenzene has a very high solubility (see section 3.1.4) for In-β-diketonates. This makes it a prime choice for use as a collecting solvent in the $In(acac)_3$ synthesis and solvent extraction. Pre-distillation, prior to its first use (as it is recycled throughout the procedure) is paramount. The pre-distillation is carried out using a rotary evaporator at 90°C and 25 mbar.

Besides the absorbances associated with the organic impurities, a large component of optical absorption introduced is due to the presence of iron contaminations that lead to the formation of $Fe(acac)_3$.

Fe purification

Acetylacetonates of e.g. iron, vanadium, cobalt and chromium absorb in the visible region. Iron is the most critical contamination of these elements. Therefore, to address this issue an iron pre-purification step was designed using a pH controlled organic-water extraction. The method is based upon differing values of $pH_{1/2}$ for iron and indium (lower for iron) in water-organic systems containing Hacac. Pure Hacac (9.7 M) is shaken with an indium aqueous solution (V_{aq}:V_{org} = 10:1) at pH ∼ 1.5 [$pH_{1/2}(Fe) = 0.75$]. The organic phase containing the $Fe(acac)_3$ is separated and the procedure is repeated three times. Experimental measurements show that the iron in the aqueous phase is reduced by a factor of up to 1000 using this procedure.

Typical starting materials of indium can have impurities in the range of a few to tens of ppm of iron. For the case of non-reagent In strips (e.g. as used in gaskets) the iron content was measured at 5 ppm to 10 ppm – and in these cases full synthesis of pure $In(acac)_3$ requires the Fe removal step. The indium that was used has an iron concentration of less than 0.5 ppm (Indium Corporation of America, Utica, NY, USA 99.999 wt.% $InCl_3$ in 2 kg lots). For a case such as this, the iron purification step can be eliminated. The measured levels of iron impurities in the other reagent materials are typically negligible, and do not contribute contaminations in the overall procedure.

The iron reacts to form $Fe(acac)_3$ which has its absorption peak around 440 nm. The extinction coefficient ϵ of this molecule at the absorption peak was determined. To do so a solution of approximately 2 % acetylacetone in water was doped with iron. At a pH around 4.5 all the iron is essentially in the form of $Fe(acac)_3$. The absorption spectra at varying Fe-concentrations were measured in a quartz cell with a path length of 1 cm and the spectrum of a Fe-free H_2O/Hacac solution was subtracted to obtain the $Fe(acac)_3$ absorbance (absorbance is defined as the logarithm of the ratio between the incident light and the transmitted light; further details in section 4.1.1). In Fig. 3.4 the absorbance at the absorption peak is plotted versus the iron concentration. There is a linear relationship between the absorbance A and the concentration c of the absorbing material (Beer-Lambert Law). If the data points in Fig. 3.4

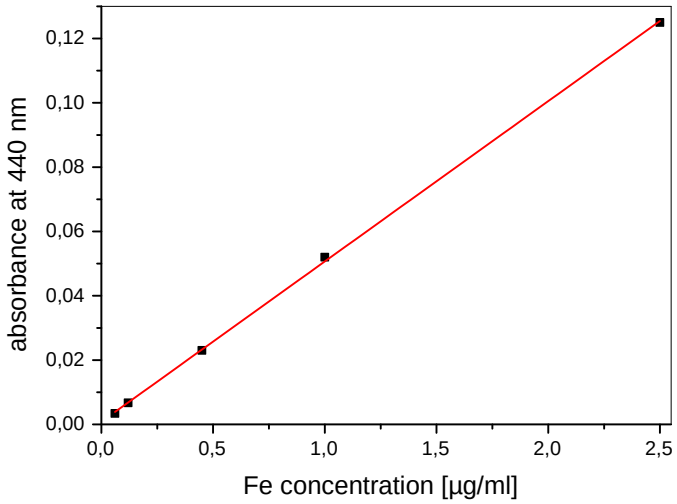

Figure 3.4: *Absorption (1 cm cell) of $Fe(acac)_3$ at 440 nm in dependence of the concentration.*

are fitted to a straight line the molar extinction coefficient ϵ (absorbance per unit path length and per unit molar concentration) can be determined from the slope. The equation relating these physical values will be given in section 4.1.1. The molar extinction coefficient is found to be (2800 ± 22) l/(mol·cm). Using this value one can then calculate that iron concentrations in the scintillator mixture [iron in the form of $Fe(acac)_3$] of more than 20 ppb will begin to restrict the attenuation length: at 20 ppb the calculated attenuation length is $\sim$ 4 m at 440 nm.

A test of the iron pre-purification procedure was made by intentionally adding iron to a very pure indium sample. The iron purification test showed that iron can be removed effectively without significant loss of the indium material. An initial iron impurity level of 9.5 ppm (measured by AAS) was reduced by at least one order of magnitude to below the sensitivity level of AAS, while the indium loss was only 3.5 %. The indium measurements are also carried out using AAS. Since the indium materials have iron levels that are typically much less than 10 ppm, the maximum indium to be lost by this method is not significant even in a worst case scenario.

Sublimation

As with most metal-β-diketonates, the vapor pressure of the $In(acac)_3$ material is relatively high when compared to metal inorganic compounds (approximately a few mbar, 150 °C to 200 °C). This offers the possibility to purify the material by sublimation.

In the sublimation process, under an applied vacuum, the material bypasses melting and goes directly into the gas phase. The sublimer unit (designed by F.X. Hartmann) is constructed to handle rates of approximately 50 grams per day. It consists of a 50 cm long tube and is 5 cm in diameter. The sample, in 10 gram amounts, is introduced into the central region of the glass tube using an Al foil 'boat'. The boat sits on an Al foil 'carpet' strip.

The central region is heated to a controlled temperature (typically 197°C) using a cylindrical heating mantle. A vacuum is drawn at the exit of the cylindrical tube while a trace flow of N_2 carrier gas (2.5 ml/s) enters from the upstream side. The carrier gas serves to sweep the vapor from the boat so that it condenses subsequently onto the Al carpet immediately downstream of the Al boat. It is important to have a tight system to obtain optical transparent material. The pressure is usually below 1 mbar. Air leakages in the system will lead to some yellow color in the sublimed $In(acac)_3$.

The proper conditions are achieved (as determined and adjusted experimentally) by sliding loosely fitted cylindrical glass inserts having closed faces into the tube, prior to the downstream vacuum connection, such that the exit side of the cylinder is loosely plugged. In this manner, the exiting N_2 gas stream does not carry uncondensed $In(acac)_3$ directly out of the tube, such that a major part of the residual material collects on the leading edge of the first glass cylindrical insert. Within the sublimer, clear crystals form inward from the surface of the glass sublimer tube, above the Al carpet. These crystals are subsequently removed from the apparatus by prodding with a stainless steel rod and poured then out. Besides the crystals also some white powder forms during sublimation. It was found that the optical clarity of that powder is much worse than the one for the big crystals. Therefore the sublimed material is sieved and only crystals with a grain size of more than 1 mm are used. The overall yield after sieving is approximately 70 %.

The sublimation step has the ability to separate the $In(acac)_3$ from partially hydrolyzed species, to aid in the removal of any $Fe(acac)_3$ and to remove other yellowing organic trace materials. These three items are discussed next.

First, in each run mixtures of indium materials of the form $In(acac)_{3-x-y}(OH)_xCl_y$ are produced. It is necessary to remove this material since it can add a weak yellow color. These impurities are present in the final material and are found to be removed during the sublimation process. The typical residue is < 3 % of the weight of the starting material in the sublimer, and is of a light yellow to beige color. The weight of this residual material was determined directly, and the In-content measured by AAS. The stoichiometric indium composition could be identified to be close to that of '$In(OH)_3$'.

Second, the sublimation step itself was tested to have the ability to separate $Fe(acac)_3$ from $In(acac)_3$ to some extent, in the absence of the iron pre-purification step using solvent extraction. The visible absorption spectrum, recorded as a function of wavelength in the 400 nm to 600 nm region of a sample of $In(acac)_3$ which intentionally contains $Fe(acac)_3$ is shown in Fig. 3.5. A factor of 5 reduction in the absorbance is achieved by the subliming procedure in a single pass. The sublimation, as far as iron is concerned, can be exploited, as needed, in accordance with the quality of starting material and the extent to which the iron (solvent extraction) pre-purification procedure is incorporated.

Third, the sublimation step achieves a final purification for it is a re-crystallization process – from the gas phase. As such, it not only leaves behind the non-volatile mixed hydrolysis products, but is also a good ultimate step to exclude any other final remaining impurities. In particular, the $In(acac)_3$ collects as clear crystals in the chamber, and the formation of the crystals tends to exclude foreign matter. In regards to the volatile impurities, traces of organic material left over following the 2-propanol wash of the $In(acac)_3$ that is re-crystallized from dichlorobenzene (the step just prior to sublimation) are observed to be eliminated. It was found that these collect in a separate, downstream, section of the sublimer tube.

The overall effect of the sublimation step is shown in Fig. 3.6. Here the absorbance of $In(acac)_3$ material with and without purification by sublimation (from a particular test batch

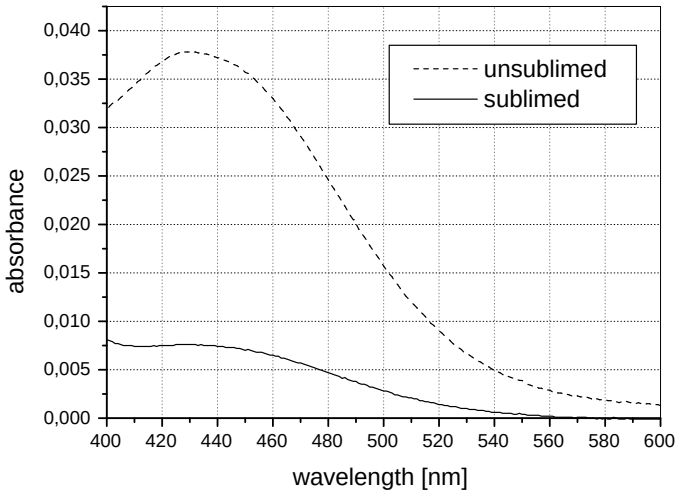

Figure 3.5: *Absorption spectrum (1 cm cuvette) of sublimed and unsublimed In(acac)$_3$ (5 w.% In) made in an intentional Fe-doped synthesis for test purposes. Sublimation contributes to a reduction of absorbance due to the presence of Fe, the main problematic inorganic contaminant.*

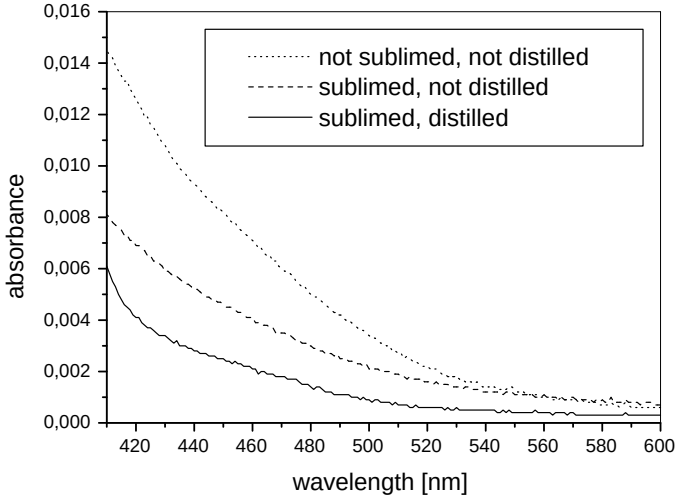

Figure 3.6: *Absorption spectrum (1 cm cuvette) of several In(acac)$_3$ (5 wt.% In) samples in anisole showing the sequential effect of two important purification steps: sublimation of the final material and Hacac distillation.*

prepared for purposes of the test variations) as dependent on the wavelength recorded from 410 nm to 600 nm is shown. In addition to sublimation the pre-distillation of the Hacac is essential. In the same figure the effect of not carrying out the distillation is also shown. Without the sublimation of the $In(acac)_3$ and the distillation of the Hacac the purity of the In-material would not meet the scintillator requirements.

Column purification

Furthermore, as an alternative approach to the sublimation, a column purification of $In(acac)_3$ dissolved in anisole was tested. For this test a weak acidic alumina oxide column was used. A 5 ml solution containing 5 wt.% In was poured through 1 g of the Al_2O_3. In the beginning the $In(acac)_3$ material used was impure compared to other samples (attenuation length at 430 nm below 1 m). After the column the absorption was remeasured and no significant difference was found in the spectra. This indicates not only that no $In(acac)_3$ was lost, but also that the column has not the ability to remove impurities.

3.1.4 Solubility

Theoretical introduction

One of the main requirements for a scintillator in an indium solar neutrino detector is high In-loading. Therefore a solvent had to be found that has a high solubility for an In-β-diketone molecule. In an ideal liquid mixture the components are soluble in all proportions. An ideal mixture is a mixture in which the interactions between unlike molecules are identical to those between like molecules in the same state. High solubility is expected where the molecular properties of solute and solvent with respect to polarizability, dipole moments and molar volumes are similar.

The dissolution of a solid in a solvent is equivalent to the melting of the solid followed by mixing of the resulting liquid solute with the solvent. The enthalpy of solution ΔH_s is given by

$$\Delta H_s = \Delta H_f^T + \Delta H_{mix} \tag{3.13}$$

where ΔH_f^T is the enthalpy of fusion at the absolute temperature T of the solution and ΔH_{mix} is the enthalpy of liquid-liquid mixing. For an ideal solution ΔH_{mix} is zero. Assuming that ΔH_f^T is independent of the temperature, $\Delta H_f^T = \Delta H_f$, classical thermodynamics shows [GRA90] that the ideal mole fraction solubility x^{id} follows the equation:

$$\ln x^{id} = -\frac{\Delta H_f}{R}\left(\frac{1}{T} - \frac{1}{T_m}\right) \tag{3.14}$$

where T_m is the melting point of the solid solute. Using the expression $\Delta S_f = \Delta H_f / T_m$ for the entropy of fusion of the solid at T_m the above equation can be written as

$$\ln x^{id} = -\frac{\Delta S_f}{R}\left(\frac{T_m}{T} - 1\right) \tag{3.15}$$

The ideal mole fraction x^{id} increases with increasing temperature until, when $T = T_m$, the solid forms a liquid in absence of solvent, so $x^{id} = 1$.

In the regular solution theory[2] by Hildebrand and Scott [HIL50] the solution process can be divided into three steps. In the first step, one molecule of the solute surrounded by other solute molecules is transferred into the vapor phase. In the second step, a hole is created in the solvent just large enough to accept the solute molecule. Finally the hole is filled by the free solute molecule.

Hildebrand introduced the solubility parameter δ which is the square root of the cohesive energy density. The cohesive energy density is the molar energy of vaporization divided by the molar volume. This parameter can be used to predict the solubility of a solute A in a solvent B. In Hildebrands model the relation between the mole fraction x of the solute in the saturated solution and the solubility parameters δ_A and δ_B is the following

$$\ln x \propto -(\delta_A - \delta_B)^2 \tag{3.16}$$

Thus the theory predicts that the smaller the difference between δ_A and δ_B the higher is the solubility. This model is limited in its predictions when the solute and solvent molecules are polar, when specific molecular orientation effects occur in solution or when the solute and solvent molecules have rather different sizes. From the results of the solubility measurements of $In(acac)_3$ in several solvents presented later in this section the parameter δ for $In(acac)_3$ can be estimated.

Concentration measurement using atomic absorption spectroscopy

The solubility of indium in the organic solvents was determined by atomic absorption spectroscopy. It uses the absorption of light to measure the concentrations of gas-phase atoms. There is a linear relationship between absorbance and concentration of an absorber of electromagnetic radiation.

The sensitivity of the method is strongly dependent on the element of interest. As a light source a hollow-cathode lamp is used, which emits the characteristic spectrum of the investigated element. The liquid analyte sample is vaporized and atomized in an air/acetylene flame at about 2500 K. For some elements that form molecules hard to break down, a nitrous oxide (N_20)/acetylene flame is used to achieve higher temperatures. The sample solutions are aspirated with a nebulizer and a fine aerosol is created for introduction into the flame. The respective resonance line is isolated from the photons passing the flame by a monochromator and the remaining intensity of the light beam is detected in a photo multiplier. The absorption is finally readout by the data acquisition system. Deionized water was aspirated between the samples. To calibrate the spectrometer four standards with a known In-concentration are prepared. A typical calibration curve is plotted in Fig. 3.7.

For the solubility measurement the In-β-diketone is first dissolved as a powder in the organic liquid. The solvents are allowed to equilibrate with an excess amount of the solute. The solution is shaken from time to time, and sits at least overnight before the sample is taken. At the investigated In-concentrations which are in the percent level the saturated liquid can be diluted in a 3 molar aqueous HCl-solution by a factor of 1000. The acidity is sufficient to break up the complex and to dissolve the indium ions in the aqueous phase. The samples and standards are prepared with duplicate acid concentrations. For most solutions at

[2]In Hildebrands terminology a regular solution is one involving no entropy change when a small amount of one of its components is transferred to it from an ideal solution of the same composition, the total volume remaining unchanged.

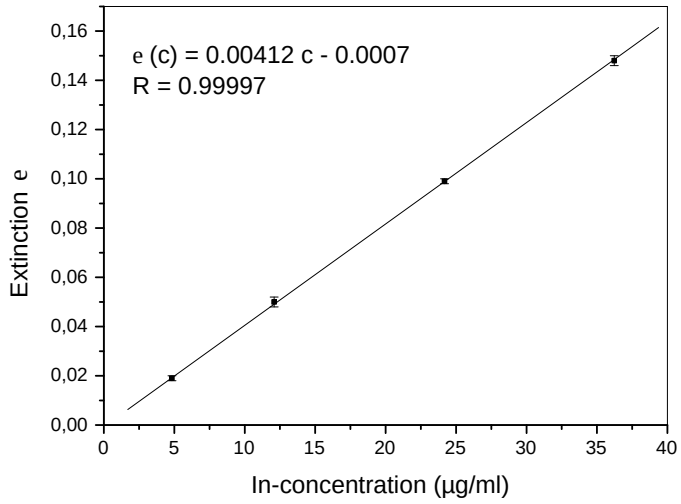

Figure 3.7: *Calibration curve in a typical atomic absorption measurement. Four standards were used at varying In-concentrations.*

least two samples were taken and measured in different concentrations. An aqueous solution, with the correct amount of acid, and no analyte, is regularly used as a blank measurement.

Solvent selection

Ionizing particles which can be detected in a liquid scintillator excite mainly the solvent molecules. Therefore aromatic molecules are often the basis of a liquid scintillator, the presence of the proper number of π-electrons ensure that there is an efficient energy transfer between the primary electrons and the solvent molecules. Of the possible solvent candidates the aromatics PC, PXE and anisole were tested in more detail. Some of their chemical and physical properties are summarized in Table 3.2. They are all clear, colorless liquids.

Pseudocumene (1,3,4-trimethylbenzene, C_9H_{12}, PC) is often used as scintillator base in neutrino experiments. For example, the Borexino experiment currently plans to use pure PC as solvent along with the fluor PPO or the KamLAND experiment in Japan uses a PC/dodecane mixture at a ratio 20:80 to detect neutrinos from nuclear reactors. PC has been found to achieve high purity levels in the range needed for low energy solar neutrino detection. As most organic solvents, PC is classified as harmful to health and hazardous for the environment. This is disadvantageous since safety is one of the most important criteria for the solvent selection in large experiments. The solubility in water is small (0.057 g/l), but it dissolves in ethanol.

Besides PC/PPO the Borexino experiment also investigated PXE (Phenyl-o-xylylethane, $C_{16}H_{18}$) in combination with the fluors p-Tp and bis-MSB as a possible scintillator for the experiment [PXE04]. The Borexino prototype CTF could demonstrate that the level of radiopurities in this scintillator is also low enough to meet the goals of the experiment. PXE is an industrial product with different applications. It is produced by reacting styrene and xylene using an acidic catalyzer. In comparison to PC, it is less dangerous. It has a higher

flash point and is contrary to PC a legally non-hazardous liquid, items of relevance for safety aspects in a big experiment. The density of PXE is higher than that of PC and is very close to that of water. Approximately 0.01 g PXE dissolves in one liter of water.

aromat	formula	wt. [g/mol]	flash pt.	dens. [kg/l]	boiling pt.	vapor press. [hPa]
PC	C_9H_{12}	120	43°C	0.88	169°C	2.8 (at 25°C)
PXE	$C_{16}H_{18}$	210	145°C	0.985	295°C	< 0.00014 (20°C)
anisole	C_7H_8O	108	43°C	0.99	156°C	3.5 (20°C)

Table 3.2: *Properties of some aromatic solvents which could be used as scintillator base. The density is given at 20 °C.*

Anisole (methoxybenzene, C_7H_8O) is more polar than the aromatics mentioned above and therefore a higher solubility of the In-β-diketone is expected. Like PXE anisole has a density which is slightly below unity. Anisole is chemically more aggressive than PXE or PC. One liter water dissolves approximately 1.6 g anisole. Anisole also readily dissolves in ethanol. In addition the solubility was tested for several other solvents, scintillating and non-scintillating, which were of interest for various reasons.

Results

The results of the solubility measurements are listed in Table 3.3. The maximal loading of $In(acac)_3$ in PC and PXE is in the range of 1.2 wt.% indium at room temperature. At higher temperature the $In(acac)_3$ solubility in the solvent increases. However, the temperature dependence of the solubility of the solute was not found to be strong for the PC system. For example, the solubility stays below 1.5 wt.% indium at 50 °C. A solvent which has similar properties to PXE concerning flash point and density is Ruetasolv DI. This odourless liquid is a mixture of diisopropylnaphtalene isomers and has a favourable environmental and toxicological profile. The solubility in that solvent is a factor of three lower compared to PXE or PC. To improve the chemical compatibility with acrylic PC is often mixed with mineral oil or dodecane. Therefore the solubility in dodecane was also tested. It was found to be below 0.1 wt.%.

One possibility to improve the solubility in a scintillating solvent, is to mix it with other non-scintillating solvents which dissolve the molecule better. For this reason and to investigate the solubility behavior in various solvents several non-aromatic organic liquids were tested. Most of the measured solubility values (for ethanol, 2-propanol, cyclohexane, diethylether and carbon tetra chloride) were below the value for PC. High solubility of more than 3 wt.% was found in chloroform (trichloromethane), toluene (methyl benzene), methoxybenzene (anisole), dimethoxybenzene and dichlorobenzene which is used in the synthesis.

Another feature of this scintillator approach is that one can consider modifications of the various different side chains of the β-diketone and thus fine tune the chemical properties of the In-molecule. In this regard, a comparison of the solubility of $In(acac)_3$ was made along with $In(dpm)_3$ and $In(dbzm)_3$ in PC. The dpm version, expected to be more soluble because of its larger organic side groups and its lower melting point, was nearly 3 times more soluble than the acac version. This solubility increase also correlates with the higher vapor pressure of the dpm complexes versus the acac complexes.

solvent	$\beta-$dik.	In sol. [w.%]	mol. fract. x [%]	δ	μ [D]
diethylether	Hacac	1.00 ± 0.05	0.67 ± 0.03	15.1	1.15
dodecane	Hacac	0.03 ± 0.01	0.05 ± 0.02	16.0	0
cyclohexane	Hacac	0.13 ± 0.02	0.10 ± 0.02	16.8	0
CCl_4	Hacac	0.58 ± 0.05	0.79 ± 0.07	17.5	0
PC	Hacac	1.20 ± 0.05	1.29 ± 0.05	18[1]	
PC	Hdpm	3.1 ± 0.1	3.8 ± 0.1		
PC	Hdbzm	0.15 ± 0.03	0.16 ± 0.03		
toluene	Hacac	5.4 ± 0.2	5.1 ± 0.2	18.2	0.3
chloroform	Hacac	3.8 ± 0.1	4.4 ± 0.1	19.4	1.1
anisole (methoxybenzene)	Hacac	7.9 ± 0.1	9.4 ± 0.1	19.5	1.2
1,2-dimethoxybenzene	Hacac	4.9 ± 0.1	6.7 ± 0.1		1.29
1,3-dimethoxybenzene	Hacac	5.5 ± 0.2	7.6 ± 0.2		
dichlorobenzene	Hacac	5.8 ± 0.1	8.6 ± 0.1	20.6	2.1
propanol	Hacac	0.22 ± 0.02	0.12 ± 0.01	23.5	1.7
ethanol	Hacac	0.52 ± 0.02	0.22 ± 0.01	26.1	1.7
PXE	Hacac	1.25 ± 0.05	2.4 ± 0.1		
Ruetasolv DI	Hacac	0.39 ± 0.05	0.73 ± 0.09		

[1] value for 1,3,5-trimethylbenzene

Table 3.3: *In solubility at room temperature using various β-diketones in several solvents. All the values were determined using atomic absorption spectroscopy. Additionally the values of the solubility parameter δ and the permanent dipole moment μ (1 Debye = $3.336 \cdot 10^{-30} Cm$) are given for some solvents [RID86].*

Of all the solvents investigated highest solubility was found in anisole. Ultimately, the use of this solvent avoids the need to go to larger side groups (e.g. the dpm complex). At room temperature, an In-loading of up to 7.9 % by weight in the form of $In(acac)_3$ was found. This is sufficient for the goals of the 5 % to 8 % loading.

In Table 3.3 the dipole moments and solubility parameters δ for some of the solvents are listed. One can see that high solubility is obtained in polar aromatic solvents having a permanent dipole moment. Hildebrands model of regular solutions seems to give reasonable predictions. The solubility of the $In(acac)_3$ increases with increasing δ until $\delta \approx 19.5$. Above that number it drops again indicating that the solubility parameter of the $In(acac)_3$ is approximately 20. The deviations from the model, e.g. for diethlyether and chloroform are probably due to the permanent dipole moment of these solvents, since it has a big influence on the solubility. The dipole moments of bonds have sometimes a stronger impact on the solubility than the dipole moment of the whole molecule. This fact can be seen in the similar results for 1,2-dimethoxybenzene and 1,3-dimethoxybenzene.

In summary, the highest $In(acac)_3$-solubility was found in anisole. This solvent allows a high In-loading in the liquid scintillator of more than 5 wt.% that is needed for a compact detector design. The maximum In-solubility in the other investigated scintillator solvent candidates PXE and PC was in the 1 wt.% range. At such In-concentrations the experiment would be presumably limited by the detector size and the resultant costs.

3.1.5 Chemical stability

One of the basic requirements on a In-liquid scintillator is chemical stability over several years. Instability of the In-complex can affect the solubility of the In-material in the solvent and the optical properties of the scintillator. Metal β-diketonates are known for their strong metal to ligand bonding. The $In(acac)_3$ materials, here, are heated to the 200°C range. Above that temperature decomposition starts.

In addition to temperature stability, reactivity of the molecule is also an important issue. The reactivity with water was studied since water molecules are omnipresent. Normally the indium ion is readily hydrolyzable due to the high 'charge-to-radius' ratio; In^{3+} begins to react with water to form hydroxy species even at pH 1. A test of the stability of $In(acac)_3$ was conducted by dissolving it in anisole ($In(acac)_3$ is insoluble in water) and constructing a two-phase system with the organic layer in physical contact with water. The pH of the aqueous phase is then raised using NaOH. The result was that no hydrolysis product was observed up to a pH of approximately 8.5. Above this pH value the scintillator clearly started to decompose. The results show that the $acac^-$ complex is stable against OH^- exposure.

3.1.6 The fluor

The molecules of anisole in the scintillator are the 'primary' molecules excited in the initial excitations resulting from the neutrino induced nuclear gamma-ray or electron emissions. Codoped fluors are adjusted to maximize the non-radiative energy transfer to achieve significant light output in the visible (blue) region. The $In(acac)_3$ itself can act as a 'sink' by absorbing UV light, consequently fluor selection and loading are crucial. The fluors investigated [PPO (2,5-diphenyloxazole, 221.24 g/mol), butyl-PBD (2-(4-biphenyl)-5-(4-tert-butylphenyl)-1,3,4-oxadiazole, 354.42 g/mol), PBD (2-(4-biphenyl)-5-phenyl-1,3,4-oxadiazole, 298.32 g/mol), p-Tp (1,4-diphenyl-benzol, 230.29 g/mol) and PMP (1-phenyl-3-mesityl-2-pyrazoline, 264.37 g/mol)] are reagent grade and used as received. The fluors BPO (2-(4-biphenyl)-5-phenyloxazole, 297.33 g/mol) and BBO (2-(4-biphenyl)-5-(4-biphenyl)-1,3,4-oxazole, 372.39 g/mol) were specially prepared by scientists from INR, Moscow. The secondary fluor, bis-MSB (1,4-bis(2-methylstyryl)benzene, 310.42 g/mol) is a reagent grade wavelength shifter used in conjunction with a primary fluor.

fluor	solubility [g/l]
BPO	$150 - 200$
butyl-PBD	> 200
PPO	> 500
PBD	$25 - 35$
BBO	< 20
PMP	> 200
pTP	$6 - 12$

Table 3.4: *Solubility of fluors in anisole. The solubility is given in grams per liter anisole.*

At the desired high In-loading unusually high fluor concentrations are needed to obtain reasonable light yields (see next chapter). Therefore the solubility of the fluor in the scintillator solvent is of importance. Table 3.4 gives some order of magnitude estimations for

the solubility of several fluors in anisole. The values were determined by increasing the fluor concentration in anisole until the solution was saturated.

3.2 Carboxylates

The development of a liquid scintillator based upon a single carboxylic acid was studied for ytterbium as well as for indium. A synthesis method was invented by F.X. Hartmann in which stability is achieved using pH control and the scintillator is kept in a stable region.

The reactions and equations in the synthesis of a metal (M) loaded carboxylic acid (HA) system are similar to the reactions in the metal-β-diketone synthesis:

$$3\,HA_{org} \longleftrightarrow 3\,HA_{aq} \qquad K_s^3 \tag{3.17}$$

$$3\,HA_{aq} \longleftrightarrow 3\,A^-_{aq} + 3\,H^+_{aq} \qquad K_a^3 \tag{3.18}$$

$$M^{3+}_{aq} + 3\,A^-_{aq} \longleftrightarrow M(A)_{3,org} \qquad K_r \tag{3.19}$$

$$M^{3+}_{aq} + 3\,HA_{org} \longleftrightarrow M(A)_{3,org} + 3\,H^+_{aq} \qquad K_{net} \tag{3.20}$$

with the overall equilibrium constant

$$K_{net} = K_s^3 \cdot K_a^3 \cdot K_r = \frac{[M(A)_3][H^+]^3}{[M^{3+}][HA]^3} \tag{3.21}$$

The equilibrium constants K_a and the solubility in water is listed in Table 3.5 for some carboxylic acids consisting of 4 to 9 carbon atoms. The pK_a value reflects the ability for the acid to release a H^+ in aqueous solution. The more carbon atoms in the HA the less willing the molecule is to lose the H^+ and the lower is the acid strength. Therefore systems with higher carbon numbers are expected to form stronger bonds to the central metal ion. This would stabilize them more against water substitution reactions. In fact scintillator systems using carboxylic acids with 6 to 9 carbons are found to be more stable compared to systems having a HA with 5 carbons or less. Also the solubility of H_2O that affects the stability of the system is lower in the acids with more carbon atoms. On the other hand the higher the number of carbon atoms the lower is the aromatic fraction in the scintillator at the same metal loading. The use of hexanoic acid or 2-methylvaleriate (both 6 carbon HAs) seems to be a good compromise.

carboxylic acid	formula	C number	pK_a	sol. in H_2O [wt.%]
butyric acid	$CH_3(CH_2)_2$-COOH	4	4.82	inf.
valeric acid	$CH_3(CH_2)_3$-COOH	5	4.86	2.4
hexanoic acid	$CH_3(CH_2)_4$-COOH	6	4.88	0.96
octanoic acid	$CH_3(CH_2)_6$-COOH	8	4.90	0.08
nonanoic acid	$CH_3(CH_2)_7$-COOH	9	4.95	0.02

Table 3.5: *The K_a and pK_a values reflecting the acidic strength of the molecules is given for varying carbon numbers. Additionally the solubility in water is listed. The numbers were taken from [RID86].*

To determine the pK_a experimentally, the organic and the aqueous fraction can be separated from each other after establishing equilibrium and the HA in the water fraction can be measured by titrating with a strong base. A titration curve is obtained from which the pK_a can be found.

3.2.1 The Ytterbium system

In an early stage of the LENS project ^{176}Yb was considered as target isotope. In this period F.X. Hartmann and T. Lasserre worked on a Yb-carboxylate scintillator. As starting material for the scintillator synthesis $YbCl_3$ dissolved in an acidic solution was used. If the Yb material is added directly to water, then hydrolysis occurs. This means that OH^- groups in the water stick to the Yb ion. The hydrolysis constants were determined from the analysis of the behavior of Yb as a function of pH. The following results were obtained:

$$pK_{h1} = 5.47 \qquad (K_{h1} = 3.39 \cdot 10^{-6}) \tag{3.22}$$

$$pK_{h2} = 6.86 \qquad (K_{h2} = 1.38 \cdot 10^{-7}) \tag{3.23}$$

The final white material formed is $Yb(OH)_{2.5}$. Extensive precipitation is observed at pH= 6.93.

The Yb-loaded scintillator can be produced in a pH–controlled water/organic synthesis method. $YbCl_3$ is dissolved in water and the solution is mixed with HA together with the scintillator solvent. Some of the HA reacts with the Yb, but an HA excess will remain in the organic phase.

A scintillator sample with 4.8 wt.% Yb-loading was synthesized using this method. The synthesis was made with the 9 carbon acid TMHA (3,5,5-trimethylhexanoic acid). The 'free' TMHA concentration in the organic solution was 0.6 M and the scintillator solvent pseudocumene was used.

Based upon the above equations one can calculate the Yb fraction in the organic phase at a given pH-value and HA concentration. In Fig. 3.8 the HA concentration is plotted versus the pH-value. In the black region all Yb is dissolved in the aqueous phase. At each line that is crossed the Yb amount in the organic phase increases by 10 % of the total amount. In the white region more than 90 % are dissolved in the organic fraction. During the synthesis the HA concentration can be assumed to be constant and the pH is increased. The dashed box shows the stable region in the parameter space at the end of the synthesis. The regions in the graph were calculated for TMHA as acid.

The light yield of the scintillator produced was measured with radioactive sources (^{54}Mn and ^{137}Cs) to be (35 ± 1) % compared to a BC505 standard at a PPO concentration of 5 g/l. The light yield of BC505 corresponds to approximately 12000 photons/MeV. With bis-MSB added, the light yield increased to (46 ± 1) % relative to BC505. The measured attenuation length was in the 3 m range. No degradation of the scintillator was found for the first two years [FXH03]. After 3 years the attenuation length was reduced by approximately one order of magnitude and the light yield dropped by a factor of three. The expected reason for the instability is the inappropriate storage of the material, e.g. the Yb solution was in contact with normal air during the whole period.

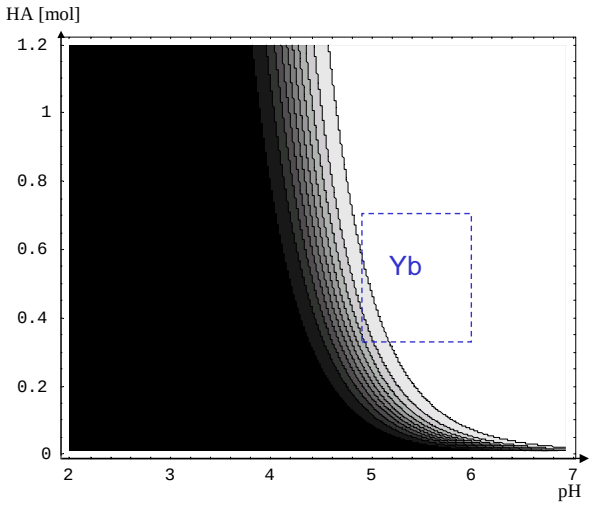

Figure 3.8: *This plot shows the stability region (dotted line box) for an Yb carboxylate system in contact with water (plot made by T. Lasserre). On the ordinate is the molarity of the acid (TMHA in this case) excess and on the abscissa the pH. In the white region all the Yb is in the organic phase, in the black region the Yb is still dissolved in the aqueous phase. The transition lines are calculated using equation 3.21.*

3.2.2 The Indium system

For the case of Indium the hydrolysis is much more severe than for Yb. The material is significantly hydrolyzed when added to distilled water, leading to an acidic solution (pH just above 1.0). To estimate the hydrolysis constants an aqueous solution containing indium is acidified to a pH of about 0.5. At that pH nearly all the indium material in the solution is In^{3+}. Then the solution is titrated with a strong base. From the resultant curve one can determine the constants:

$$pK_{h1} = 1.1 \tag{3.24}$$

$$pK_{h2} = 3.5 \tag{3.25}$$

Consequently, it is more difficult to make stable In-carboxylate scintillators due to the high reactivity with water, even during the synthesis.

Indium based scintillators were made by F.X. Hartmann using e.g. hexanoic acid (6 C). A quantity of 2.7 g of In in HCl was boiled to dryness, and then dissolved in 4 ml H_2O. The aqueous phase is placed into equilibrium with 30 ml pure hexanoic acid. The pH is adjusted using concentrated NaOH solution until a final pH of 4. The indium amount in the aqueous and in the organic phase were determined by AAS, and 97 % of the indium material was found to be in the organic phase. The organic phase with an In-loading of 6 wt.% to 8 wt.% is used as stock solution for the scintillators. This stock solution can be placed in equilibrium with water and remains stable, but it has zero light output. Therefore the solution has to be diluted with an aromatic solvent. PC, PXE and anisole were used in these tests. Fig. 3.9 shows the stability region for indium. Compared to the Yb-system the molarity of the HA has to be higher and one has to operate at lower pH-values because otherwise the system starts to see severe hydrolysis. At the aromatic solvent concentrations needed to get reasonable light

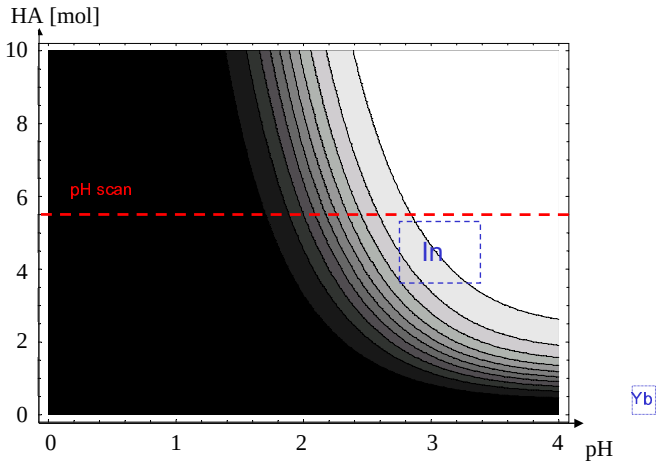

Figure 3.9: *This plot shows the stability region for an In carboxylate system in contact with water (plot made by T. Lasserre). The relative position of the Yb stability region, from the previous Fig. 3.8, is also shown in the lower right.*

yields the molarity of the HA is too low and the solution leaves the stability region in the parameter space.

All scintillators were unstable when directly made. Tests showed that these instabilities were due to the presence of water. The water causes a white indium hydrolyzed material to form. The water content in the HA and in the solvents was removed by drying agents as sodium sulfite. This improved the situation, but not completely.

The addition of some ethanol to the scintillators produced clear solutions. The ethanol presumably serves to:

- offset the hydrolysis reaction by adjusting the water chemistry
- delay or stop the polymerization by complexing with the HA's
- increase the solubility of the hydrolyzed material
- shift the equilibria of the reactions

In Table 3.6, the properties and the results of light yield measurements under irradiation with a radioactive source for some samples are summarized (method is described in Chapter 4). PPO was used as a fluor without the secondary wavelength shifter bis-MSB. The reason for the lower values obtained for the light yield as compared to the previous case of Yb is due to the high HA concentration, but as HA is lowered stability is lost.

For all the samples listed in Table 3.6, the fluorescence yield was also measured in a fluorimeter (see chapter 4) by light excitation of the scintillator at the absorption peak of the solvent. The fluorescence yields of the emission spectra were higher than the light yields obtained in the γ–source measurement. This indicates that the energy is efficiently transferred from the solvent to the PPO. The primary electrons after the Compton scattering of the gammas from the ^{137}Cs source lose energy in reactions with the hexanoic acid. Therefore

In [wt.%]	solvent	HA conc.	EtOH ratio [wt.]	LY [% BC505]
3.2	PC	2.8 M	0.05	10 ± 2 %
3.4	PXE	2.8 M	0.05	15 ± 2 %
4.4	Anisole	2.8 M	0.02	11 ± 2 %
4.2	Anisole (dried)	2.8 M	0	12 ± 2 %
4.4	PXE (dried)	2.8 M	0	18 ± 2 %

Table 3.6: *The light yields compared to a BC505 standard are given for some In-carboxylate scintillators. The HA (hexanoic acid) stock solution containing the indium is mixed with the scintillator solvent in a ratio of 50:50. The fluor PPO was used in all of the samples.*

the light yield is reduced. This effect is not observed in the fluorimeter, because there is no excitation of the acid at the excitation wavelength of the anisole absorption peak.

Carboxylic acid systems containing indium were extensively investigated by a Russian/ Italian group at Gran Sasso [DAN03]. They tested systems at varying carbon numbers and found that for the synthesis of scintillators operating with acids from 3 to 5 carbon atoms, neutral organophosphorus compounds are needed. These systems are very transparent (> 7 m attenuation length at 430 nm), but unstable and limited in light yield. The presence of the organophosphorus could be one of the reasons for the instability. So the use was avoided by going to acids with higher carbon numbers where these compounds are not needed any more.

The indium molecule in the scintillator produced at Gran Sasso is not $In(HA)_3$. Instead the molecule contains mainly OH^- groups. The rest (X) is a mixture of acetate- and carboxylic acid anions. The general description of the chemical compound they find in the scintillator is $[In(OH)_aX_{3-a}]_n$. The replacement of carboxylic acid by OH-groups has the advantage that the non-aromatic fraction in the scintillator is reduced and therefore the light yield becomes higher. With increasing pH values in the water fraction during the synthesis more and more carboxylic ligands are replaced by OH-groups. Therefore the amount of acid in the organic solution decreases and the light yield increases. Although hydrolysis occurs the group discovered that they could suspend the In-hydroxide in the organic medium. In fact, they achieved that the In remains in the organic phase until a pH of about 8. At this optimum pH-value (concerning light yield) the OH^- fraction a per indium molecule is approximately 2.5. At higher pH-values the In-solubility in the organic solvent (PC) decreases and also the light yield starts to drop.

The best results were obtained using the 6 carbon acid 2-methylvaleriate ($CH_3(CH_2)_2$-$CH(CH_3)$-COOH). At an In-loading of 80 g/l, a light yield of 64 % compared to the unloaded scintillator was achieved. The attenuation length was determined to be 2.8 m at 430 nm.

Chapter 4

Optical properties of the In-loaded scintillator

In this chapter the optical properties of various scintillators as light absorption, fluorescence emission and light yield under irradiation with a γ-source are described. The goal of these measurements was to optimize the fluor and solvent composition for an $In(acac)_3$ loaded liquid scintillator. Part of the results described in this chapter are summarized in [BUC04].

4.1 Absorption measurements

4.1.1 Measuring apparatus and definitions

The absorption measurements were carried out using a UV/Vis–spectrophotometer from Varian (Cary 400). It is a double beam instrument; one beam passes through a reference cell, the other beam passes through the sample cell. The spectrometer can be used in a wavelength region between 175 nm up to 900 nm. It is operated at room temperature. As sample containers UV-transparent quartz cells were used with a length of 1 cm (3,5 ml volume) and 10 cm (30 ml volume).

The intensity I of the light emitted in the spectrometer decreases exponentially, when it propagates through the sample.

$$I(x) = I(0) \cdot \exp\left(\frac{-x}{\Lambda}\right) \tag{4.1}$$

In this equation Λ is the attenuation length and x is the pathlength in the cell. The absorbance A is defined by the following equation:

$$A(x) = \log_{10}\left(\frac{I(0)}{I(x)}\right) \tag{4.2}$$

A combination of the two equations results in

$$\Lambda = \frac{x}{A} \cdot \log_{10}(e) = 0.4343 \cdot \frac{x}{A} \tag{4.3}$$

This equation is used to calculate the attenuation lengths. In the case that there are several absorbing components in the sample, the absorbances of the single components can be added

to get the overall absorbance. Using the above equation this leads to the following relation for the overall attenuation length Λ_{sample}

$$\frac{1}{\Lambda_{sample}} = \frac{1}{\Lambda_1} + \frac{1}{\Lambda_2} + ... \tag{4.4}$$

The validity of this equation will be shown experimentally for the system used.

The molar extinction coefficient ϵ is related to the absorbance A as follows:

$$\epsilon = \frac{A \cdot M}{c \cdot d} \tag{4.5}$$

where c is the concentration, M the molecular weight and d the pathlength. In this thesis the unit (l/mol·cm) is used for ϵ. It may be thought of as the absorbance per unit path length and per unit molar concentration. The linear relationship between absorbance and concentration of a sample follows from the above equation. This relationship is known as the Beer-Lambert Law. At high concentrations there can be deviations from this law.

The order of magnitude for the baseline variation of the instrument used in these investigations for A is 10^{-4}. The sensitivity for Λ is therefore in the 5 m range when the 1 cm cuvette is used. In a 10 cm sample, the sensitivity increases by one order of magnitude.

To determine the absorbance of a solute a quartz cuvette filled with a solvent in the sample beam of the spectrometer was measured versus a similar cell also filled with the pure solvent in the reference beam as a baseline. Then the solvent in the sample beam is replaced by the solution containing the sample material and the absorbance of the solute is measured. The same results are obtained if the baseline is taken with an air filled cuvette in the sample beam and air in the reference beam. In this case the absorbance of the pure solvent is measured first and afterwards the solution containing the sample. Finally one subtracts both spectra and gets the absorbance of the material of interest. Corrections for different Fresnel reflections due to changes in the refraction index of the liquid are neglected.

4.1.2 Sample preparation

Before the measurements most samples were sparged with nitrogen to remove oxygen dissolved in the liquid. Oxygen absorbs strongly in the region around 185 nm, however the tail of the absorption spectrum reaches wavelengths up to approximately 400 nm. The region of interest for most of the measurements is around 430 nm and above. At these wavelengths the absorption due to dissolved oxygen can be neglected in most cases. In cases in which the absorbance was investigated at lower wavelengths or the absorbance was small the samples were sparged for 5 minutes when the smaller cuvettes (3.5 ml) were used and for approximately 30 minutes when the larger cuvettes (30 ml) were used. Sometimes there are bubbles in the sample after the sparging which affect the absorbance. Therefore it is preferable to wait for two minutes for the sample to stabilize after introducing it into the spectrometer.

In the cases where high concentrations of the $In(acac)_3$ or the fluor are used (> 10 g/l) the sample was filtered using a 0.2 μm single-use regenerated cellulose (RC) membrane syringe filter with a polypropylene housing to remove insoluble contaminations. A test was performed to check if there is a negative effect of the optical transparency on the solvent due to the presence of the filter. Absorption spectra of pure cyclohexane and pure anisole before and after filtering were compared to each other (10 cm cell). No adverse effect on the transparency was found for both solvents at least in the region between 310 nm and 600 nm.

To accelerate the dissolving process of the $In(acac)_3$ and the fluor, the samples were treated in some cases in an ultrasonic bath for approximately 5 minutes. There are indications that this procedure has negative effects on the absorbance since a yellow color was sometimes observed in the liquid sample, especially when PXE was used as a solvent. Perhaps this is due to oxygen picked up from the air above the sample during the shaking. Another possibility is that the effect is due to the higher temperature in the bath.

4.1.3 Results

One of the objectives of scintillator production is to achieve long transmission lengths for wavelengths longer than 400 nm where the PMT is most sensitive. The two major absorbance contributions in this region are the indium material ($In(acac)_3$) and the fluor. Furthermore, the absorption bands of the $In(acac)_3$ and the fluors determine the energy transfer rates between the excited solvent molecules and the other scintillator components.

In Fig. 4.1 the wavelength dependence of the molar extinction coefficient is shown for $In(acac)_3$ in absence of fluors. The solvent is ethanol and the $In(acac)_3$-concentration for the measurement is 18 mg/l (molecular weight: 412.15 g/mol). The maximum of the absorption peak is at 285 nm. This means that there is significant energy transfer from the solvent to the In-material since the light emission of aromatic liquids is typically in the same wavelength region.

To obtain a large overlap between the solvent emission spectrum and the primary fluor absorption spectrum, the fluor absorbance has to be in a similar wavelength range. The molar extinction coefficient of the most carefully investigated fluors and of the secondary wavelength shifter bis-MSB are shown in Fig. 4.2. For the fluors the maximum of the absorbance is slightly above the $In(acac)_3$ peak at 303 nm for PPO and 323 nm for the BPO. The bis-MSB absorbs mainly in the region where the PPO emission is strong. The maximum is at 348 nm. To determine the molar extinction coefficient over the whole spectrum from the absorption peak up to 600 nm measurements at different concentrations were needed to be within the sensitivity region of the spectrometer. The PPO curve is a combination of literature values (280 nm to 350 nm) [BER71] and measured values (371 nm to 600 nm). The region between was interpolated. In the bis-MSB curve the instrument was not sensitive in the region above 450 nm at the concentrations used.

Absorbance measurements of all scintillator components (In-material, fluors, primary scintillating solvent) were recorded in the wavelength region where highest transmission is most important. In Fig. 4.3 the attenuation length Λ of the different components of a 5 wt.% In scintillator mixture as determined from the experimental measurements is shown. The attenuation lengths are in the range of a few meters. The attenuation length was derived from the absorbance of the single components as described above. To determine the absorbance, the components were dissolved in anisole. The baseline was taken after introducing two 1 cm cuvettes filled with pure anisole into the photospectrometer. The curve for the $In(acac)_3$ represents the optical quality of an average material after the sublimation. Other samples showed better or worse results. After having some experience with the sublimation apparatus and the optimization of the sublimation parameters the crystals obtained showed only small variations. Nearly all 5 wt.% In-loaded samples produced nowadays have an attenuation length of 3 m to 5 m at 430 nm sufficient for the needs of a low energy solar neutrino detector. The light loss mechanism applicable in the low absorbance region could still be due to scattering or absorption of any impurities.

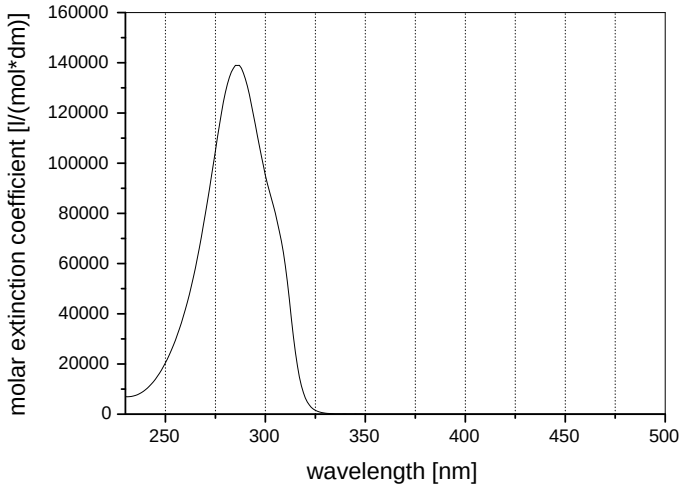

Figure 4.1: *Absorption spectrum, in units of the molar extinction coefficient, of specially prepared $In(acac)_3$ dissolved in ethanol (18 mg/l; 43.8 μmol/l) showing a maximum at 285 nm.*

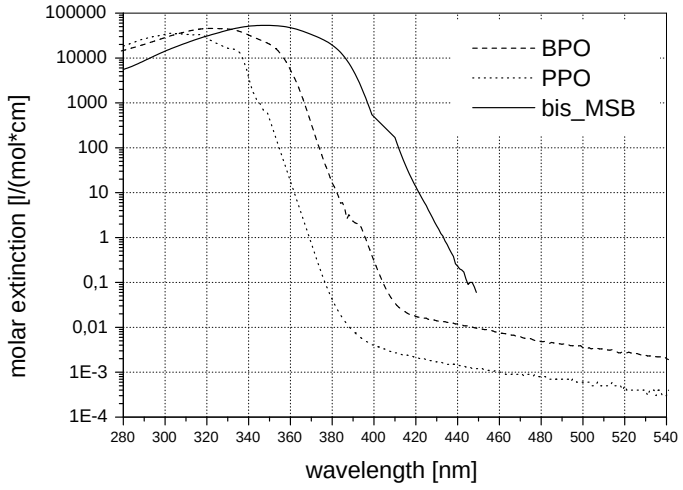

Figure 4.2: *Molar extinction coefficient of BPO (maximum at 323 nm), PPO (maximum at 303 nm) and bis-MSB (maximum at 348 nm).*

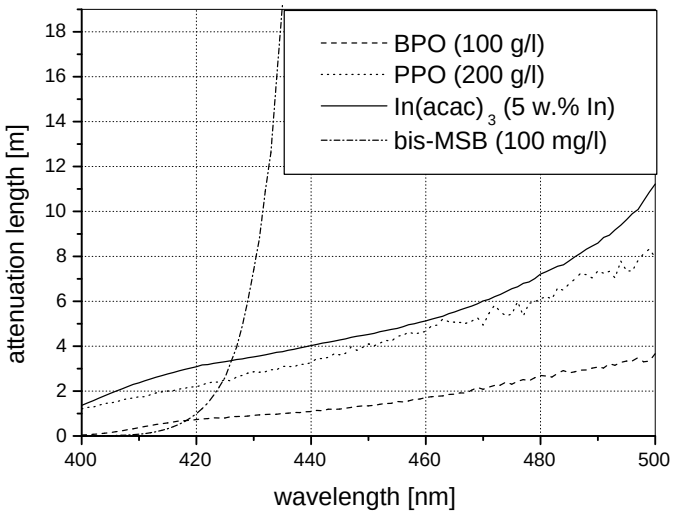

Figure 4.3: *Wavelength dependence of the attenuation length for components of the main scintillator versions: PPO (200 g/l, 0.90 M) or BPO (100 g/l, 0.34 M), bis-MSB (100 mg/l, 0.32 mmol/l) measured in 1 cm cells and 5 wt.% indium loading (0.44 M) measured in a 10 cm cell. The contribution of the anisole solvent is small.*

Fig. 4.3 also shows a plot of the attenuation lengths for possible fluor components of the scintillator. Unusually high fluor concentrations in the $In(acac)_3$-loaded scintillator are needed to get a sufficient light output. The reason is discussed later in the thesis. For PPO at a concentration of 200 g/l and an In-loading of 5 wt.% both ingredients contribute approximately the same amount to the absorbance. In a system using BPO at a concentration of 100 g/l the attenuation lengths are shorter at a given wavelength than those for the PPO system. The absorption spectrum of BPO is shifted to longer wavelengths compared to that for PPO. At these BPO concentrations, the absorbance in the region of interest is dominated by the fluor. Thus, the attenuation length can be improved by a lower fluor concentration. However, this implies also a reduction in the light yield. The attenuation length of butyl-PBD (Aldrich, 99%) was also measured at a concentration of 200 g/l and found to be worse than for the other fluors. At 430 nm it was only in the range of 30 cm.

Finally the bis-MSB contribution at a much smaller concentration of 100 mg/l is shown. Above 430 nm the contribution is negligible, but below 420 nm it starts to dominate the absorbance in the system. It will be shown later that the light absorbed by the bis-MSB at 420 nm and below is reemitted at longer wavelengths. This light is mainly lost in the spectrometer measurement, because the probability that it is emitted in the direction of the light beam and hits the PMT is small. In a bigger LENS-like cell such light can be reflected at the cell walls and has much higher probability to be detected.

In addition to the contributions of the In-material and the fluors to the attenuation length there is also a small absorbance around 430 nm due to impurities in the anisole. It is possible to remove such impurities in the anisole by a column purification procedure using a weakly acidic Al_2O_3 column packing. The attenuation length of the unpurified anisole (Aldrich, 99%) was measured to be between 5 m and 11 m at 430 nm depending on the production

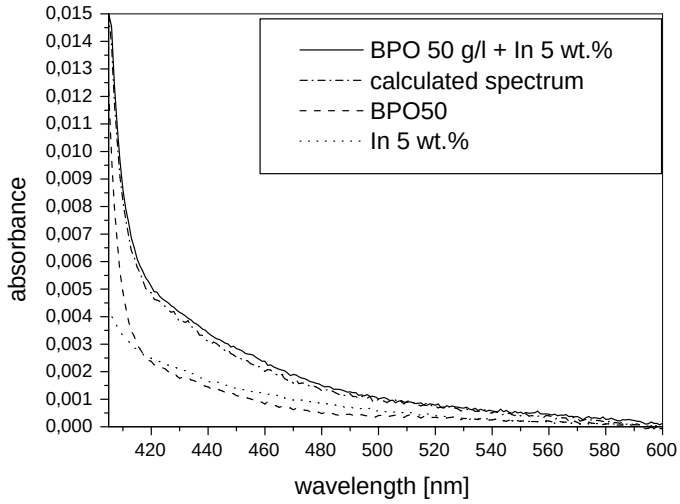

Figure 4.4: *The absorbance of In(acac)$_3$ (5 wt.% In) and BPO (50 g/l) when dissolved in anisole is shown. The components were first measured separately and then together in the same solution. The measured absorption spectrum of the full scintillator mixture (anisole contribution neglected) is compared to the calculated spectrum.*

number of the sample. For the samples being below 8 m the attenuation length increases to at least 9 m after purification. For these measurements a 10 cm cuvette was used for better sensitivity, and the baseline was taken with the empty cuvette versus air. It was assumed that the attenuation length is infinite (namely the absorbance is zero) at the minimum (580 nm) of its absorbance spectrum.

The reciprocal of the scintillator attenuation length $1/\Lambda_{scint}$ equals approximately the sum of the reciprocals of the attenuation lengths of all single components.

$$\frac{1}{\Lambda_{scint}} = \frac{1}{\Lambda_{solvent}} + \frac{1}{\Lambda_{fluor}} + \frac{1}{\Lambda_{In}} + \frac{1}{\Lambda_{bis-MSB}} \tag{4.6}$$

To test the validity of this equation the absorbance of a specific In(acac)$_3$ sample (5 wt.% In) and of 50 g/l BPO were measured separately. Then 50 g/l BPO were added to the In(acac)$_3$ solution. It is shown in Fig. 4.4 that the calculated sum of the In(acac)$_3$ and the BPO absorbance matches well with the spectrum of the mixture determined experimentally. Small corrections of the equation are expected due to dilution effects (e.g. the anisole concentration in the sample) at the high fluor and In(acac)$_3$ concentrations.

In summary, a combined attenuation length of approximately 1.5 m (0.7 m) at 430 nm using PPO (BPO) is achievable in a 5 wt.% In-anisole-fluor mixture using equation 4.6 and the concentrations of Fig. 4.3. With the In(acac)$_3$ of the highest quality that was produced (approximately 5 m attenuation length at 5 wt.% In-loading) the dominating contribution to the absorbance at the used concentrations comes from the fluor. If the results are due to impurities possible further improvements in the absorbance properties can be achieved for the PPO (Aldrich, 99%) or BPO (non-commercial synthesis). If the absorption of the fluor at long wavelengths is due to intrinsic molecular properties then further purification steps will

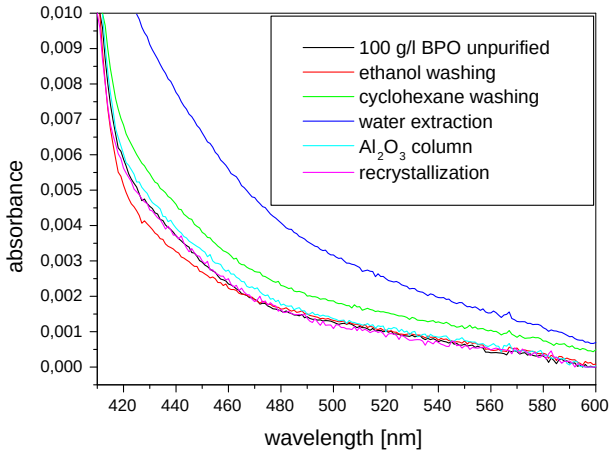

Figure 4.5: *The purification of BPO was tested by several methods. An improvement in the transparency was only found by ethanol washing. The BPO concentration was 100 g/l in most of the measurements. In case the concentration was lower the absorbance was upscaled. The high absorbance after the water extraction is probably due to residual water in the organic solution.*

not help. As will be described later there are indications that the BPO absorption is due to impurities. Therefore several attempts were made to purify the material.

4.2 BPO purification tests

Although the BPO material was delivered pure several additional purification tests were performed to improve the transparency around 430 nm. The BPO purification tests were carried out in collaboration with one of our Russian colleagues, Igor Barabanov. Several methods as recrystallization, washing, column purification and water extraction were investigated. The results are summarized in Fig. 4.5. No major improvement in the transparency could be achieved with these methods.

4.2.1 Recrystallization

In a first purification test, BPO was dissolved in anisole at a high concentration of 150 g BPO per liter anisole. Then the sample was filtered to remove insoluble impurities and the solution was kept overnight in an icebox at –15°C (melting point of anisole: –37°C). Approximately half of the material recrystallized. The sample was filtered and dried at 41°C. An absorption measurement at 50 g/l BPO in anisole showed no improvement in the optical transparency.

4.2.2 Washing

The next attempt was based on the idea to wash the material in a solvent that has only small solubility for the fluor, but dissolves the impurities. Ethanol and cyclohexane were tested. A

BPO amount of 0.5 g was mixed with 10 ml of each liquid and the solutions were shaken in an ultrasonic bath for 15 minutes. After three days the samples were filtered and dried.

In Fig. 4.5 there is an offset for the measurement of the purified BPO using cyclohexane. This offset is probably due to surface contaminations on the quartz cuvette. If one assumes that the offset is constant for all wavelengths and is subtracted the obtained curve matches well the spectrum of the unpurified BPO.

The absorbance was approximately 10 % lower after the ethanol washing of the BPO than before. The BPO-concentration in the ethanol was determined with the spectrometer in a diluted sample knowing the molar extinction coefficients of BPO. The solubility in ethanol was found to be in the 5 g/l scale. Therefore, the BPO loss in the ethanol is in the 10 % range at the used concentrations. The ethanol washing was the only investigated method in which a improvement in the transparency could be observed.

4.2.3 Column purification

Very positive effects were obtained by purifying solvents as anisole and PXE using a weakly acidic Al_2O_3 column. The same method was tested with an anisole BPO solution in order to purify the BPO. A solution of 20 ml containing BPO at a concentration of 100 g/l was sent over a 7.5 cm long column in a cylindrical glass tube. The volume of the column was 6.5 ml. The anisole/BPO solution before and after the column was diluted in cyclohexane until the BPO-concentration was in the 1 mg/l range. At this concentration the spectrometer is sensitive (1 cm cell) at the maximum absorption of BPO (323 nm) which was a factor 0.64 lower for the solution after the column than before. This indicates a BPO-loss of 36 % to the column material. The absorption is proportional to the concentration. Dividing the absorption spectrum obtained after the column with 0.64 reproduces the spectrum measured before. This means that there was no purification effect by the column.

4.2.4 Water extraction

A final attempt to purify the BPO was water extraction. The density of anisole (0.99) is very similar to that of water, therefore the separation between the two liquids is difficult. At high BPO-loading the density increases and becomes greater than unity. Therefore the solution of 100 g BPO per liter anisole used for the extraction settled down at the bottom of the separation funnel. The H_2O:organic ratio was 2:1. The mixture was shaken for a few minutes and the two phases were separated the next day. The absorbance seemed to be much worse than before (see Fig. 4.5). A possible explanation could be the presence of water in the organic fraction which forms bubbles. In such a case the light can be scattered at these bubbles. As will be shown in the next chapter after water extraction and drying of the organic phase using a silica gel column a minor improvement in the absorption is observed.

4.2.5 Conclusion

In summary, no purification method was found to reduce the absorbance significantly in the wavelength region of interest around 430 nm. The best result was achieved with the ethanol washing, but even with this minor improvement the BPO is still the component limiting the absorbance at the scintillator emission. In case that the absorbance is really due to an impurity it is likely that the chemistry of the impurity is similar to the chemistry of the BPO molecule.

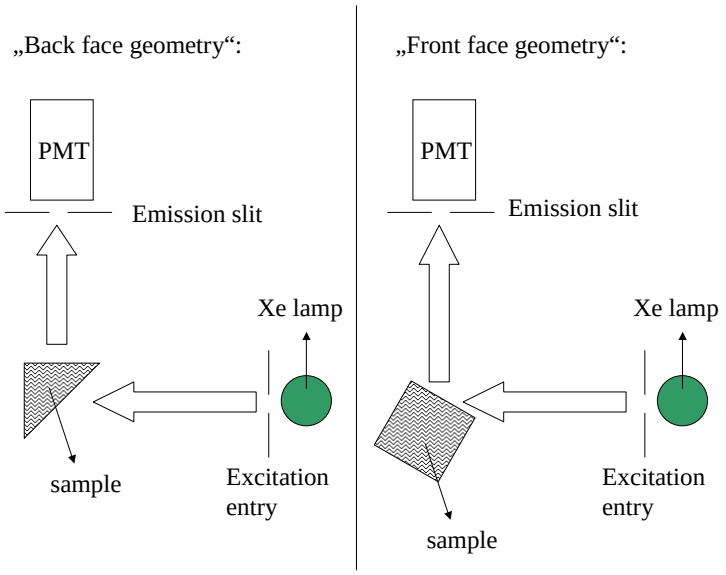

Figure 4.6: *The two most commonly used geometries for the fluorescence measurements. In the back face geometry the fluorescence light propagates several mm through the sample before the emitted light is detected in the instrument. In the front face geometry the excitation light enters on the same side of the cuvette which is observed by the PMT.*

4.3 Fluorescence measurements

In the fluorescence measurements the light emission spectra of scintillator samples were investigated after excitation at a certain wavelength, typically the absorption maximum of the scintillator solvent. The light yields and the emission wavelengths of the various scintillators are determined from the observed spectra. Different geometries are available in the measurements to examine radiative and non radiative energy transfer properties.

4.3.1 The fluorimeter

For the fluorescence measurements also a device from the company Varian was used (Cary Eclipse) which is operated at room temperature. The wavelength range that can be used in this instrument is 190 nm to 900 nm. As light source a Xenon flash lamp is used in the instrument. It flashes at a rate of 80 flashes/s at a pulse width of 2 to 3 μs. The light is collected by Schwartzschild collector mirrors and then focused through a lens onto the excitation entry slit. Two extended range PMTs act as detectors for the emitted light. Furthermore the fluorimeter consists of two Czerny-Turner monochromators, selectable filters and a range of fixed width selectable slits for excitation and emission. For the monochromators the accuracy is ± 1 nm. The optics of the instrument is protected by a quartz overcoating.

Two different geometries for the position of the sample were mainly used, depending on what kind of information one would like to obtain (see Fig. 4.6). The most frequently used geometry was the front face geometry. In this mode, the excitation light enters on the same side of the cuvette containing the sample as that which is observed by the detector of the emitted light. This geometry ensures that the reabsorption of the emitted light in

the scintillator is negligible because the light is absorbed and emitted in a thin layer close to the wall of the cuvette when the solvent is excited at its absorption maximum. Some measurements were performed using the backface geometry which is also shown in Fig. 4.6. For this geometry a triangular cell is used. The excitation light enters the cell at 45 degrees to the hypotenuse and exits through the liquid out a side, with the emission viewed under 90 degrees to the incident excitation beam. Therefore the fluorescence light propagates several mm through the scintillator mixture before detection. This geometry was chosen to examine the effect of short range self-absorption.

The emission spectrum of a fluorescent molecule is typically determined by dissolving it at low concentrations in the mg/l scale in a non fluorescent liquid as cyclohexane or ethanol. Then the sample is excited at the absorption peak of the molecule under investigation. The fluorimeter was also used to measure the emission spectra of the full scintillator mixtures. Oxygen can have a quenching effect on the light yield of the samples. Therefore the samples were sparged with nitrogen for 5 minutes before each measurement.

4.3.2 Emission spectra of the basic ingredients

The primary fluor is the central ingredient for light emission in the visible region. Since it is present in relatively large quantities in the In-loaded scintillator the fluor is either directly excited by the initial radiation or excited by energy transfer from the solvent. However, the secondary fluor (e.g. bis-MSB) present in small quantities, shifts the emission to longer wavelengths. The solvent itself is an UV fluorescent aromatic and dissolves the In-material.

The absorption and the emission spectrum of anisole diluted in cyclohexane is shown in Fig. 4.7. The emission maximum for anisole is at 293 nm when excited at its absorption peak at 271 nm. For some aromatic molecules the position and structure of the fluorescence spectrum depends on the dielectric constant and the index of refraction of the solvent. In a polar solvent like ethanol the sharpness of the band structure can be lost and the fluorescence spectra as well as the absorption spectra can be shifted towards longer wavelengths [BER71]. This effect is stronger for the fluorescene spectrum. For anisole no shift in the emission peak was observed using ethanol instead of cyclohexane as solvent.

The emission peak of pure anisole excited at the absorption maximum in the front face geometry is shifted to longer wavelengths by a few nm (peak at 296 nm). This effect can be explained by a non-radiative energy transfer between the anisole atoms. The probability for such a transfer is higher at lower wavelengths and therefore the emission spectrum appears to be shifted to higher wavelengths.

The main shift of the anisole UV emission to longer wavelengths (around 360 nm) is done by the primary fluor. The absorption and emission spectra of similar fluors are shifted to longer wavelengths if the number of phenyl groups in the molecule is increased. The number of rings increases from two to four between PPO, BPO and BBO. It was observed experimentally that for each additional phenyl group the absorption and emission spectra are shifted by approximately 20 nm. The absorption and emission peaks of the oxadiazoles are shifted to shorter wavelengths compared to the corresponding oxazoles, e.g. for the oxadiazole PBD the maxima in the spectra are around 20 nm below the ones of BPO which is a oxazole. Both fluors have three phenyl rings in the same position.

For some fluors the emission spectrum in anisole is rather different compared to the emission spectrum in cyclohexane. In cyclohexane the spectrum of PPO shows three peaks at 341 nm, 358 nm (global maximum) and 374 nm (the PPO absorption peak is at 303 nm

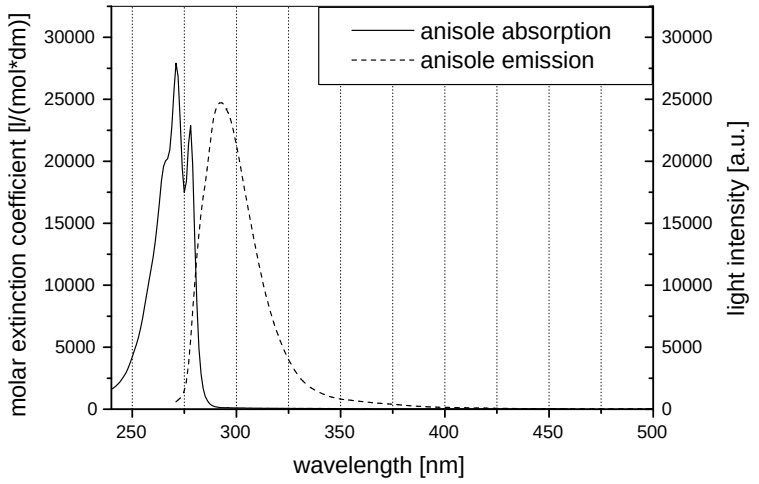

Figure 4.7: *Absorption (molar extinction coefficient, left scale) and emission (relative light intensity, right scale) spectra of anisole diluted in cyclohexane (16 mg/l, 0.15 mmol/l). The absorption maximum is at 271 nm, the emission maximum at 293 nm (271 nm excitation).*

if dissolved in cyclohexane). Using the same fluor concentration the spectrum in anisole shows only one peak at 367 nm. Apart from the solvent effect there is also a concentration effect. When the fluor concentration is increased the peaks occur approximately at the same wavelength, but the light yield at the emission peak is reduced and the tail of the spectrum becomes larger at longer wavelengths. Similar effects are observed for BPO. The emission peak for this fluor diluted in cyclohexane is at 383 nm. In anisole at the high BPO concentrations used the peak shifts slightly above 400 nm. In the wavelength region of the primary fluor emission the absorbance due to the fluor itself or due the In-material is still high. Therefore further wavelength shifting is needed.

To shift the wavelength to longer than 400 nm bis-MSB was used as a secondary fluor. The bis-MSB leads to a broad emission peak having a maximum at 425 nm in the scintillator system. The emission spectrum of a scintillator sample containing bis-MSB at the 100 mg/l level and PPO as primary fluor was measured using a triangular cell in backface geometry in order to investigate short range absorption effects. The spectrum shows a cutoff at 400 nm due to self-absorption of the bis-MSB in the cell. In fact, in this mode 50 % of the light is emitted above 440 nm. The effect of bis-MSB is discussed in more detail in the next section.

Indium diverts some of the useful light since it also absorbs photons in the region of the anisole emission, however, there is insignificant light emission from the $In(acac)_3$ molecule. A measurement was performed where a sample of $In(acac)_3$ dissolved in ethanol at a concentration of 18 mg/l was placed in a 1 cm cuvette and excited at its absorption peak maximum of 285 nm. It was observed that negligible light emission was found from the absorption peak to 600 nm. Energy transferred to the $In(acac)_3$ material is therefore lost and this process should be avoided. The key to significant light output is the tuning of the transfer processes so as to maximize the solvent-to-primary fluor energy transfer pathway over the solvent-to-In material mode.

4.3.3 The effect of bis-MSB

The energy of the excited fluor molecules can be transferred to the bis-MSB in a radiative or a non-radiative energy transfer process. Which process is dominant in a scintillator system depends first on the overlap between the emission spectrum of the fluor and the absorption spectrum of the bis-MSB. Second the bis-MSB concentration is essential for the energy transfer behavior.

The emission spectra of fluors like PPO and p-Tp are well matched to the absorption maximum of bis-MSB (345 nm). Therefore non-radiative energy transfer between the fluors is likely. For the case of BPO as primary fluor the overlap integral is smaller, because the BPO emission spectrum is shifted to longer wavelengths compared to PPO or p-Tp.

Which mode is responsible for the energy transfer can be investigated using the fluorimeter in front face geometry. If all the energy of the excited fluors is transferred in a non-radiative way, then no fluor emission peak is seen in that measurement. The emission and detection of real photons originating from the primary fluor indicate energy transfer by radiation.

In Fig. 4.8 some emission spectra of several samples taken in front face geometry are shown to demonstrate the different non-radiative energy transfer rates from PPO and BPO to bis-MSB. The intensity of the light emission is given in arbitrary units. All samples had an In-loading of 5 wt.% and were excited at the anisole absorption peak of 271 nm. The bis-MSB concentration was varied at a constant BPO concentration of 100 g/l. At a bis-MSB concentration of 100 mg/l the spectrum is still similar to the pure BPO spectrum demonstrating that there is only minor non-radiative energy transfer from BPO to bis-MSB. If the bis-MSB concentration is increased by one order of magnitude to 1 g/l the energy transfer rate increases and one starts to see the features of a pure bis-MSB spectrum with the characteristic peak around 425 nm.

The spectrum of a 5 wt.% In-loaded scintillator using PPO as fluor at a concentration of 200 g/l is illustrated in the same figure. The height of the peak at 425 nm was normalized to the maximum of the spectrum for the 1 g/l bis-MSB/BPO system. In fact the light emission in the PPO system is less than in the BPO system. In the case of PPO the bis-MSB spectrum is already seen at much lower bis-MSB concentrations compared to the BPO system. At 100 mg/l bis-MSB already a significant energy fraction is transferred non-radiatively to the secondary fluor. Nevertheless the PPO-peak around 370 nm is still present showing that some PPO molecules emit real photons in that kind of system. At higher bis-MSB concentrations the bis-MSB peak would be increased at the cost of a lower PPO peak.

The energy transfer between BPO and bis-MSB by emission and absorption of photons can also be investigated with the fluorimeter. In that case the backface geometry and a triangular cell are used to include short range self absorption. Some of the results are shown in Fig. 4.9. The same scintillator samples were used as for the measurements in front face geometry. The attenuation length of bis-MSB at a concentration of 100 mg/l at the emission maximum of BPO around 400 nm is in the mm range. With increasing bis-MSB concentration the spectrum is shifted to higher wavelengths. This is not only due to the energy transfer from the BPO to the bis-MSB. There is also self-absorption of the bis-MSB followed by reemission at higher wavelenghts.

In small samples, there is no gain in light yield by using bis-MSB together with BPO since the energy transfer rate is small. However, the use of bis-MSB in this system is advantageous if one goes to longer pathlengths. In this case radiative energy transfer from BPO to bis-MSB occurs and the scintillator emission is in a more transparent region.

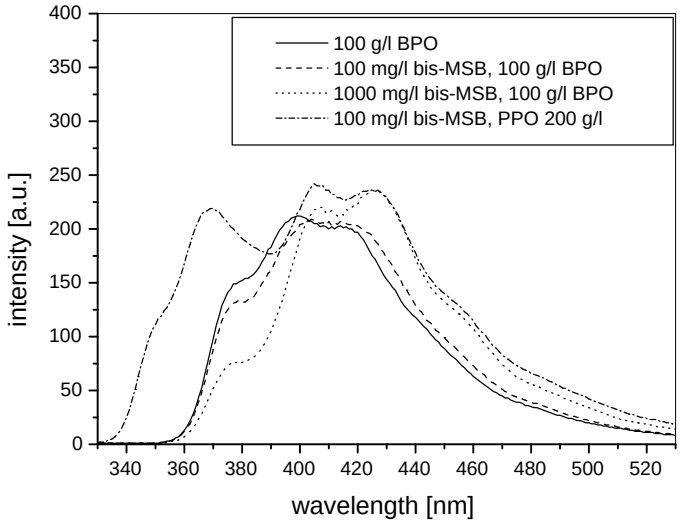

Figure 4.8: *The emission spectra of 5 wt.% In-loaded scintillators are shown when excited at the anisole absorption. For these measurements the front face geometry was used. The effect of increasing bis-MSB concentrations at 100 g/l BPO is shown. For comparison a similar spectrum at 200 g/l PPO and 100 mg/l bis-MSB is plotted.*

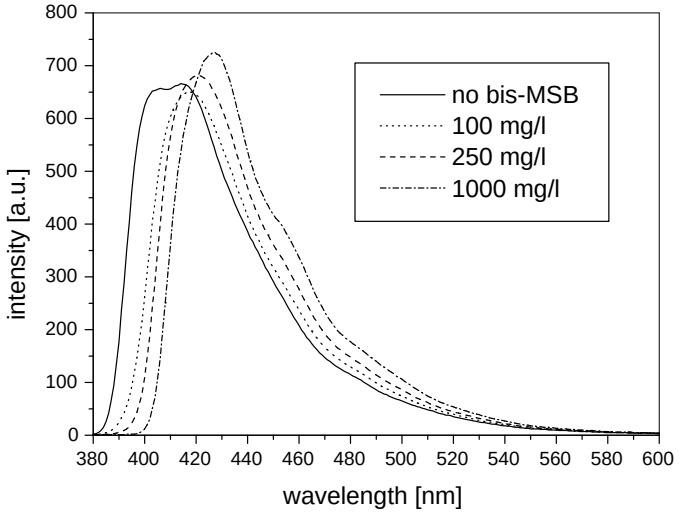

Figure 4.9: *The emission spectra of 5 wt.% In-loaded scintillators are shown when excited at 271 nm (anisole absorption peak). They were measured in backface geometry using a triangular cell. The effect of wavelength shifting at increasing bis-MSB concentrations and a constant BPO-concentration of 100 g/l is shown.*

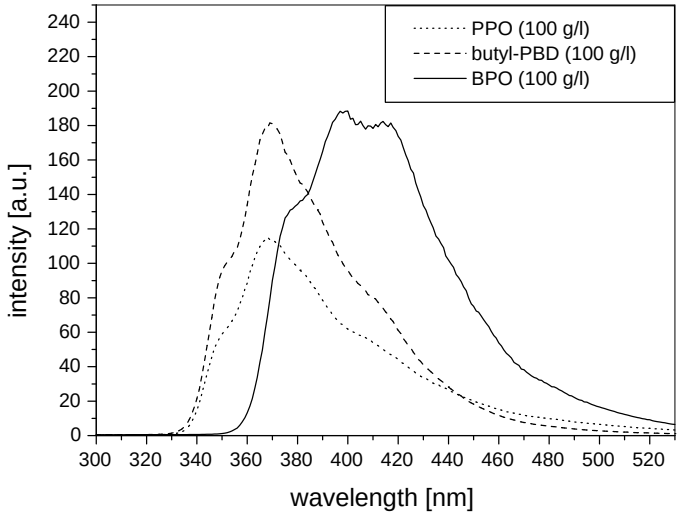

Figure 4.10: *Emission spectra of 4.5 wt.% (0.40 M) In-loaded scintillators excited at 271 nm in front face geometry. Data shown for equal weight primary fluor loadings (or 0.34 M BPO, 0.28 M butyl-PBD, 0.45 M PPO) in the absence of the secondary fluor bis-MSB.*

4.3.4 Maximization of energy transfer to the fluor

There are three different possible approaches towards improving the light yield involving the transfer of energy from the solvent to the fluor. One is to increase the transfer rate from the solvent to the fluor by using higher fluor concentrations (examined in the next section), second is to optimize the light from a given fluor by choice of fluor, and the third is to try to decrease the competing transfer rate from the solvent to the $In(acac)_3$.

Fluor optimization

To optimize the light yield by choice of fluor, the performance of several fluor candidates was investigated experimentally. The results obtained lead to PPO, butyl-PBD and BPO as the best candidates since these have high solubility in anisole and thus can be used in higher amounts so as to emit more light. No aggregation was observed even at fluor concentrations of more than 100 g/l. Furthermore, with similar In-concentrations and comparable fluor amounts, the three fluors mentioned above emit notably more light than PMP or p-TP. In Fig. 4.10 the emission spectra of 5 wt.% In-loaded scintillators are shown using these three fluors at a common weight loading of 100 g/l. The integrated emission spectrum (integrated as a function of wavenumber, using front face geometry) is 45 % higher for the butyl-PBD scintillator compared to the PPO system. Correspondingly, the integrated BPO spectrum is 70 % higher than the PPO spectrum.

Finally, as seen in Fig. 4.10, the BPO system has the advantage that it emits at longer wavelengths than the other fluors. Since PPO and butyl-PBD both emit photons around 370 nm, the emission still overlaps somewhat with the absorbance of $In(acac)_3$. Therefore, the bis-MSB wavelength shifter is more needed for these fluors than it is for the BPO case.

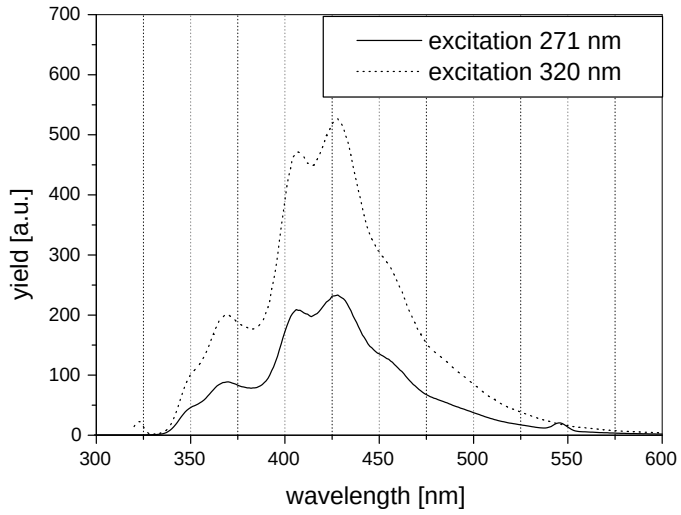

Figure 4.11: *Emission spectra of a 5 wt.% In-loaded scintillator (200 g/l PPO, 500 mg/l bis-MSB) excited at 271 nm and 320 nm. These measurements were made in front face geometry.*

Solvent optimization

To reduce the transfer rate from the solvent to the $In(acac)_3$, the third variation, one would prefer a solvent which emits at a longer wavelength than the ansiole. The intensity of the fluorescent emission of an In-loaded scintillator using PPO and bis-MSB as fluors increases as the wavelength of the excitation light increases from the anisole absorption at 271 nm to longer wavelengths. Up to 305 nm, slightly beyond the absorption peak of the PPO (303 nm), the difference is small, but when the excitation light is increased past 320 nm there is a significant increase in fluorescence light emission (see Fig. 4.11). Consequently, a solvent having an emission greater than 300 nm would be of interest. Such solvent components exist in the form of the dimethoxybenzenes (dmb). They have a high solubility for $In(acac)_3$ (see solubility section) and emit photons mainly above 300 nm. The isomer 1,4-dmb, a solid at room temperature, has a fluorescent emission at 321 nm when dissolved in anisole at a wt. ratio of 20:1. Tests of the actual light yield however revealed no improvement in the light yield for In-loaded scintillators compared to the pure anisole based version of the scintillator. Probably the rate of energy transfer to the 1,4-dmb is too slow such that it does not decrease the rate of transfer to the In-molecule.

In the In-free scintillator systems the light yield decreases with increasing 1,4-dmb concentrations. At a 1,4-dmb:anisole ratio of 1:1 a second light emission peak appears at longer wavelengths. This is a well known effect that sometimes occurs at high solute concentrations. The effect can be explained by the formation of excimers. An excimer is a transient excited dimer, formed in the process [BER71]

$$S^* + S \rightarrow (SS)^* \rightarrow S + S + h\nu$$

where S,S^* and $(SS)^*$ represent a solute molecule in the ground state, a similar molecule in

an excited state and an excimer. Generally the energy of the excited state of the transient dimer $(SS)^*$ lies below that of S^*, so that the fluorescence from an excimer state lies in the region of longer wavelengths.

Besides the solid 1,4-dmb, two other dimethoxybenzenes being liquids at room temperature were also investigated. The first is 1,2-dmb which has an emission maximum at 305 nm when diluted in cyclohexane. The light yield was determined to be approximately 80 % of an In-free anisole scintillator at the same fluor concentration. For the case of an In-loaded scintillator the difference in the light yield is smaller, but no significant improvement could be observed using 1,2-dmb as solvent.

Finally the performance of 1,3-dmb, also a liquid at room temperature, was investigated. When dissolved in cyclohexane it has strongest emission at 299 nm. This is close to the anisole emission therefore only a minor improvement in the energy transfer to the fluor is expected. The light yield of an unloaded scintillator version with 1,3-dmb as solvent was more than a factor two below the corresponding anisole system. The 1,3-dmb used had some yellow color indicating that it contained some impurities. In summary, all the dimethoxybenzenes tested gave no improvement in light yield compared to anisole.

Another solvent emitting at higher wavelengths than anisole is Ruetasolv (tradename) which is a mixture of diisopropylnaphtalene isomers. The emission peak of the pure liquid measured in front face geometry to avoid self-absorption is at 342 nm. Therefore the energy transfer to the $In(acac)_3$ is expected to be small. The maximum In-loading in this solvent is below 0.5 wt.%. Therefore this solvent is not suitable to an experiment where high In-loading is needed, but it could be of interest in other applications where a lower metal loading is sufficient.

To investigate the influence of the solvent on the light yield the performance of PXE and PC as solvents was compared to the anisole case at 1 wt.% In-loading. These solvents all emit in the same wavelength region between 280 nm and 295 nm when dissolved in cyclohexane. Thus, the energy transfer rates to the other scintillator components are expected to be similar. The deviations of the integrated emission spectrum from the anisole case were 10 % and below. The light yield seemed to be best for the PXE system and worst for the PC system.

From the measurements presented above it can be concluded that the best solvent for an In-detector using $In(acac)_3$ dissolved in a liquid scintillator at high In-concentrations is anisole. Of all the fluors under investigation BPO gave the best results concerning the scintillator light yield.

4.3.5 Reemission of BPO and bis-MSB

To test if the BPO absorption above 400 nm is due to the fluor itself or due to impurities in the BPO an anisole/BPO solution at a fluor concentration of 100 g/l was excited at various wavelengths around 400 nm. In this test, a triangular cell was used in backface geometry. If the light is absorbed by the BPO itself then reemission of the photons at longer wavelengths is expected. If the light is absorbed by non fluorescent impurities then no reemission should be observed.

As seen in Fig. 4.12 there is clearly emission when the wavelength of the excitation light is at 400 nm or below. Excitation at 410 nm is still followed by the emission of a small amount of light. At 420 nm corresponding to a molar extinction coefficient ϵ of approximately 0.018 l/(mol·cm) no light was reemitted indicating that the absorbance in that region is due to impurities and not due to the tail of the BPO spectrum. The peak around the excitation

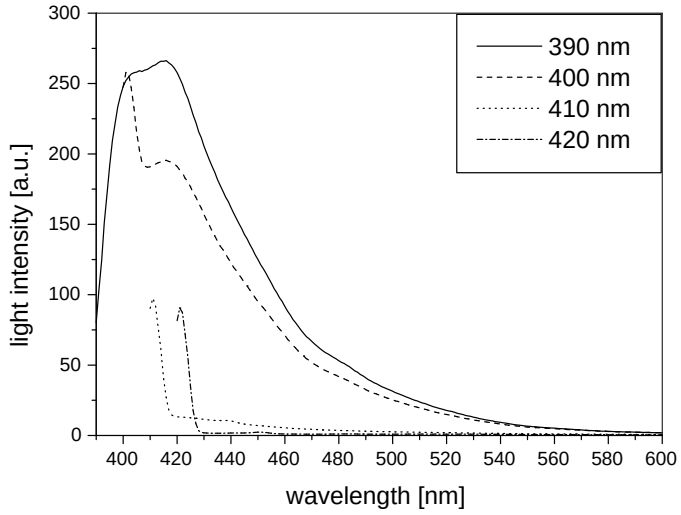

Figure 4.12: *Emission spectra of BPO at excitation energies between 390 and 420 nm (backface geometry).*

energy is due to scattered light of the excitation beam.

A similar test was performed using bis-MSB at a concentration of 2.5 g/l. In this system reemission was still observed for excitation at 440 nm. The molar extinction coefficient at that wavelength is 0.23 l/(mol·cm). At the used concentrations this corresponds to an absorbance which is a factor of 3 below the one for the BPO system at 420 nm showing that we are not limited by the sensitivity of the fluorimeter.

So it seems that the BPO absorbance around 430 nm is due to an impurity and light absorbed by the BPO in this wavelength region is therefore lost. On the other hand the light absorbed by bis-MSB in the same wavelength region is reemitted at longer wavelength and is still detectable by the PMTs of the detector cells.

4.4 Light yield under irradiation with a γ-source

4.4.1 Experimental setup

The light yield measurements were performed using a vial filled with liquid scintillator viewed by a PMT. A ^{137}Cs-source (662 keV photons) is used to excite the sample. The photons scatter off of electrons in the scintillator, ejecting energetic electrons. These lead to light production primarily through the direct excitation of the solvent and primary fluor components.

The experimental setup for the light yield measurements is located in a dark room. The temperature in this room varies between 20 °C and 30 °C. A drawing of the setup is shown in Fig. 4.14. A blue sensitive bi-alkali photocathode PMT (Photonis XP2262) is exposed to a 1 cm quartz cuvette containing the scintillator sample. The cuvette is surrounded by a teflon reflector except on the side which is optically coupled to a glass window and viewed by the PMT. The sample is irradiated by the radioactive source in a closed box housing sample and reflector.

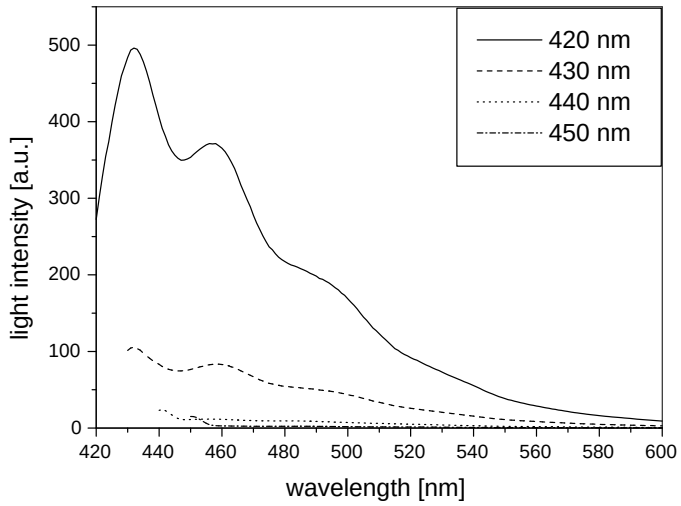

Figure 4.13: *Emission spectra of bis-MSB at excitation energies between 420 and 450 nm (backface geometry).*

Fig. 4.15 shows the electronic circuit used for the light yield measurements. The PMT is operated at a high voltage (HV) of 1750 V. The PMT signal is split by a linear Fan Out (FO). The gate for the trigger is generated by a Constant Fraction Discriminator (CFD) and a Gate/Delay Generator. It has a width of 80 ns. The trigger and the time delayed PMT signal meet at a charge sensitive ADC (QADC) which is part of a VME acquisition system. The light signal is proportionally converted into a current pulse which is integrated to give the 'PMT charge signal'.

The light yield is found by recording the characteristic Compton spectrum (number of events vs. PMT charge signal) and determining for a given deposited energy at the Compton shoulder the corresponding PMT signal. The PMT signal at the Compton edge is then compared to the signal of a BC505[1] standard at the same energy. To compare the values between sample and standard, the pedestal has to be subtracted. The pedestal is determined by taking data using the same settings as in a 'real' measurement except that the time delay between trigger gate and multiplier signal is changed in such a way that during the time period when the gate is open there is no signal from the PMT.

Examples of two measured Compton-spectra are plotted in Fig. 4.16. The figure shows the Compton edge of a BC505 standard on the top and the Compton spectrum of an In-loaded scintillator sample below. A higher light yield of the scintillator corresponds to a shift of the Compton edge to higher PMT signals (abscissa in the plot). The maximum of the Compton spectrum at the Compton edge and the high energy tail is approximated by a gaussian fit. The light yield of the In-scintillator in Fig. 4.16 is 44 % of BC505. In some cases the light yield was measured using a digital oscilloscope instead of the VME system. Here the PMT pulse was integrated and a histogram of the results was plotted on the screen. From this

[1]Bicron BC505 (also known as NE 224) is a product of the Compagnie de Saint-Gobain, Paris, France available through Saint-Gobain Crystals and Detectors. It has a light yield of 80 % relative to the light yield of anthracene and maximum emission at 425 nm.

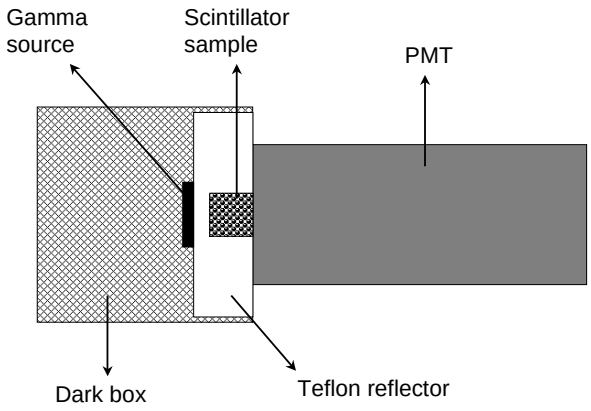

Figure 4.14: *A simple drawing of the setup used for the light yield measurements is shown.*

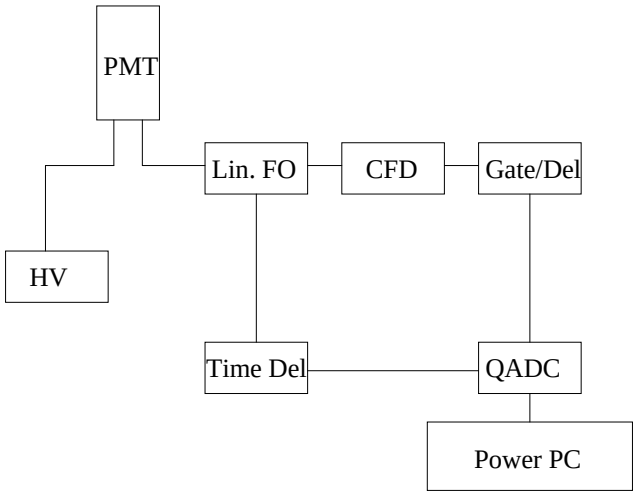

Figure 4.15: *Electronic circuit used for the light yield measurements.*

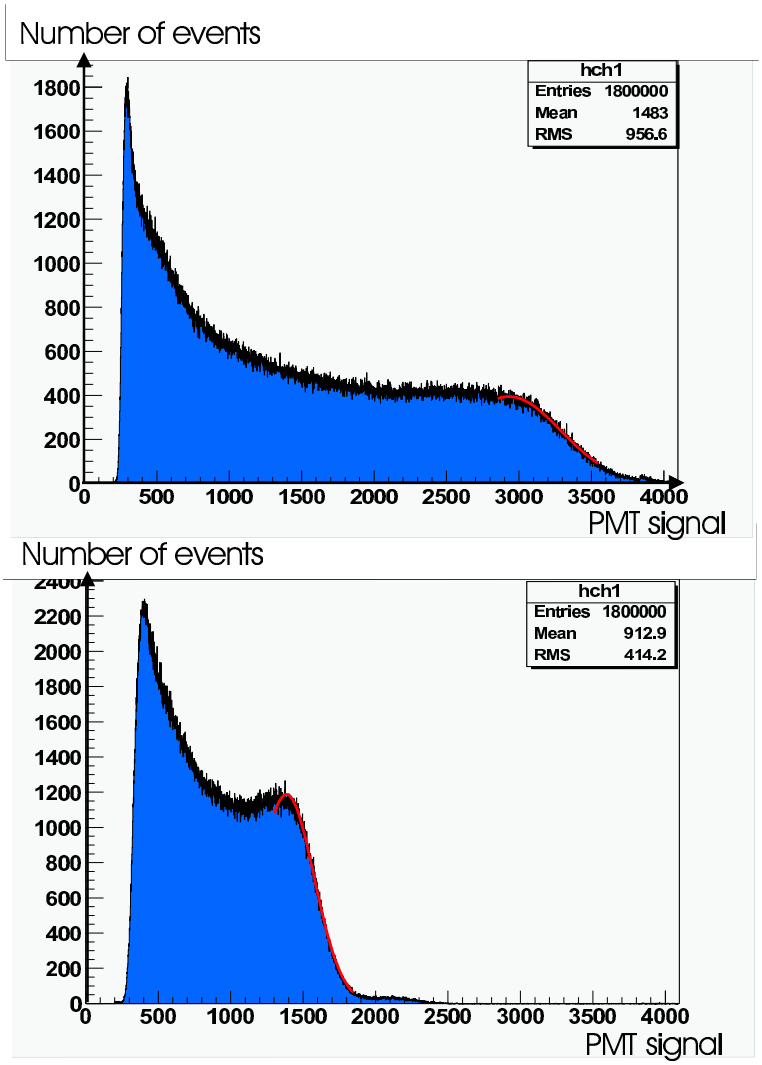

Figure 4.16: *Compton spectra of BC-505 (top) and a 7 wt.% loaded In-LS (bottom) under irradiation with a ^{137}Cs source measured in a 1 cm cell. For the In-loaded scintillator one can see a little photopeak above the Compton edge due to the higher Z of In compared to the other elements in the scintillator.*

histogram the Compton edge was estimated and compared to a standard. It will be explicitly mentioned in this thesis when this less precise method was used.

Before the scintillator samples were irradiated with the ^{137}Cs source to create a light pulse they were sparged with N_2 for 5 minutes and filtered if needed. The measurements were started approximately 5 minutes after the high voltage (HV) was turned on. It was tried to keep this time period constant for all measurements to avoid drifting effects of the HV after some time or a possible oxygen pickup in the sample.

4.4.2 Standards

In order to check the stability of BC505 and for a better comparison with results obtained in other groups using different standards additional standards are regularly used. A standard of 5 g/l BPO in pseudocumene and the BC505 are cross-checked with colleagues at the Laboratori Nazionali del Gran Sasso, Italy. The light yield of the PC/BPO standard was measured to be 8 % to 10 % higher than BC505. Another standard used is the 'Borexino mixture' of 1.5 g/l PPO in pseudocumene. The yield of this standard is approximately 5 % lower than BC505. In these mixtures pseudocumene of the Borexino experiment was used. Mixtures based on this pseudocumene have significant higher light yields than scintillators using 'commercially' available pseudocumene.

In most cases the unloaded version of the In-loaded scintillator mixture was used as a standard since the comparison of the two directly shows the effect of the In-material on the light yield. For the case of PPO as a fluor the values were compared to a solution of 6 g/l PPO in anisole. At this concentration the light yield is (77 ± 2) % compared to the BC505 standard. The error is estimated from repeated measurements and represents the typical relative error in these measurements for light yields in that region. For 6 g/l BPO in anisole the light yield is (89 ± 2) % compared to the BC505 standard.

Anisole samples of different companies were tested and compared to each other. Anisole from the Fluka company showed the same light yield at 6 g/l PPO as a sample obtained from Aldrich (99%). Both were measured to be (75 ± 2) % BC505. Together with these two samples a third sample (Aldrich 99%+) was tested. Here the result was (70 ± 2) %. This sample had a broad bump around 500 nm in the absorption spectrum indicating the presence of some impurities.

No significant effect on the light yield of the scintillator is observed when the anisole is purified with the Al_2O_3 column. In general the reproducibility of the results using different anisole batches is high.

4.4.3 Fluor variation

As seen in the previous chapter the fluor choice and concentration has a major impact on the light yield of the highly In-loaded scintillators. The light yield under irradiation with the γ-source was measured for several fluors with and without the addition of bis-MSB. Table 4.1 summarizes the main results for these fluor variations. A wide range of useful light yields are found. For the case of a 5 wt.% In-loaded scintillator the light yield is (35 ± 2) % compared to BC505 at 200 g/l PPO and 500 mg/l bis-MSB. At a weight concentration of 100 g/l of primary fluor and 200 mg/l bis-MSB approximately 10 % more light using butyl-PBD instead of PPO (at 5 wt.% In) results. Using BPO at the same weight concentration a light yield of (51 ± 2) % BC505 is measured without any additional secondary wavelength-shifter; a result

which is more than a factor two higher than the value obtained using PPO at the same weight concentration. With bis-MSB in addition to BPO, only a small increase in the light yield is observed, but as shown in section 4.3.3 the emission is shifted to longer wavelengths.

fluor	wt. conc. [g/l]	In-conc. [wt.%]	bis-MSB	light yield
BPO	100	4.7	–	51 ± 2 %
BPO	100	4.6	200 mg/l	52 ± 2 %
BPO	150	7	–	44 ± 2 %
Butyl-PBD	100	4.6	–	20 ± 1 %
Butyl-PBD	100	4.4	200 mg/l	29 ± 2 %
PPO	100	5.0	–	19 ± 2 %
PPO	100	4.8	200 mg/l	26 ± 2 %
PPO	200	4.8	500 mg/l	35 ± 2 %
PMP	100	5	–	< 5 %

Table 4.1: *Light yield of In-loaded scintillators relative to a BC-505 standard for varying fluor combinations.*

One can convert the unit of the In-concentration given in weight percent into grams per 100 ml by multiplying the number in the table by the density. The density of one scintillator, (BPO + bis-MSB), entry two in Table 4.1, was determined by measuring the weight of a thin glass cylinder first filled with water and then filled with the scintillator at the same level. From the difference of these values the calculated number for the density is 1.044 kg/l illustrating the typical value for this kind of scintillator.

All other fluors tested had lower solubility and/or lower light yields than the fluors mentioned above. PBD was compared to PPO at the maximum possible fluor loading for PBD which is 30 g/l. These measurements were done with the digital oscillscope. At a In-loading of 1 wt.% the light yields obtained in a PBD system were 10 % to 20 % higher than in a PPO system. The relative improvement is similar in PBD-systems that contain bis-MSB in addition. In a 5 wt.% In-loaded scintillator at 30 g/l PBD and no bis-MSB, the yield is 13 % relative to BC505.

Several systems containing p-Tp or PMP as fluor were also investigated. The light yields found were a factor two or more below that of PPO at the same weight concentrations. In the case of p-Tp this could be due to the fact that it emits photons at lower wavelengths than PPO. Therefore there is a larger overlap between the fluor emission with the $In(acac)_3$ absorption resulting in a higher energy transfer from the fluor to the In-material. PMP has an unusually large Stokes shift [DES89]. It absorbs (peak at 295 nm in cyclohexane) at shorter wavelengths than PPO or BPO, but emits at higher wavelengths (peak at 425 nm) than PPO. One of the reasons that the light yield in the PMP system is so low relative to PPO or BPO could be due to the fact that its absorption band is closer to the $In(acac)_3$ absorption band. In the BPO or PPO system the maximum of the overlap integral between the anisole emission and fluor absorption spectra is at higher wavelengths compared to the PMP system and therefore well separated from the $In(acac)_3$ absorbance. Another reason for the lower light yield of the PMP system could be the longer decay time of the excited PMP molecule. In summary, as expected from the fluorescence measurements the highest

light yield is obtained using BPO as fluor.

4.4.4 Light yield at varying fluor concentrations

The light yield variations at varying fluor concentrations were mainly investigated for the fluors PPO and BPO. At a typical concentration of 6 g/l PPO in anisole the light yield drops with the addition of $In(acac)_3$ at an In-concentration of 1 wt.% to about 20 % compared to the unloaded scintillator. The light yield increases with increasing PPO-concentration. Higher PPO-concentrations increase the overall energy transfer rate to the PPO component and therefore the light yield. Additionally, there are more directly excited primary fluor molecules. For a loading of indium at 1 wt.%, scintillator light yields of more than 50 % BC505 could be reached by adding primary fluors to levels of 100 g/l PPO and secondary fluors to 500 mg/l bis-MSB. The results of the measurements at 1 wt.% In-loading, varying PPO-concentrations and no bis-MSB are listed in Table 4.2. In the same table results of light yield measurements of the same samples using the fluorimeter in front face geometry are given. The scintillators were excited at the anisole maximum absorption of 271 nm and at the PPO-absorption of 303 nm. For excitation at 303 nm the curve is steeper. At this wavelength there is still strong anisole absorption, but at increasing PPO-concentrations the number of PPO molecules excited directly increases leading to more light. The fluorimeter numbers in Table 4.2 correspond to the fluorescence spectra integrated over the wavenumber. The value at 48 g/l was set arbitrary to 36 for a better comparison with the results of the source measurement. A similar shape of the light yield curve is observed for the fluorimeter and the γ-source measurements. The 1 wt.% In-loaded scintillator was essentially investigated to learn about the system.

PPO concentration [g/l]	6	12	24	48
Light yield (source) [%][1]	15	22	31	36
Light yield (fluorimeter) [a.u.]	13	21	29	36

[1] Light yield versus BC-505 using a ^{137}Cs source.

Table 4.2: *Light yield measurements at 1 wt. % In-loading and varying PPO concentrations. The numbers determined with the fluorimeter (271 nm excitation) are given in arbitrary units. The value at 48 g/l PPO is set to 36 as the value of the source measurement for better comparison.*

The goal in the scintillator development presented here is an In-loaded scintillator with 5 wt.% In-loading. Therefore, as a next step, the light yield was measured at varying PPO-concentrations for a constant In-concentration of 5 wt.%. In Fig. 4.17 the experimental light yield relative to the BC505 light yield is plotted versus the fluor concentrations c (here in grams per liter anisole). In fact, for the lower curve in Fig. 4.17 the In-concentration was somewhat diluted by the addition of the PPO. At low PPO-concentrations the In-loading was 5 wt.% and dropped to 4.1 wt.% at 200 g/l. This could be the reason for the little difference between the last point on the lower curve and the first point on the upper curve (bis-MSB variation) which had a 5 wt.% In-loading. Unsublimed $In(acac)_3$ was used in the set of measurements at varying PPO-concentrations. It seems that the sublimation mainly

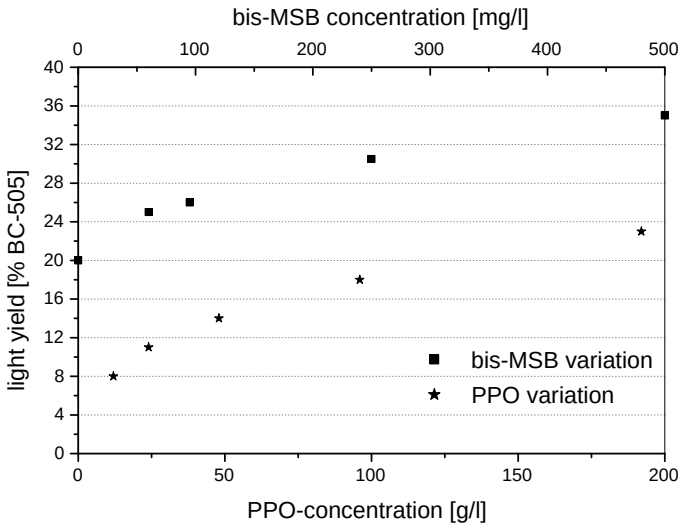

Figure 4.17: *Light yield for a 4.1 wt.% In liquid scintillator as a function of PPO weight concentration up to 200 g/l, no bis-MSB (bottom axis) and for a similar 5.0 wt.% In scintillator with PPO fixed at 200 g/l and increasing bis-MSB concentration (top axis).*

affects the optical transparency of the sample and has only a minor effect on the light yield.

For the case of no PPO the light yield is zero. From that there is a rapid increase in light output followed by a tendency towards leveling off. For the larger fluor concentrations self-quenching is seen to occur. Despite this, the light still increases with increasing fluor concentration because the more dominant effect of the $In(acac)_3$ quenching is still being overcome.

Higher light yields are obtained using BPO as fluor. The experimental results of the measured light yield curves at varying BPO concentrations are discussed in the next section together with the theoretical predictions of the models.

4.4.5 Light yield at varying In-concentrations

To increase the scintillator light yield the In-concentration could be lowered. A lower In-concentration would on the other hand increase the size and cost of an In-detector. The dependence of the light yield on the In-concentration was determined in a set of measurements in which the BPO concentrations were kept constant at 100 g/l. The results of these measurements are shown in Fig. 4.18. The light yield is given in percent of the unloaded scintillator at a BPO-concentration of 100 g/l (72 % of BC505). There is approximately a linear relationship between the light yield and the In-concentration above 1 wt.% In-loading. A faster decrease is observed between the unloaded scintillator and 1 wt.% In-loading.

One sample was tested at a In-concentration of 7 wt.% which is close to the solubility limit in anisole. In this measurement a different BPO concentration of 150 g/l was used and therefore this data point is not included in Fig. 4.18. A light yield of 44% relative to BC505 was measured (62% compared to 100 g/l BPO in anisole). If the data points are fitted by a straight line the additional data point at 7 wt.% indium is above the fit line which is expected

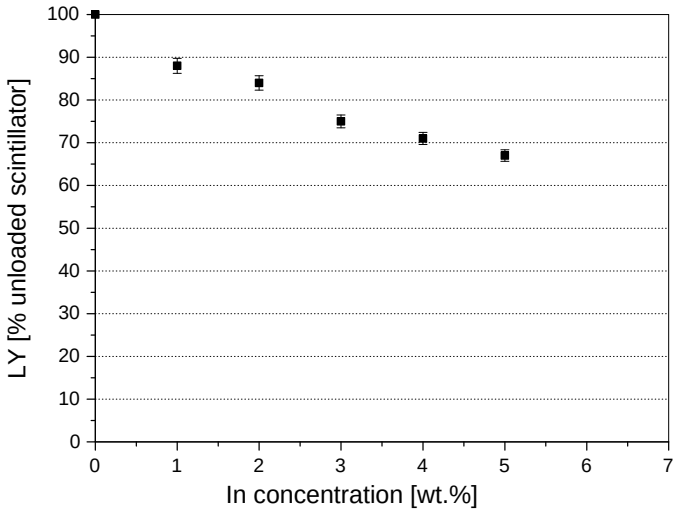

Figure 4.18: *Light yield (LY) relative to the unloaded scintillator as a function of the In concentration. The fluor (BPO) concentration was kept constant at 100 g/l.*

due to the higher BPO concentration. These measurements combined with the theoretical model described in the following section allows to calculate the light yield at every given indium and BPO concentration.

4.5 Comparison with theory

4.5.1 In-free scintillator

Fig. 4.19 is a plot of the experimental data of the light yield of an In-free liquid scintillator with varying PPO-concentrations. The solvent is anisole and the light yield was measured in a 1 cm cuvette under irradiation with a ^{137}Cs-source as described previously. There is a steep increase at low fluor concentration until a plateau is reached at a PPO-concentration of about 5 g/l.

The data set is fitted by some of the models presented in Chapter 2. The best fit was computed by finding those values of the free parameters that minimize the sum of the squares of the deviations of the theoretical curves from the experimental data points weighted by the error bars (χ^2). The χ^2 is minimized by an algorithm[2] that starts from initial parameter values and performs a series of iterations on the parameter values. In Table 4.3 the two free parameters in the fit, the saturation value of the light yield (I_0) and the critical concentration (c_0), are given as obtained by the fit. Additionally the chi squares are listed. All the models give good fits to the data points. The model by Stern Volmer is less good than the other ones by Perrin and Förster, especially because the saturation is already reached at 6 g/l. This model would expect a further increase. The most advanced model by Förster gives a very good fit to the data. For this fit only the first five data points were used. In this model the

[2]The computer program used for the fitting uses the Levenberg-Marquardt algorithm [PRE88]

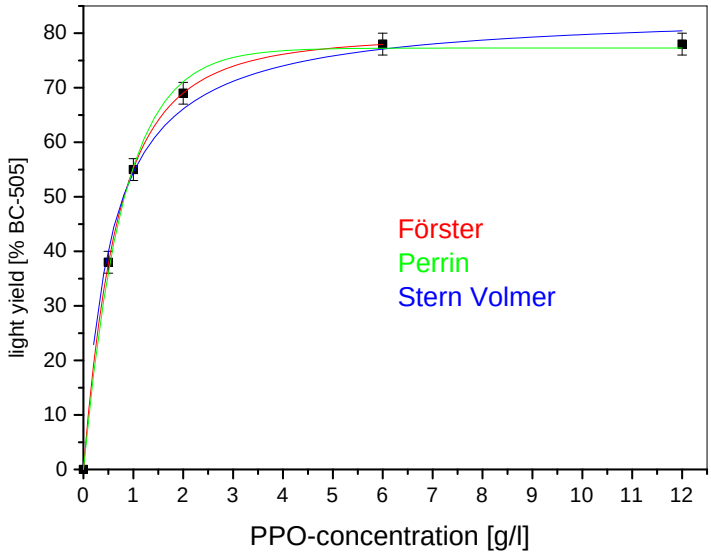

Figure 4.19: *The experimental data points of the light yield in percent (relative to BC505) are shown for an In-free scintillator at varying PPO concentrations (solvent anisole). The curves are fits to the data of the models of Perrin (green, top curve at 3 g/l PPO), Förster (red, middle curve at 3 g/l PPO) and Stern Volmer (blue, bottom curve at 3 g/l PPO).*

critical concentration is at a PPO-concentration of 1.11 ± 0.01 g/l.

model	χ^2	I_0	c_0 [g/l]
Perrin	0.56	77.3 ± 1.0	0.79 ± 0.04
Stern Volmer	1.71	84.1 ± 2.3	0.54 ± 0.07
Förster	0.005	79.57 ± 0.14	1.11 ± 0.01

Table 4.3: *The quality of the fit, the critical concentration c_0 and the asymptotic value for the light yield in % BC-505 are given.*

However, none of these models includes the self-quenching that occurs at high fluor concentrations. Self-quenching is related to the formation of a double molecule or occurs after the collision between two fluorescent molecules. To investigate this effect in more detail the light yield was measured at PPO-concentrations up to 200 g/l. For this set of measurements the fluorimeter was used in the front face geometry since this method is faster compared to the measurements with the γ-source and gives similar results. As solvent for the PPO anisole was used. The light yield was determined by integration of the emission spectrum.

In Fig. 4.20 eleven data points are shown together with a fit using the extended Kallmann model (including direct excitation of the fluor). In this model there are four free parameters. The χ^2 of the fit is 0.21. Some of the data points were measured twice in an independent set of measurements and the average value is given in the Figure. The errors were estimated

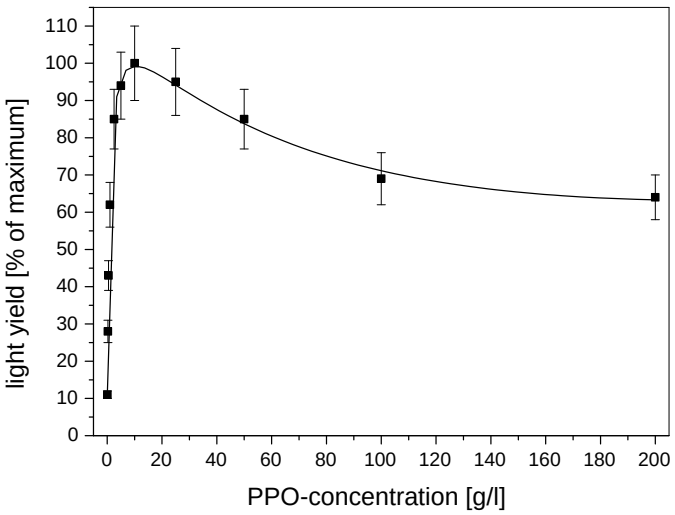

Figure 4.20: *The light yield in percent of the maximum value at 10 g/l is shown for an In-free scintillator at varying PPO concentrations (solvent anisole). The data points which are measured with the fluorimeter in front face geometry are fitted by the extended Kallmann model.*

from the variations in these two measurements. At a PPO-concentration of 200 g/l the light yield drops to approximately 65% of the maximum at 10 g/l.

A similar curve with less data points was measured with BPO instead of PPO using the γ-source. The maximum of the light yield is reached at a BPO-concentration of approximately 5 g/l and above. Also in this system self-quenching was observed. The light yield at 100 g/l BPO is 80 % of the maximum. The modeling of scintillator systems containing indium will be discussed next.

4.5.2 In-loaded scintillator

The In-loaded scintillator system is more complicated compared to the In-free scintillator system since there are two acceptor molecules. In Fig. 4.21 the light yield is plotted at varying fluor concentrations with a constant In-concentration q. For the upper curve the In-concentration is kept at 2 wt.% In and for the lower one the concentration is 5 wt.% In. The curves show the same characteristics as the PPO-curve presented in the previous chapter, but saturation is reached at much higher fluor concentrations.

In this system the useful light is mainly due to excitation of the primary fluor acceptor (A) by energy transfer from the solvent (anisole) donor molecules (D), $D^* \rightarrow A^*$. The In ('quencher' Q) concentration q enters the situation by opening up an energy quenching pathway, $D^* \rightarrow Q^*$. This possibility is closed by adjustment of the concentration c of the acceptor A molecules. In this system the processes $D^* \rightarrow A^*$ (rate constant k) and $D^* \rightarrow Q^*$ (rate constant k') dominate over spontaneous D^* emission, λ_D. If direct fluor excitation and self-quenching of the fluor are neglected the probability for energy transfer from D^* to the

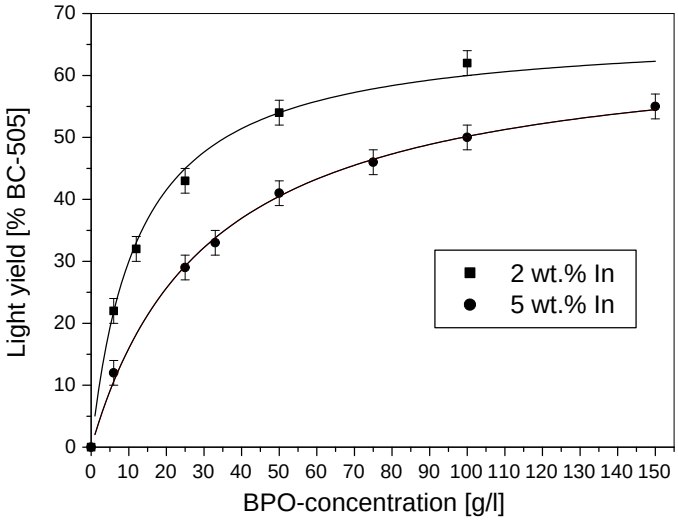

Figure 4.21: *Light yield for a 5 wt.% and a 2 wt.% In liquid scintillator as a function of BPO concentration. Both curves are fitted by the model as described in the text. For the 2 wt.% fit the ratio of the energy transfer constants determined in the 5 wt.% data fit was used to predict the shape of the measured curve.*

acceptor (fluor) can be expressed by the ratio

$$r = \frac{kc}{(\lambda_D + kc + k'q)} \tag{4.7}$$

If the contribution of λ_D is neglected an equation can be derived describing the light output curve at varying fluor concentration c:

$$I = I_0 \cdot \left(\frac{1}{1 + K \cdot \frac{q}{c}} \right) \tag{4.8}$$

where I_0 is the light output in the limit of large c and K is the ratio of energy transfer rates (k'/k). The use of rates is similar to the spirit of the Stern-Volmer equation. A similar equation would also be obtained in the Kallmann model when fluor quenching is neglected. The equation gives a good fit to the data at 5 wt.% In-loading ($\chi^2 = 0.17$). To check if the model gives also good predictions for other concentrations the ratio of energy transfer rates K obtained from the 5 wt.% curve fit was used as a fixed parameter in the 2 wt.% curve. Again a good fit was obtained ($\chi^2 = 0.57$).

At a low acceptor concentration in the light curves, the ratio (q/c) is high and the quenching pathway is flooded leading to no light output. For an 'infinite' c, on the other hand, there is no effective quenching by the indium material, so that the light from D* →A* in this case rises to the maximum I_0. From the fits we get an I_0 of (65.9 ± 1.3) % relative to BC505 for the 5 wt.% curve and (67.5 ± 1.0) % for the 2 wt.% curve which is close to the value of the In-free scintillator at 100 g/l BPO loading of approximately 70 %.

There is a point where $I = I_0/2$ and $K \cdot \frac{q}{c} = 1$. In this case the rates of the quenching and the acceptor pathways are equally at play. From the fit of the curve at 5 wt.% In-loading (0.44 M) one finds that this is the case at a BPO-concentration of 31 g/l (0.10 M). The lower molarity of the fluor at that point demonstrates that energy is transferred more easily to the BPO than to the In-material. To the left of this point at lower fluor concentrations the quenching path begins to dominate and the light yield drops. Increased values of the critical concentration c_0 compared to the unloaded scintillator are indicative of the need to overcome the quenching rate.

4.5.3 Critical transfer distances and critical concentrations

With the absorption and the normalized emission spectra of the relevant components one can calculate the critical distances R_0 for the resonant non-radiative energy transfer via the dipole–dipole interaction using the formulas of chapter 2. The results for a system with anisole as donor molecule are summarized in Table 4.4.

component	J [10^{-14}cm^6/mol]	R_0 (Förster) [nm]	$c_{0,calculated}$ [mmol/l]	$c_{0,exp}$ [mmol/l]
In(acac)$_3$	0.70	2.5	26	
BPO	2.3	3.0	15	
PPO	2.2	3.0	15	5.02 ± 0.05

Table 4.4: *The overlap integrals J, the critical distances R_0 and the critical concentrations $c_{0,calculated}$ calculated according to Försters model for ansiole as donor and In(acac)$_3$, PPO and BPO as acceptors are listed. Additionally the experimentally observed critical concentration $c_{0,exp}$ for PPO is given.*

For PPO the calculated value is a factor of 3 above the one determined experimentally. One expects a lower number for c_0 in the experiment compared to Försters theory for two reasons. First, Försters model explains only energy transfer due to dipole-dipole interaction. At the used concentrations the excited donor molecule is often close enough to the acceptor molecule that the exchange interaction becomes relevant. This results in faster transfer rates than those predicted by the Förster theory. Second in his model donor and acceptor molecules are both diluted in an inert medium. In the system discussed here the donor molecules are the molecules of the solvent itself and are present in high concentrations. Therefore energy 'hopping' between the donor molecules has to be included which also increases the transfer probability to the acceptor.

At the In(acac)$_3$–concentrations used (in the range of 0.4 mol/l) one finds on average one molecule in a volume of 4 nm^3. This means that the distance between two In(acac)$_3$–molecule is in the order of 1.5 nm which is a factor two below the critical transfer distance. Therefore significant energy transfer from the solvent to the In(acac)$_3$ is expected at these concentrations.

The critical distances were also calculated for bis-MSB as acceptor and the fluors PPO and BPO as donors. The results are listed in Table 4.5. As observed in the experiment the critical distance is longer corresponding to a better energy transfer in a PPO/bis-MSB system as compared to a BPO/bis-MSB system. The calculated critical concentrations correspond to approximately 1 g/l bis-MSB in the case of PPO and 2 g/l bis-MSB in the case of BPO.

fluor	J [10^{-14}cm^6/mol]	R_0 (Förster) [nm]	$c_{0,calculated}$ [mmol/l]
BPO	2.7	3.8	7
PPO	5.4	4.3	5

Table 4.5: *Critical distances and concentrations calculated according to Försters model for bis-MSB and two fluors as acceptors.*

Non-radiative transfer was already observed experimentally at lower values. This effect can also be explained by the limitations of Försters model.

4.6 Long term stability of the optical properties

One of the main motivations for the In(acac)$_3$ approach is the expected stability of the scintillator. Long term stability tests of the optical properties light yield and attenuation length were performed. Typically the stability of the attenuation length is more critical than the stability of the light yield. The handling of the sample has a large impact on its optical properties. Therefore it is in some cases hard to distinguish whether a degradation of the scintillator performance is due to improper handling or due to intrinsic instability of the scintillator.

To test the stability of the light yield a sample (approximately 5 ml) was prepared with 5 wt.% In-loading and a BPO-concentration of 150 g/l. The sample was stored in a glass vial and flushed with nitrogen after each measurement. For the measurements the sample had to be transferred to the quartz cuvette. In this step there is always the risk to catch up some contamination, therefore this measurement was done only few times in large lags. In the test period of 15 months only a minor decrease in the light yield was observed. The results of the four measurements are listed in Table 4.6. In the first measurement the light yield was (53.0 $\pm$ 2.0) % relative to the BC505 standard. The value measured after 15 months was (50.5 $\pm$ 2.0) % relative to the BC505. This demonstrates that even at the high fluor concentration used, the light yield of the In(acac)$_3$-loaded scintillator is stable.

date	8 Nov.'02	26 Mar.'03	25 Nov.'03	3 Feb.'04
Light yield	53.0 $\pm$ 2.0	53.5 $\pm$ 2.0	49.5 $\pm$ 2.0	50.5 $\pm$ 2.0

Table 4.6: *The light yield of a 5 wt.% In-loaded scintillator relative to BC-505 and the date of the measurement is given. The BPO-concentration in this scintillator is 150 g/l.*

The stability of the attenuation length was tested for several samples. In Fig. 4.22 the time dependence of the attenuation length at 430 nm is plotted for several In-loaded samples. To avoid contamination due to liquid handling the samples were stored under N_2 atmosphere in 10 cm quartz cuvettes which are used in the photospectrometric measurements. As a baseline air was measured versus air to obtain reproducible conditions in the measurements. The absorbance of the empty cuvette was determined before the cell loading and subtracted from the absorbance of the filled cell. The absorbance was assumed to be zero at the minimum of the resulting spectrum.

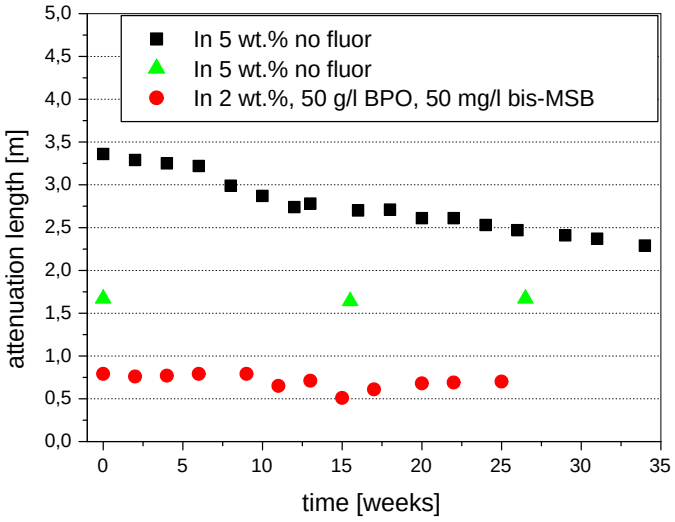

Figure 4.22: *The time dependence of the attenuation length at 430 nm is plotted for several In-loaded solutions.*

Two 5 wt.% In-loaded samples were investigated using In-material from different synthesis batches. As solvent anisole was used and no fluors were added to the solution. The attenuation length of one of the solutions (squared symbol in Fig. 4.22, batch 1) was originally measured at 3.3 m (430 nm). This number includes the contribution of the solvent to the absorbance. In this sample the measured attenuation length slightly decreased over time. The reduction was approximately 2 cm to 3 cm per week. After 8 weeks there seemed to be a systematic difference to the measurements before, since there was a small offset in the spectrum compared to previous measurements accompanied by a more rapid decrease in the transparency. This effect could be due to changes on the surface quality of the cuvette and demonstrates the sensitivity of the measurement to changing conditions. However, there seems to be a constant intrinsic decrease in the transparency of this solution. A similar sample of 5 wt.% In in anisole showed no change in the attenuation length over more than 25 weeks (triangular symbol, batch 2). This sample had an original attenuation length of 2.4 m. After 20 weeks the attenuation length dropped to 1.6 m, however in that time period the sample was not stored in the quartz cuvette. Therefore this change can be due to wrong storage or handling of the sample. After it was loaded into the 10 cm cell (zero point in Fig. 4.22) the attenuation length stayed constant at 1.6 m. Another possibility for the primary variation can be the reaction of trace impurities in the solution resulting in the formation of absorbing material.

To investigate the influence of the fluors on the scintillator stability a sample containing 2 wt.% In, 50 g/l BPO and 50 mg/l bis-MSB was also studied (circled symbol). The attenuation length of this scintillator composition was initially 0.79 m at 430 nm (dominated by the fluor absorbance). During the test period of approximately half a year there were some variations of instrumental origin, but the attenuation length remained stable in the 0.7 m region.

In summary, even at the high In-concentrations in the few percent range the solutions

remained rather stable over time. The reasons for the observed variations in some of the samples can be manifold. The tests have shown that long term stability of light yield and attenuation length can in principle be achieved, but a careful handling of the sample is mandatory. In general, it is more difficult to test the stability on small scales compared to large samples that are observed continuously and kept under unchanged conditions. Therefore, the ultimate stability test will be the prototype measurement described in the following chapter.

Chapter 5

Prototype measurements

5.1 Background measurements in the LLBF

The final scintillator test is a measurement in a prototype detector. This prototype has to be in a radiopure environment. For that purpose the LENS Low Level Background Facility (LLBF) was constructed in the underground laboratory at Gran Sasso. A drawing of the LLBF is shown in Fig. 5.1. It consists of a passive shielding system of about 80 tons and was setup in a cleanroom. The inner volume is 70 cm × 70 cm × 400 cm. Radiation from the surrounding rocks and materials are absorbed by three layers: 20 cm polyethylene, 23 cm steel and 15 cm of electrolytically refined copper. External radiation is shielded by the LLBF equivalently to about 3 m of water. After the copper production the time of exposure of the material to cosmic rays was minimized. The copper was analyzed with the GeMPI detector at Gran Sasso [NED00] and new purity records were achieved: $^{238}\mathrm{U} < 2 \cdot 10^{-12}$ g/g (determined from $^{226}\mathrm{Ra}$), $^{232}\mathrm{Th} < 7 \cdot 10^{-12}$ g/g, $^{40}\mathrm{K} < 4 \cdot 10^{-9}$ g/g and $^{60}\mathrm{Co} < 11$ μBq/kg [HEU03]. The detector system can be mounted on a copper floor that can be moved in and out of the shielding with the help of a removable train working with air pressure. A system for radon removal was hooked up and background measurements were performed inside the shielding.

5.1.1 Radon

Radon and other radioactive gases present in the inner volume of the shielding are removed by nitrogen (N_2) flushing. The nitrogen flow is monitored by flowmeters at the inlet and at the outlet. Nitrogen bottle packages of 12 or 16 bottles (each 50 l volume) connected in series are used. In the beginning the bottles are pressurized up to 200 bar, so that each bottle contains 10 m^3 of gas at standard conditions. In saturation the typical ^{222}Rn-activity in one bottle is in the range of 0.5 mBq [BUC01]. Therefore the activity in the nitrogen would be approximately 50 μBq/m^3 for a full bottle. This is about 6 orders of magnitude below the ^{222}Rn activity in the underground lab and low enough for the current purpose of the LLBF.

In Fig. 5.2 the ^{222}Rn-activity A versus time t is plotted during the N_2-flushing at a flux of 300 l/h. Due to air leakages in the shielding the flux at the outlet was approximately half of the inlet flux. The main leaks were probably at the feed throughs for the electronic cables of the detector which were sealed using silicon sealant. Another source of air leaks are the two big top flanges of the LLBF. The leaks are not that critical for the background, because the volume is flushed continuously. This means that there is always a slight overpressure in the shielding reducing the radon diffusion from the outside to the inside.

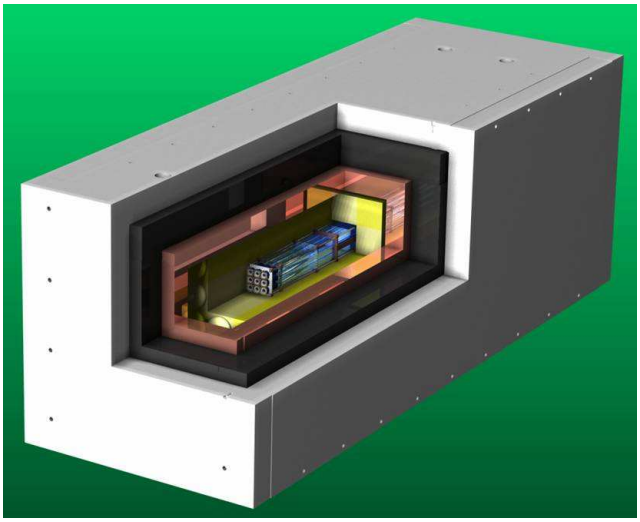

Figure 5.1: *The cutaway view shows the different layers of the LENS Low Level Background Facility (LLBF): 20 cm polyethylene, 23 cm steel and 15 cm copper.*

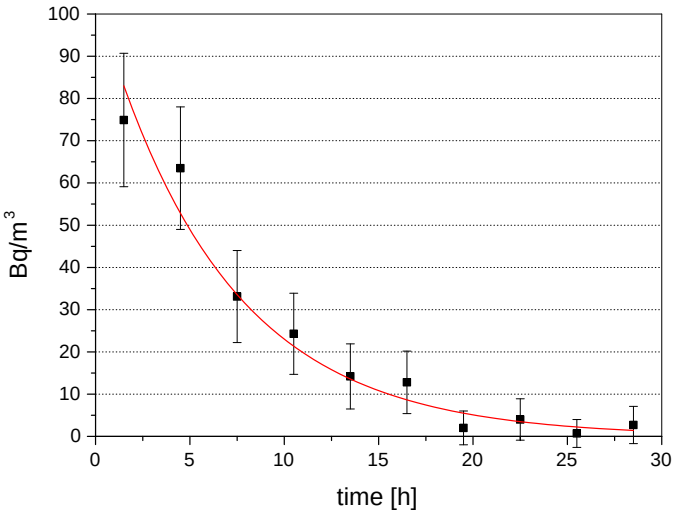

Figure 5.2: *^{222}Rn activity in the LLBF at a flux of 300 l/h measured with a commercial Rn-monitor.*

The data show that the N_2-flush adequately lowers the Rn-activity. The data points in the plot of Fig. 5.2 are fitted by an exponential decay. The best fit is obtained by the equation

$$A(t) = 104 \cdot \exp\left(-\frac{t}{6.6}\right)$$

From the fit one gets a 'decay time' of (6.6 ± 1.1) h. Assuming perfect mixing one would assume that the activity decreases by a factor e after one volume exchange if one neglects the radioactive decay of the radon during that time period. The inner volume is approximately 2 m^3 which matches with the total amount of N_2 flushed into the LLBF after 6.6 h.

In this measurement the activity was determined in every three hours using a commercial Rn-monitor. The first data point was set at 1.5 h after the start of the flushing although it was obtained three hours after starting, because the measured activity is integrated over the last three hours. To improve the sensitivity of the Rn-monitor the time period for one cycle was increased. In that mode the final activity stayed below 1 Bq/m^3 which is the maximal sensitivity of the instrument.

5.1.2 Background measurement using a Ge-detector

The background inside the LLBF shielding system was first measured with a high purity Ge-detector. For this measurement the whole detector was placed inside the shielding during the measurement. A dewar containing liquid nitrogen (LN_2) for the detector cooling was also placed inside the shielding. To reduce the background signal created by the dewar, a shielding was mounted between the detector and the dewar. Next to the detector a 15 cm thick wall was constructed out of radiopure copper bricks. The copper was stored underground for several years. Therefore the background due to cosmogenic activation is low. An additional shielding of 10 cm lead (also material of low radioactivity) was mounted on the dewar side.

The LN_2 had to be refilled at least once per week. This procedure could be done during the measurement without opening the shielding. There was a connection from the dewar to the outside of the shielding. Inside the LLBF a silicon tube was used and outside a steel pipe could be connected to an external LN_2 dewar. The nitrogen was refilled using overpressure in the mobile outside dewar. The temperature below the top cap of the dewar was monitored using a PT100. When the dewar was filled up, the PT100 was in contact with LN_2, so the temperature was at -197 °C. At a lower nitrogen level the sensor measured the temperature of the gas phase above the liquid, which was approximately 10 °C above liquid nitrogen temperature.

The inner volume of the LLBF shielding was continuously flushed with N_2-gas during the measurement. To avoid overpressure of more than 200 mbar corresponding to a force of 10000 N on the top flanges, the pressure inside the shielding was monitored with a manometer. Small flanges were prepared with suitable feed throughs for all cables and connections.

In Fig. 5.3 the Ge-spectrum measured inside the shielding is shown together with a measurement taken outside the shielding. The spectrum measured without shielding has the features of a typial Ge-spectrum with the outstanding Compton edges and lines of ^{208}Tl (2.615 MeV) and ^{40}K (1.461 MeV). The detector measured outside for 22 h and inside the LLBF there were 21.8 days of 'good' data taking. The first one or two days after the closing of the shielding and after the exchange of the nitrogen bottles were not used in the analysis, because in these periods the background was dominated by the daughters in the ^{222}Rn and ^{220}Rn chains.

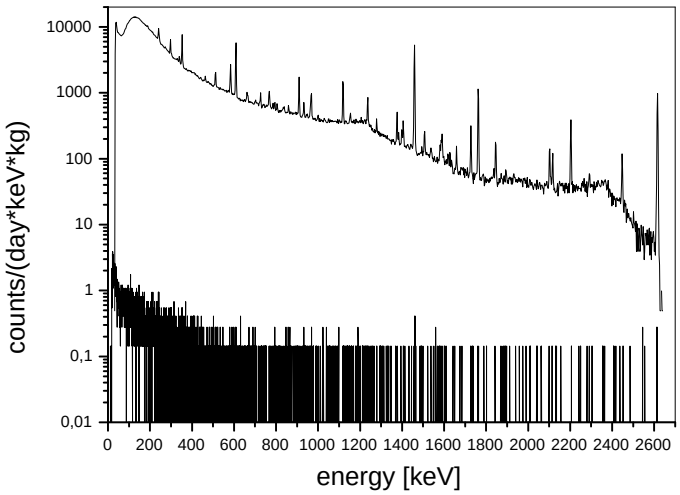

Figure 5.3: *Germanium spectrum measured inside the LLBF shield (21.8 days) compared to the spectrum without shield.*

From the measurements a reduction factor of at least 10^4 is found for the continuum and of more than 10^5 for the lines. In the energy range between 400 keV and 2600 keV the background signal was 4 counts/(kg y keV). This is nearly a factor two below the value given for the intrinsic background of the detector [HMO02] demonstrating that it was the best shielding the detector has ever had. In the range 2000 keV to 2080 keV six counts were detected in the 21 days corresponding to an activity of 1.5 ± 0.6 counts/(kg y keV). This number can be compared to a background of 0.19 ± 0.01 counts/(kg y keV) [HMO01] in the Heidelberg–Moscow germanium $\beta\beta$-experiment in the same energy window.

In Table 5.1 the event rates for some characteristic lines are summarized. The assumed internal background of the detector is also given in that Table. All numbers above 400 keV are within the errors consistent or below the values for the background, except for ^{40}K which is 3 σ above. There are several possibilities for the increased count rate for ^{40}K which do not involve the LLBF shielding material itself. It could be due to the additional shielding against the dewar, or due to the transport system of the floor which was inside the shielding during the measurement. The counts in the ^{208}Th line could be due to residual ^{212}Pb ($T_{1/2} = 10.6$ h) from the ^{220}Rn decay chain.

5.1.3 Background measurement using a liquid scintillator

Setup

In a next phase the background of an In-free liquid scintillator inside the shielding was measured. For this measurement the quartz (Herasil 102) cells which were foreseen for an In-loaded prototype detector were used. The quartz cells have been designed in collaboration with Heraeus (Hanau) and Hellma (Müllheim). Neutron activation analysis showed that the radiopurity of the quartz is high: U $< 1 \cdot 10^{-12}$ g/g, Th: $26 \cdot 10^{-12}$ g/g and K: $45 \cdot 10^{-9}$ g/g [HEI02]. The radiopurity was one of the reasons why quartz was used as cell material. An-

Isotope	Energy [keV]	LLBF [c/d]	Background [c/d]
^{214}Pb	352	1.1 ± 0.2	0.55 ± 0.09
e^+e^-	511	0.28 ± 0.11	0.74 ± 0.10
^{214}Bi	609	0.21 ± 0.11	0.35 ± 0.07
^{137}Cs	662	0.32 ± 0.12	0.50 ± 0.09
^{228}Ac	911	0.18 ± 0.09	0.27 ± 0.06
^{60}Co	1173	< 0.15	1.32 ± 0.11
^{60}Co	1333	< 0.1	1.36 ± 0.12
^{40}K	1461	0.64 ± 0.17	0.14 ± 0.05
^{208}Tl	2616	0.32 ± 0.12	0.19 ± 0.05
integral	$100 - 400$	69 ± 8	49
integral	$400 - 2700$	26 ± 1	46

Table 5.1: *Count rate per day in the LLBF Ge measurement at selected energies and intrinsic background count rate of the detector.*

other reason was the inertness of quartz with the various solvents under study. The prototype cells have a squared cross section (5×5) cm^2 (outside) and are 1 m long. They can be filled up with approximately 2 l of liquid. The filling can be done through two holes on the top of each side of the cell which are sealed by two conic teflon plugs. The teflon plugs have screw threads for removal.

For a better light collection the cells are wrapped with a foil having very high reflectivity (VM2000 from 3M). So in case the angle of the light is too large for total internal reflection at the walls of the quartz cell, there is still high probability that there is specular reflection at the foil. Each cell is equipped with UV transparent rectangular acrylic light guides at both ends with a length of 0.5 m. They are used as a shielding against radiation emitted by impurities in the photomultipliers (PMTs). These light guides, which have the same cross section as the cells, are also wrapped with the VM2000 foil. The PMTs are equipped with low-background glass for further reduction of the radioactive background. In addition special low-background voltage dividers were used. The PMTs and the voltage dividers were both delivered by ETL. They have a two inch diameter and their circular planar surface is coupled to the acrylic buffer using optical grease. Some light is lost due to the differing geometries of the cross sections of the buffer and the PMT. The VME based DAQ electronics is read out by a Motorola powerPC operating under LINUX. The analysis of the data is performed under a ROOT/C++ platform [MOT04].

Nine identical cells were mounted in an array structure of 3×3 cells. In a second phase the scintillator of some cells was replaced by In-loaded scintillators as described later. For calibration purposes four teflon tubes are inserted along the cells at the inner edges of the outer cells. So each teflon tube is surrounded by four cells. The outer diameter of the tubes is 4 mm, the inner diameter is 2 mm for two of them and 3 mm for the other two. They are sealed at the end inside the LLBF by silicone sealant. A thin wire with a ^{137}Cs source at one end can be inserted into the calibration tubes from the outside. With that system the source can be placed along the cells at every distance from the PMTs. Two copper flanges were prepared with feed throughs for the teflon tubes, the nitrogen connections and the electronic cables. Only one cable per PMT was used for high voltage and for the signal to minimize the

number of cables to be fed into the shielding.

Cell preparation

Before each cell was filled with liquid scintillator a special cleaning procedure was applied. In a first step the nine cells were rinsed with approximately 50 ml of 2-propanol to remove organic contaminations. Then they were rinsed twice with 50 ml of distilled water to remove the propanol. In the next step the cells were washed with a 10 % nitric acid solution. The main purpose of this purification step is the removal of radon daughters which accumulate with time on the surface of the quartz cells. The cells were then again rinsed with water to remove the acid and filled up with water for storage. Before the filling of the organic scintillator the residual water in the cells was removed using 2-propanol. The final rinsing was done with the scintillator itself.

Before the filled cells were mounted in the LLBF oxygen, radon and other disturbing gases in the scintillator were removed by sparging the liquid for one hour with nitrogen. A thin teflon tube connected to the N_2-supply was introduced into the cell at one end and placed at various positions. During the measurement the cells are kept under N_2-atmosphere by flushing the inner volume of the LLBF continously with the gas.

The liquid scintillator

A PXE based mixture, with p-Tp as primary and bis-MSB as secondary solute, was used as the first scintillator tested. The PXE was obtained from Koch Special Chemical Company, Corpus Christi, Texas, USA. The scintillator has been used in the Borexino CTF prototype detector as well. The CTF was first loaded with PXE in October 1996. It was purified by silica gel solid column purification. In that step initial trace impurities, e.g. ^{238}U at $3.2 \cdot 10^{-14}$ g/g could be purified to levels below $1 \cdot 10^{-17}$ g/g [PXE04]. The PXE was reloaded into CTF in 2000 and emptied from a Borexino liquid handling system in February 2001. From that time it was stored in clean barrels underground under a N_2-atmosphere. Some of this scintillator was then loaded into the LLBF in 2003.

The p-Tp concentration in the scintillator is 2.3 g/l, the bis-MSB concentration is much lower at 20 mg/l. After the silica gel column purification in one of the Borexino scintillator purification systems the attenuation length of the scintillator mixture was 2.6 m to 3.0 m at 430 nm [PXE04]. It was measured with a photospectrometer in a 10 cm cuvette. After more than two years storage in barrels the attenuation length of a sample was remeasured at Gran Sasso and a consistent result (2.7 m at 430 nm) was found. This shows that the attenuation length of the scintillator did not change over the years.

Before the filling of the 1 m quartz cells used in the LLBF, the scintillator was purified again using a weakly acidic Al_2O_3 column. This provides the first data on the Al_2O_3 purification of a PXE compound. The system was first pre-equilibrized in a beaker at a scintillator:Al_2O_3 ratio of 2:1. 200 g of Al_2O_3 was used for 6 l to 7 l of scintillator. At this ratio no breakthrough of impurities was found. The attenuation length improved to more than 10 m at a wavelength of 430 nm. The attenuation length of the scintillator before and after the purification with the alumina column is plotted in Fig. 5.4.

To test if the column removed part of the fluor which is not expected for the pure hydrocarbons [FXH03], the light yield of the scintillator was measured before and after the column. The light yield was determined by two different methods. In one method the solvent was

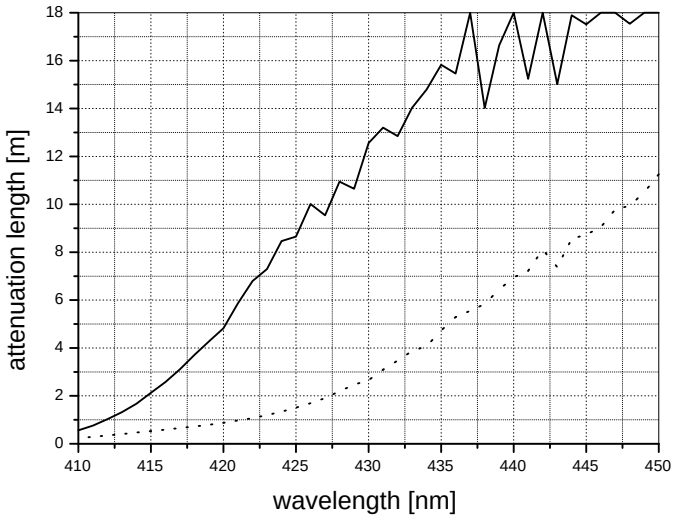

Figure 5.4: *Attenuation length of the PXE/p-TP/bis-MSB scintillator before (dotted) and after (solid) column purification with a weak acidic alumina column.*

excited by photons using a fluorimeter and in the other method the solvent was excited by γ-rays of a ^{137}Cs-source. In the measurement with the γ-source a light yield of 83 % with respect to a BC505 standard was found for the sample without column purification. The value obtained after purification was 3 % higher which is within the errors consistent with the number determined before. This indicates that only a minor fraction of the fluors was lost in the column in this geometric design, because the concentrations were already at the lower limit to get the optimum light yield. This was confirmed in fluorimeter measurements in which only small deviations of less than 10 % for the emission peak maxima of the scintillator before and after the column were observed.

Results

In Fig. 5.5 the spectrum measured inside the LLBF is shown with one of the cells filled with liquid scintillator. The overall trigger rate was $2.1 \cdot 10^{-3}$ counts/(s kg) above a threshold of (50 ± 10) keV. In the Borexino CTF 5 t of the same liquid scintillator were used. Radio carbon levels of $^{14}\mathrm{C}/^{12}\mathrm{C} = 11.74 \pm 0.03 \cdot 10^{-18}$ have been measured [LOW02]. The β-decay of ^{14}C has an endpoint energy of 156 keV and the isotope has a half life of 5730 years.

The unique potential of the LLBF as a detector for low radioactivity physics is illustrated by the ^{14}C result. In 1 kg pure PXE there are $(4.76 \cdot N_A)$ molecules where N_A is Avogadro's number. Each PXE molecule has 16 carbon atoms. The total number of ^{14}C molecules in the PXE expected from the CTF result is therefore $5.37 \cdot 10^8$ corresponding to an activity of 4.3 mBq/kg. Although a significant part of the spectrum is below the threshold of 50 keV, this number shows that the main part of the single hits ($2.1 \cdot 10^{-3}$ counts/(s kg)) in the cells can be explained by ^{14}C in the PXE. The shape of the spectrum is also consistent with the expectations from the ^{14}C decay.

A background source in the scintillator are the gammas emitted by the daughters of the

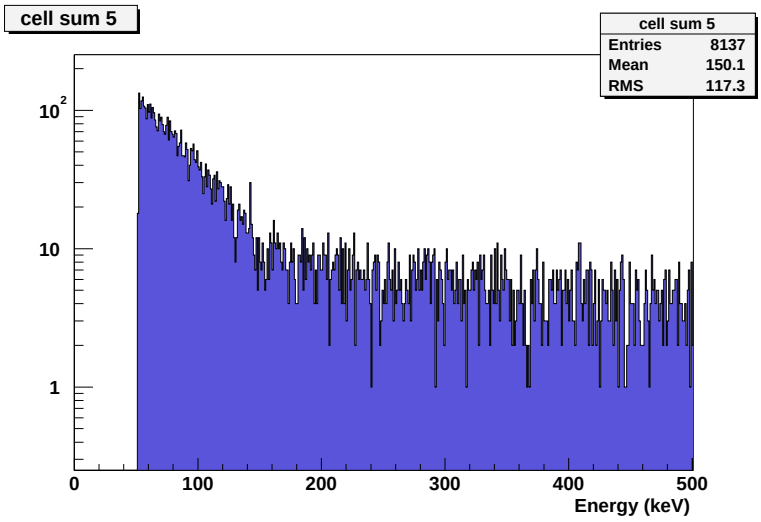

Figure 5.5: *The measured background spectrum inside the LLBF using a PXE based liquid scintillator. The ^{14}C β-spectrum can be seen above a threshold of 50 keV. The trigger rate of single hits is $2.1 \cdot 10^{-3}$ counts/(s kg) (plot made by D. Motta).*

Rn-decay chain inside the teflon tubes used for calibration. These tubes are open to the outside, so air with an ^{222}Rn-activity of approximately 100 Bq/m^3 can enter the detector. The tubes are 2 mm and 3 mm thick. This corresponds to a total volume of approximately 20 ml along the cell length of 1 m for the sum of all four tubes. Under the assumption that on average 2 gammas are detected per ^{222}Rn-decay (e.g. one in the ^{214}Pb- and one in the ^{214}Bi-decay) in one cell one expects a count rate of 2 mBq in all nine cells. This correspond to a rate of $0.11 \cdot 10^{-3}$ counts/(s kg) which is the order of magnitude for the background if the ^{14}C activity is subtracted.

There were some variations in the background of the different cells. The array was placed closer to one of the side walls inside the shielding, and the distance to the bottom was much smaller than the distance to the top. The cells closer to the shielding had lower background indicating that there was still a signal from radon in the gas phase of the shielding.

5.2 Optical properties in long quartz cells

5.2.1 Light transport in a long cell

To optimize the scintillator composition for the prototype detector it is also essential to know about the light transport mechanisms in a long cell. There are two ways how scintillation light from the ionization site can be transported to the PMTs: total internal reflection (TIR) or specular reflection (SR). The cells which will be used in LENS have a large length to cross section ratio. Therefore, a lot of reflections at the walls of the cells are expected before the light is detected by the PMTs.

TIR is the reflection of the total amount of incident light at the boundary of two media. It only takes place when the light is in the more dense medium and approaches the less dense medium. When a light beam is directed to the boundary of two media A and B at a angle Θ_A towards the normal the light is reflected or refracted depending on Θ_A. The angle of

refraction can be calculated using Snell's Law

$$n_A \cdot \sin(\Theta_A) = n_B \cdot \sin(\Theta_B)$$

where n_A and n_B are the indices of refraction of the materials. When the angle of incidence is greater than a critical angle Θ_c the light is completely reflected. The critical angle Θ_c can be calculated using Snell's Law when $\sin(\Theta_B) = 1$:

$$\sin(\Theta_c) = \frac{n_B}{n_A}$$

The mechanism of TIR in a quartz cell is in principle 100 % efficient, but in practice the efficiency is a little bit lower due to light absorption in the walls and surface imperfections.

An alternative to TIR is a cell design based on SR which is nearly equally efficient at all angles. However, above the critical angle the efficiency for reflection is lower compared to TIR. The chemical compatibility of several solvents with the high reflectivity foil VM2000 was investigated in accelerated aging tests at elevated temperatures. Samples of the foils were immersed in the solvents PC, PXE and anisole at 35 °C. Destruction of the reflecting surface was observed already after 7 days starting from the edges in all tested organic liquids. For PXE the destruction was much less intensive than for PC. The most aggressive solvent was the anisole which totally decomposed the foil in its various layers after a few days. Therefore the VM2000 foil can not be used in contact with the scintillator. Nevertheless it can be used to wrap the quartz cells from the outside. In this case light which is not reflected due to TIR can still be reflected at the foil.

The transport of light in long cells has been studied using a LED (light-emitting diode) at the wavelengths of 380 nm and 428 nm, either on quartz tubes based on TIR and in light guides built out of a VM2000 foil [MOT04]. The TIR efficiency was found to be in the range of 99.5 %. For SR the reflectance was found to be approximately 98.5 %. The results of these measurements were used to predict the light transport behaviour in prototype cells filled with scintillator.

5.2.2 Measurements in a 1 cm wide and 1 m long cell

In the measurements presented up to now involving In-loaded scintillators the goal was to optimize the light yield in a short cell of 1 cm where light propagation is unimportant. The situation changes going to longer cells. The quartz cell that was used for a first series of measurements in a long cell had an outer cross section of 1.5×1.5 cm^2 with a wall thickness of 2 mm and a length of 1.08 m. The inner volume was approximately 130 ml. The corners of the cell were rounded which is a major source of light loss. The scintillation light created in the cell under irradiation with a LED (370 nm) or a γ-source was detected with a PMT at the end of the cell. For these measurements no VM2000 foil was used. Therefore the amount of detected light was quite small. The main purpose of the measurements in this cell was to find the best composition of the scintillator for the LENS prototype. In particular the effect of bis-MSB on the attenuation length was investigated. Furthermore the MC simulations on light propagation in quartz cells performed by Dario Motta [MOT04] were tested and tuned.

To study the effect of different bis-MSB concentrations on the scintillator performance in a long cell, experiments were made in which the secondary wavelength shifter, bis-MSB, was the only component that was varied. As scintillator solvent anisole was used, the In-loading was

at 5 wt.% and the BPO concentration was kept constant at 50 g/l. According to simulations the best performance is expected at this BPO concentration. At higher BPO concentrations the light yield still increases in a small 1 cm cuvette. However, in the 1 m cell used in these measurement there is significant self-absorption of the BPO in the wavelength region of the scintillator emission. Therefore, a higher BPO concentration could be disadvantageous concerning light yield in the long cell. In the small 1 cm cell the light yield is similar with and without bis-MSB when BPO is used as fluor since the non-radiative energy transfer rate from BPO to bis-MSB is small. However, as seen in the previous chapter, the bis-MSB shifts the emission spectrum to a more transparent region. Most of the light absorbed by the bis-MSB itself is reemitted. This reemitted light is detected in the PMTs unless the photons are reemitted at an angle below the critical angle for TIR.

BPO [g/l]	bis-MSB [mg/l]	In [wt.%]	Λ_{cell} [m]	Λ_{spect}^{430nm} [m]	Λ_{spect}^{450nm} [m]
3	0	0	2.2 ± 0.1	11.1	16.3
50	0	0	1.23 ± 0.06	2.5	3.8
50	0	5	0.57 ± 0.06	0.60	0.86
50	100	5	0.81 ± 0.04	0.49	0.84
50	250	5	0.72 ± 0.04	–	–
50	500	5	0.91 ± 0.05	0.30	0.79

Table 5.2: *The measured attenuation lengths for unloaded and In-loaded scintillators at varying bis-MSB concentrations are listed. The attenuation lengths were determined in a 1 m long cell with a cross section of 1.1 cm×1.1 cm under irradiation with a source (Λ_{cell}) and in the photospectrometer (Λ_{spect}). For the measurements in the spectrometer the values at 430 nm and 450 nm are given.*

Table 5.2 summarizes the results obtained for the effective attenuation length in the 1 m cell together with the results of the measurements with the photospectrometer. For comparison the attenuation lengths of two unloaded scintillator versions at BPO concentrations of 3 g/l and 50 g/l are given besides the values obtained for the In-loaded scintillators at varying bis-MSB concentrations. It should be noted that the $In(acac)_3$ used in these measurements had a shorter attenuation length compared to samples produced more recently. The main reasons for this was a higher pressure during sublimation, and the fact that the $In(acac)_3$ material was not sieved at the time of the measurement. Therefore, the $In(acac)_3$ material dominates the absorbance above 430 nm in these tests.

A comparison of the attenuation lengths determined in the photospectrometer at 430 nm and the effective attenuation lengths in the 1 m cell shows that the values measured in the photospectrometer are higher for the In-free scintillator versions. Such a behavior is expected, because in the spectrometer the light propagates straight through the sample whereas in the long cell most of the scintillation light is reflected several times at the walls and the real pathlength is longer than the distance between the origin of the light and the end of the cell. However, in the In-loaded scintillators containing bis-MSB the effective attenuation length in the cell is longer than the attenuation determined in the spectrometer at the emission peak of approximately 430 nm. This effect is partly due to the fact that the light is reflected at the border between the quartz and the air and therefore propagates on a major part of the way to the PMT through the quartz where transmission is high compared to the scintillator.

Furthermore with bis-MSB as an additive a lot of light absorbed by bis-MSB at 430 nm is reemitted in a more transparent region above 430 nm, especially at high concentrations of the secondary wavelength shifter. The probability to detect these reemitted photons is much higher in the long cell compared to the spectrometer measurement.

The bis-MSB has no effect on the light yield in a small (1 cm) cuvette which was shown in light yield measurements under irradiation with a ^{137}Cs source of two of the In-loaded scintillators. For the In-loaded sample in Table 5.2 containing no bis-MSB the light yield was (39.5 ± 1.0) % relative to BC505. At 500 mg/l bis-MSB and similar BPO- and In-concentrations it was (40.5 ± 1.0) % relative to BC505. These values are consistent with other measurements using $In(acac)_3$ samples of different synthesis and sublimation batches at similar concentrations. Therefore, these results also demonstrate that the light yield of optically less pure $In(acac)_3$ is similar to purer samples with higher transparency.

One can learn from these measurements in a long cell that it is advantageous to use bis-MSB in an In-loaded scintillator with BPO as fluor. A bis-MSB concentration of 100 mg/l is already sufficient. At higher concentrations there is no significant improvement in the attenuation length. This result is also predicted by the simulations.

5.2.3 Measurements in a LENS-like cell

In a next step various scintillator compositions were tested in a prototype cell of 1 m length and (5×5) cm^2 cross section. To minimize light losses the cell was wrapped with a VM2000 foil. PMTs with 2 inch diameter were attached to both ends. Part of the produced light is lost due to incomplete coverage of the squared cell ends by the round PMTs. Before the measurements the scintillator in the cell was sparged with N_2 using a teflon tube that was inserted into the cell. The $In(acac)_3$ based scintillator system was investigated at two different In-concentrations. In the following, the results of these measurements will be described.

A 2 wt.% In-loaded scintillator

First an optical characterization of a 2 wt.% In-loaded scintillator was performed. To do so, sublimed $In(acac)_3$ and BPO is mixed with anisole and filtered using a 0.2 μm filter. The BPO-concentration is adjusted to 27 g per liter anisole. At that concentration best performance is expected in the 1 m long cell when self absorption is included. The light yield in a 1 cm cell is (44 ± 1) % relative to BC505 for this composition. After filtering, bis-MSB was added at a concentration of 50 mg/l. The In-concentration of the scintillator that entered the cell was checked by AAS (atomic absorption spectroscopy) and an In-loading of (1.86 ± 0.05) wt.% was measured. The density of this scintillator composition was determined to be (1.012 ± 0.002) g/cm^3.

The expected attenuation length in the photospectrometer is calculated under the assumption that the contribution of the single components to the absorbance sum. The extinction coefficients at the wavelengths of interest were determined for all components separately. The used anisole was purified using a weak acidic Al_2O_3 column and had an attenuation length of 9 m at 430 nm, the wavelength region of the scintillator emission peak. Taking into account the contribution of the other components and assuming an average molar extinction coefficient of 0.003 l/(mol·cm) at 430 nm for the $In(acac)_3$ material, the attenuation length of the final scintillator mixture can be calculated. It is 1.65 m at 430 nm which is consistent with the measured value of 1.45 m. At these concentrations the absorbance above 430 nm is

clearly dominated by the BPO.

The attenuation length in the 1 m cell was determined by a method similar to the one applied in [SUZ90]. A ^{137}Cs source was used and the backscattered Compton electrons of 477 keV were measured. The source was moved along the cell in 10 cm steps. If the amount of collected light is plotted versus the distance between the source and the PMT the attenuation length can be determined by fitting the data points with a double exponential. The value obtained for the long component is 1.54 m. This can be compared to an effective attenuation length of approximately 4 m measured for an In-free PXE based scintillator determined in the same cell. These numbers are in good agreement with the simulations.

Scintillator properties of importance for an effective background reduction in a neutrino detector, as the number of photoelectrons (pe) per MeV, the spatial resolution of an electromagnetic interaction and the energy resolution were also studied. If the number of pe are summed in both PMTs with the source placed at the center of the cell one obtains 230 pe/MeV. The spatial resolution of the source position was determined by measuring the time difference between the two PMT signals and found to be 6 cm (1σ) for this scintillator composition. The energy resolution was also measured with the Compton backscattering method using a ^{137}Cs source. At 477 keV the energy resolution was measured to be 10.2 % (1σ). After a few days the results became worse, because the liquid in the cell was in contact with the teflon plugs and anisole could exit the cell due to capillary forces. As described above the anisole destroys the VM2000 foil. Therefore the cells should not be filled to the top. The scintillator properties were also measured for a 4.15 wt.% In-scintillator using the same setup and are discussed next.

A 4.15 wt.% In-loaded scintillator

To minimize the size of the neutrino detector a higher In-loading than 2 wt.% is desirable. The 2 wt.% In-loaded scintillator used for the measurements described above was used as a basis for the next scintillator mixtures with higher In concentrations. First, the BPO concentration was increased to 47 g/l and the In-concentration to 4.15 wt.%. In this case the In-loading was also confirmed by AAS to be (4.1 ± 0.1) wt.%. The light yield in a 1 cm cell is (42 ± 2) % relative to BC505 for this scintillator composition. The density of the mixture is (1.046 ± 0.004) g/cm^3. The bis-MSB concentration was kept at 50 mg/l and in a second step increased to 100 mg/l. The composition of this scintillator is similar to the one that is tested in the LENS prototype detector.

component	anisole	indium	BPO	bis-MSB	Λ_{scint}^{calc}	Λ_{scint}^{exp}
concentration		2 wt.%	27 g/l	50 mg/l		
Λ [m]	9	7.6	3.3	15	1.63	1.45
concentration		4.1 wt.%	47 g/l	100 mg/l		
Λ [m]	9	3.7	1.9	7.5	1.00	0.96

Table 5.3: *The contribution of the single components to the attenuation length Λ is listed for two scintillator compositions. The overall attenuation lengths calculated and measured in the photospectrometer are given.*

In Table 5.3 the contributions of the single components to the attenuation lengths of the

final scintillator mixtures at 2 wt.% In and 4.1 wt.% In are summarized. The sum of the reciprocals of the attenuation lengths give the inverse of the overall attenuation length of the scintillator system. The calculated value of 0.96 m is in agreement with the 1 m measured in the photospectrometer using the standard method in a 1 cm cell.

scintillator	In-conc. [wt.%]	Λ_{eff} [m]	En. res. (1σ)	Sp. res. (1σ)	ph. el./MeV
PXE+pTP	–	4.20	5.2	3 cm	750
anisole+BPO	2.0	1.58	10.2	6 cm	230
anisole+BPO	4.15	1.28	11.6	7 cm	200

Table 5.4: *The effective attenuation length Λ_{eff} in a 1 m long cell (5×5 cm^2 cross section), the energy resolution at 477 keV, the spatial resolution and the number of photoelectrons/MeV (sum of both PMTs and source at the center of the cell) is given for some scintillator compositions.*

In Table 5.4 some relevant properties of the system are listed. For comparison also the corresponding values for the 2 wt.% In-system, and for an In-free PXE based scintillator are given. The unloaded scintillator is the one used in the Borexino prototype CTF. This scintillator contains p-Tp (2.3 g/l) and bis-MSB (20 mg/l) as fluors and has an attenuation length of approximately 10 m in the photospectrometer. The light yield is (83 ± 2) % relative to BC505 in a short cell. For the 4.15 wt.% In-loaded no significant difference in all the properties was observed when the bis-MSB concentration was increased from 50 mg/l to 100 mg/l. These scintillator properties meet the demands for a low energy solar neutrino experiment, at least for ^{7}Be neutrinos. A pp-neutrino detector would require some tuning of the In-concentration in the scintillator.

Fig. 5.6 shows the data points and the spectra that were used to determine the effective attenuation length, the energy and the spatial resolution in the cell. Details about the experimental methods and the data analysis are found in [MOT04]. The light yield for each PMT was measured as a function of the distance between the source and the end of the cell. The value at the position 50 cm from the end, the cell center, was normalized to unity. In one set of measurements the variation of the light yield was determined simultaneously for both PMTs. The result of one PMT is plotted in red (circles), the result of the other one in blue (squares). The graph on the top of Fig. 5.6 shows the characteristic shape of such a curve. There is a steep decrease in light yield close to the end of the cell and a long component of the double exponential further away from the PMT. The decision about the concentrations of the scintillator components for the prototype measurement was mainly based on the results of these measurements.

5.3 Underground measurement of In-loaded cells in the LLBF

To complete the R&D phase of the LENS project a prototype measurement is carried out in the Gran Sasso underground laboratory. The prototype consists of 9 quartz cells equipped with light guides and PMTs at both ends. Some of the cells are In-loaded and some are In-free. This measurement gives the final information about the scintillator performance as radioactive background of the scintillator composition and long term stability in an un-

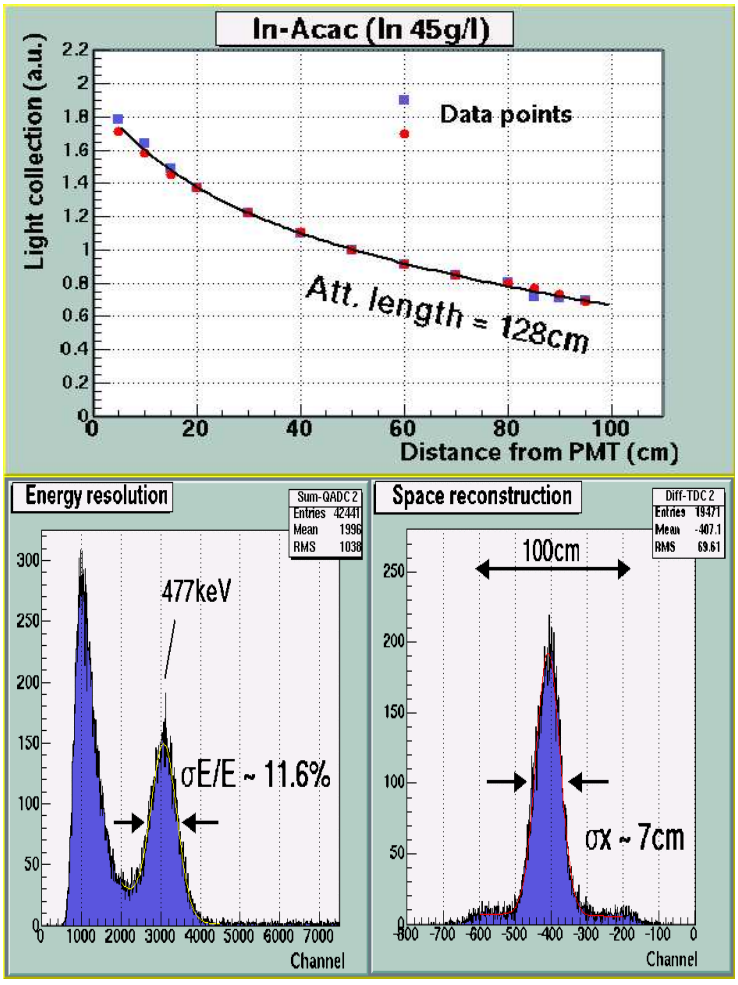

Figure 5.6: *On the top the light yield at one end of the cell is plotted versus the distance between source and PMT. The attenuation length is determined by fitting the data points with a double exponential. On the bottom the spectra that were used to determine the energy and the spatial resolution are shown.*

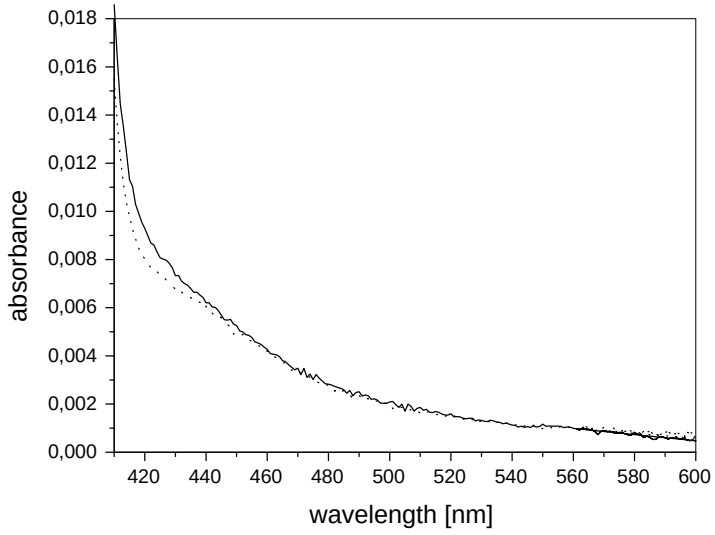

Figure 5.7: *The BPO absorbance at a concentration of 125 g/l measured in one of the four batches of the anisole/BPO master solution is shown after water extraction (dotted line) compared to the unpurified solution (solid line). The measurement was performed using a 1 cm cuvette.*

touched closed system which is kept under N_2-atmosphere. Furthermore the background due to Bremsstrahlung can be investigated in the In-free cells. The measurement also allows the comparison of different scintillator compositions in an identical setup.

5.3.1 Scintillator preparation

First, the procedure to produce the scintillator is described. The sublimed $In(acac)_3$ from the various sublimation runs were stored separately and the optical clarity of each batch was tested in a photospectrometer. Only material with a transparency of more than 2 m at 430 nm was used for the scintillator. The $In(acac)_3$ was dissolved in anisole at an In-concentration of 4.5 wt.%. After the production of 1.25 kg of the anisole/$In(acac)_3$ solution the mixture was measured in the photospectrometer using a 10 cm cell. The attenuation length of this solution was found to be 3.3 m at 430 nm (4.6 m at 440 nm). There is a significant contribution of the anisole to the absorbance at this purity level of the $In(acac)_3$.

To avoid that the high BPO amounts needed in the $In(acac)_3$ scintillator introduce radioactive contaminations into the liquid a BPO master solution was mixed and purified. This master solution had a BPO concentration of 125 g per liter anisole. It was purified by water extraction in a separation funnel at a water to anisole ratio of 2:1. The water extraction was done twice and the funnel was shaken for approximately 2.5 min. The density of anisole (0.99 g/cm^3) is close to that of water at standard conditions. At the high BPO concentration of 125 g/l the density increases to more than one and the BPO/anisole solution settles down on the bottom of the funnel. The main purpose of the water extraction was to remove the radioactive isotope ^{40}K.

After the water extraction the anisole solution is saturated with water. As mentioned previously, water can affect the stability of the scintillator. Therefore the solution was dried after the water extraction by passing it through a silicagel column of 9.9 g used for approximately 800 ml of solution (which was divided in four batches for the water extraction). The BPO-concentration was determined after the first batch (200 ml) passed the column by measuring the absorbance of a small amount of the solution before and after purification diluted in cyclohexane. The BPO loss in the column and in the water was found to be less 10 %. The absorbance was measured for each batch after the purification and compared to the unpurified solution. The absorbance of one of the batches after water extraction is shown in Fig. 5.7. Similar spectra were measured for the other three batches. There is a little improvement in the transparency after purification in the wavelength region around 420 nm.

The purified BPO master solution was then added to the In-solution in a way that the final BPO-concentration was 50 g per liter anisole. Additional $In(acac)_3$ was added to compensate for the dilution of the In-concentration. Finally the 4.5 wt.% In-solution was pumped through a 0.2 μm filter before the bis-MSB was added. A bis-MSB concentration of 100 mg/l was chosen. Then the approximately 2 l of In-loaded scintillator were transported in glass bottles to Gran Sasso for filling the cell.

5.3.2 Cell loading

Most of the scintillator synthesis was already done four to five months before the cells were mounted underground. Four of the 1 m long quartz cells filled with the In-free PXE-based scintillator which were used for the background measurements in the LLBF were emptied and refilled with In-loaded scintillators. The cells were rinsed with the pure scintillator solvent before filling. One cell was filled with the 4.5 wt.% In-loaded $In(acac)_3$ scintillator and two were filled with a scintillator having a similar In-loading produced by a Russian/Italian group. In these scintillators carboxylic acids were used to dissolve the indium in the organic liquid. Two slightly different versions were tested for that system. In addition one cell was prepared with an $In(acac)_3$ scintillator version at 0.1 wt.% In-loading. The solvent of this scintillator version is an anisole/PXE mixture with a factor 20 more PXE than anisole. The fluor concentrations are approximately 4 g/l BPO, 2 g/l p-Tp and 25 mg/l bis-MSB. The different indium to BPO ratios in the two $In(acac)_3$ scintillators can be used to estimate the contributions of the fluor and the In-material to the background.

All cells were filled so that a blanket of a few mm was left above the liquid for several reasons. First the blanket is needed to avoid that the cell breaks when there is thermal expansion of the scintillator. Second it is preferable to have no contact with the cell wall on the top, because light losses are then minimized since TIR will occur at the perfectly planar surface of the liquid. Finally the teflon plugs should not touch the liquid, otherwise part of the liquid can exit the cell due to capillary forces between the teflon and the quartz and destroy the VM2000 foil.

Before the filled cells were transported underground they were sparged with nitrogen to remove gases which decrease the performance like oxygen and radon. The cells were mounted in the LLBF in the geometry shown in Fig. 5.8. The configuration was chosen to optimize the number of In-free neighbors for each In-loaded cell. Three sides of the In-loaded cells are faced with In-free cells. This geometry allows to detect Bremsstrahlung photons in the PXE cells in coincidence with In-β-decays in the In-cells. The Bremsstrahlung spectrum obtained can be used to estimate one of the main background sources in a LENS-detector. The same

PXE cell No.7	In-Carb. 51 g/l In cell No.8	PXE cell No.9
$In(acac)_3$ 1 g/l In cell No.4	PXE cell No.5	In-Carb. 54 g/l In cell No.6
PXE cell No.1	$In(acac)_3$ 47 g/l In cell No.2	PXE cell No.3

Figure 5.8: *The configuration of the various cells in the prototype array is shown. The array consists of 5 In-free PXE based cells, 2 $In(acac)_3$ scintillator versions and 2 In-carboxylate scintillators.*

light guides and PMTs that were used for the background measurement were also used here. The inner volume of the LLBF is flushed with nitrogen during the measurement.

5.3.3 Results

The array of scintillator cells is calibrated regularly in order to check the stability of the system. The calibration is performed in the same way as in the background measurement using a ^{137}Cs source that is introduced in the inner volume through a teflon tube. The light yield at the center of the cell relative to an In-free PXE scintillator and the attenuation lengths are determined in each measurement by a comparison of the fitted Compton edges in the spectra. For the determination of the attenuation length an one exponential fit to the data is sufficient, because the short component (which is of relevance when no buffer is used) can be neglected in the presence of the 0.5 m long light guides.

The scintillator properties are summarized in Table 5.5. The value obtained for the effective attenuation length for the highly In-loaded $In(acac)_3$ scintillator is (0.95 ± 0.13) m slightly below the number determined in Heidelberg with a similar composition. The difference could be due to a systematic error of the light yield determination in the LLBF measurement [MOT04]. When the energy resolution is poor the Compton edge appears to be shifted to lower values. Therefore at larger distances from the PMTs where the amount of detected light is less the shift is expected to be larger compared to distances closer to the PMT resulting in an apparently shorter attenuation length. This effect was no issue in the measurement performed in Heidelberg since there the more precise Compton backscattering method was used to determine the attenuation length.

The light yield with the source at the center of the cell is (30 ± 7) % compared to the

Cell No.	In [g/l]	Mass [kg]	Vol. [l]	density [g/cm^3]	LY [%]	Λ_{eff} [m]
2	48	1.88	1.80	1.05	30 ± 1	0.95 ± 0.13
4	1	–	–	1.0	70 ± 14	2.65 ± 0.55
6	54	1.57	1.67	0.94	71 ± 3	1.65 ± 0.20
8	51	1.52	1.63	0.94	70 ± 3	1.08 ± 0.10
5	0	–	–	1.0	100	2.55 ± 0.45

Table 5.5: *Some properties as In-loading, light yield (LY) and effective attenuation length in the cell Λ_{eff} of all In-loaded and of one In-free scintillator are listed. The light yield was determined with the ^{137}Cs source at the center of the cell and compared to a typical In-free PXE cell.*

average PXE cell which is consistent with the Heidelberg measurement. The light yield of the scintillators produced in Gran Sasso is approximately a factor two higher than that of the $In(acac)_3$ version at similar In-concentration, but the latter is expected to be more stable. The main reason that the light yield of the scintillator loaded with 1 g/l In is not significantly higher than that of the highly loaded carboxylate systems is the lower light yield of the unloaded PXE or anisole scintillator systems compared to a PC based system. After a time period of two months all the scintillators are found to be stable within the uncertainties of the measurement.

Chapter 6

Rare earth acetylacetones in liquid scintillators

The technique to produce an In-loaded liquid scintillator described in the previous chapters can also be applied for other metal doped scintillator systems. Currently, a gadolinium loaded scintillator for a future reactor neutrino experiment [BU03, HAR03] and a Nd-loaded scintillator for a $\beta\beta$-decay experiment are under investigation. Lower metal loading is needed in these experiments compared to an solar neutrino In-detector. A Gd-loading of 1 g/l to 2 g/l which is nearly two orders of magnitude below the In loading presented before is sufficient in a reactor neutrino experiment. In a double beta decay experiment using neodynium the metal loading has to be optimized, but a concentration of 2 g/l could already be sufficient with a proper detector design. Due to the lower metal loading much higher light yields and long attenuation lengths are expected. The main requirement for metal loaded liquid scintillators used in such experiments is the long term stability. In the following sections the chemistry of rare earth acetylacetones and initial results on the two metal loaded systems (Gd and Nd) are described.

6.1 Physical and chemical properties of rare earth acetylacetones

The chemistry of rare earths, such as Nd and Gd is rather different from the chemistry of indium which has no electrons in the f shell. A major difference between the trivalent rare earth acetylacetones and $In(acac)_3$ is that the rare earth complexes form hydrates ($M(acac)_3 \cdot nH_2O$). The literature indicates that basically only two hydrates are formed: the monohydrate and the trihydrate [POP61]. The synthesis typically results in the preparation of trihydrates. From that molecule one can produce monohydrate by drying it in a desiccator above e.g. magnesium perchlorate or by crystallization from a solution of the trihydrate in e.g. ethyl alcohol or acetone. The hydrates of the rare earth elements with lower atomic number are more stable. The larger diameter of the latter probably enable them to accomodate more easily the additional water molecules. The synthesis of anhydrous rare earth trisacetylacetones is reported e.g. in the references [KOE67] and [PRZ71]. In contradiction to earlier publications ([POP61][RIC68]) the preparation of anhydrous rare earth acetylacetones by vacuum drying is reported in reference [LIS77].

Purification of the metal chelates by sublimation as performed for the $In(acac)_3$ requires

stability at high temperatures and a high vapor pressure. The melting points of some monohydrated rare earth acetylacetonates are listed in Table 6.1. All of them are about 60 °C below the value of $In(acac)_3$. It appears that the melting point decreases with increasing atomic number. There seems to be no significant difference in the melting point of the monohydrate compared to the trihydrate. Generally volatility of metal chelates with a common ligand increases with a decrease in the radius of the central metal atom [MEH78]. Therefore one would expect lower vapor pressures for the Nd and Gd complexes compared to $In(acac)_3$ due to the larger size of the metal ions.

Rare earth	Nd (60)	Sm (62)	Gd (64)	Dy (66)	Ho (67)	Er (68)	Yb (70)
Melt.p.[°C]	140	138	139	136	133	129	125

Table 6.1: *The melting points of the hydrated rare earth acetylacetonates are listed [POP61]. The atomic number of the rare earth is given in parenthesis after the element symbol.*

As seen in Fig. 6.1 the absorption spectra of most trivalent metal acetylacetones are similar. The main absorption peak around 285 nm is due to an absorption in the resonance structure arising from the carbonyl groups of the acac ligands [PRZ71]. The absorption peaks of the metal chelates are shifted to longer wavelengths compared to the pure Hacac spectrum with a maximum at 274 nm. For the case of Nd the metal ion itself has absorption bands in the visible region. The absorption spectrum of hydrated $Nd(acac)_3$ shows splitting and intensification of absorption bands compared to the metal chloride. This effect is shown in Fig. 6.2. The sample containing the metal chloride was prepared by dissolving Nd_2O_3 in a HCl-solution. Then part of this standard solution was dissolved in ethanol and the absorption spectrum was measured. The main peak is at 576 nm, at which the molar extinction is 5.8 l/(mol·cm). $Nd(acac)_3 \cdot nH_2O$ dissolved in ethanol shows splitting of the main absorption band and a shift of the peak maxima to longer wavelengths. The molar extinction coefficient peaks at 583 nm and was found to be approximately a factor 4 above the maximum for the $NdCl_3$ solution (literature value for $Nd(acac)_3 \cdot 3H_2O$: $\epsilon = 28.6$ l/(mol·cm) [LIS77]). The increase of the $Nd(acac)_3 \cdot nH_2O$ absorbance to shorter wavelengths between 450 nm and 400 nm is probably due to impurities in the material. Only a few other rare earth acetylacetones as Ho and Er absorb in the visible region [PRZ71]. None of the metal acetylacetones tested showed emission in the fluorimeter after excitation at the absorption maximum.

6.2 Gd-loaded scintillator for a reactor neutrino experiment

This section describes the synthesis of pure $Gd(acac)_3 \cdot nH_2O$ and the solubility in several scintillator solvents. The optical properties of Gd-loaded scintillators are presented. Apart from the acac scintillator version, there is also the option of a Gd-loaded carboxylate system.

6.2.1 Synthesis and dehydration of $Gd(acac)_3 \cdot nH_2O$

Synthesis and purification

Two different synthesis methods were tested to produce $Gd(acac)_3 \cdot nH_2O$. Both methods used Gd_2O_3 dissolved in a HCl-solution as a starting material. In the first method the Hacac was added and the pH was increased using an ammonia solution to about 7. The insoluble

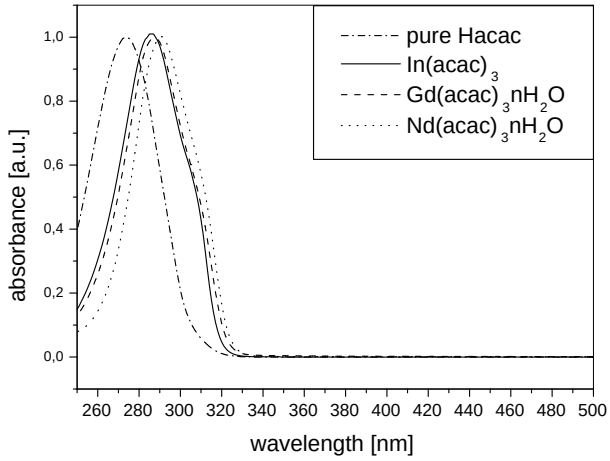

Figure 6.1: *The main absorption bands of pure Hacac (to the left in the figure), $In(acac)_3$ and the two hydrated rare earth acetylacetones $Gd(acac)_3 \cdot nH_2O$ and $Nd(acac)_3 \cdot nH_2O$ are shown. The molecules were diluted in ethanol and the height of the absorption peaks was normalized to unity.*

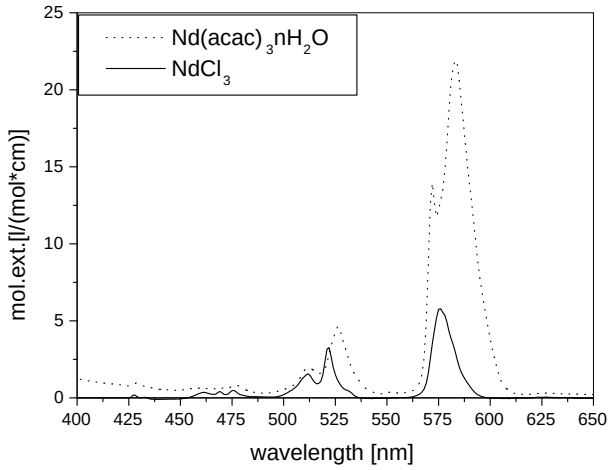

Figure 6.2: *The molar extinction coefficient at varying wavelengths is shown for $Nd(acac)_3 \cdot nH_2O$ and $NdCl_3$. The extinction was determined from absorbance measurements of the samples diluted in ethanol.*

$Gd(acac)_3 \cdot nH_2O$ forms a crystalline precipitate. The decreasing Gd content in the solution was monitored by photospectrometry during the synthesis. The reaction was found to occur at a pH of about 5. The final solution was filtered to extract the Gd complex as a powder. The yield of that procedure was slightly above 40 %.

The second method followed a procedure proposed by J.G. Stites et al. [STI48]. In this case, a NH_3 solution is added to the acidic HCl-solution containing the Gd_2O_3 until pH 5. Then Hacac dissolved in an ammonia solution (approximately 0.2 M) is added. The pH is kept around 6.3 using diluted acidic and ammonia solutions. The mixture was stirred overnight to give the Gd time to react before filtering. The pH dropped from 6.3 to 6.0 during that time period. This procedure gave a yield of only 15 %. The yields found by Stites et al. for several rare earths were in the 90 % range using hydrochloric acid and in the 80 % range using nitric acid in the synthesis. Probably the chosen pH value of 6.3 was not high enough. Therefore the pH of the solution after filtering was further increased to approximately 8. After one more day additional $Gd(acac)_3 \cdot nH_2O$ formed together with some hydrolysis product. The yield of this second step was about 50 %. There are also indications that the time needed to complete the reaction was not sufficient although the published procedure gives the reaction only 12 hours to take place. The final product is air dried for one day. Both synthesis procedures use aqueous solutions in the synthesis. Therefore the final product is essentially the trihydrate $Gd(acac)_3 \cdot 3H_2O$.

The purification used for the Hacac and the synthesized material is described in [POP61]. The Hacac is pre-purified by extraction with an 2 M ammonia solution. In addition the Hacac is twice water extracted. The water to Hacac ratio was approximately 1:3 in the extraction. Furthermore the Hacac is distilled using a rotary evaporator. The trihydrated chelate that is obtained after the synthesis is dissolved in heated ethanol and the solution is filtered. Excess acetylacetone is added to prevent hydrolysis. Then water is added to produce a 65 % ethanol solution and the mixture is permitted to cool down overnight. The purified material recrystallizes due to the decreased solubility in the water/ethanol solution at the lower temperature. The crystals were washed once with a ethanol/water (50:50) solution and twice with pure water. The Gd loss in the purification was found to be less than 20 %. A first purification test by sublimation of the hydrated $Gd(acac)_3$ was not successful.

Dehydration

A study of the dehydration of the $Gd(acac)_3 \cdot nH_2O$ was made by drying samples of the first (batch 1) and second (batch 2) synthesis procedure after the purification step described above in a desiccator above silicagel. The change in the weight due to the removal of the water molecules was measured for several days until equilibrium was reached. According to the literature [POP61] one expects that the starting material is basically a trihydrate and the resulting product a monohydrate. The time dependence of the molar fraction n of water molecules per $Gd(acac)_3$ during the drying of batch 1 and batch 2 is plotted in Fig. 6.3. It was assumed that the material is pure $Gd(acac)_3 \cdot nH_2O$ and that at the beginning n equals 3. The weight of the material indicates that after one week of drying the chelate is a monohydrate. For both batches the final estimated number for n is below one. The most probable explanation is that the starting material has on average slightly more than 3 H_2O molecules per Gd-complex.

It was tried to remove the last water molecule to obtain anhydrated $Gd(acac)_3$ following the method described in reference [LIS77]. The dehydration was carried out at 60 °C and under vacuum (10^{-6} mbar) for a period of 5 days. For this test material specified as

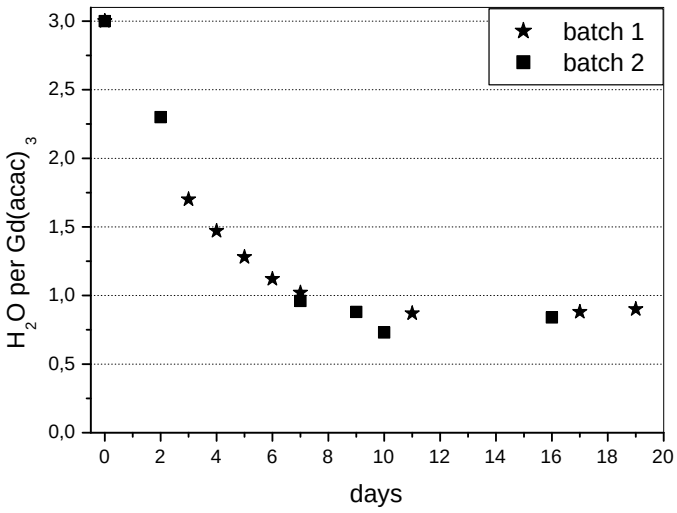

Figure 6.3: *The molar fraction of H_2O molecules per Gd-complex is shown during the drying period in the desiccator. It was determined by weight under the assumption that the material at time 0 is pure $Gd(acac)_3{\cdot}3H_2O$ and that only water molecules are removed.*

$Gd(acac)_3{\cdot}nH_2O$ (Aldrich, 99%) was used. A measurement of the Gd fraction in the material indicated that it is basically a monohydrate. A filter was installed to avoid that the powder is pumped away. The Gd-content in pure $Gd(acac)_3$ is 34.6 %. A stoichiometric determination of the Gd-content in the material produced resulted in a higher value of 38 ± 1 % indicating that the material is partially decomposed. Some authors (e.g. [POP61]) suggest that the monohydrates of rare earth acetylacetones are under vacuum partially converted to the monobasic form ($Gd(acac)_2OH$) which is reported to be stable for Gd [PRZ71].

Solubility

The optimum Gd-loading in a reactor antineutrino experiment is in the 1 g/l range. The solubility of $Gd(acac)_3{\cdot}nH_2O$ (Aldrich) in several solvents of interest was determined by photospectrometry. An excess amount of the material was first dissolved in the various solvents. After treatment in an ultrasonic bath and several days of sitting the solutions were filtered. Then the solvent was evaporated, and the Gd amount in the residue was determined. For that purpose the residue was first dissolved in a HCl-solution. Then the Gd-concentration was measured in a photospectrometer using a color complex. For the PXE sample a different procedure had to be applied. Due to the low vapor pressure of that solvent evaporation is hardly possible. The Gd was extracted into the HCl solution by mixing of the acidic aqueous phase with the Gd-loaded PXE.

The results of the solubility measurements are summarized in Table 6.2. The measurements show that a Gd-loading of 0.1 wt.% corresponding to approximately 1 g/l is possible in solvents like anisole, PXE, dodecane or Ruetasolv DI (diisopropylnaphtalene). The lowest solubility was found in PC. However, the solubility would be sufficient in a PC/dodecane mixture when the dodecane fraction is chosen high enough.

solvent	Gd sol. [wt.%]
PXE	0.16 ± 0.01
dodecane	0.14 ± 0.01
pseudocumene	0.009 ± 0.002
anisole	0.35 ± 0.01
Ruetasolv DI	0.30 ± 0.01
H_2O	0.049 ± 0.005
ethanol	> 1

Table 6.2: *Gd solubility at room temperature using $Gd(acac)_3 \cdot nH_2O$ in several solvents. The values were determined with photospectrometric methods.*

6.2.2 Solvent selection

In the experiments Chooz [CHO99] and Palo Verde [PAL01], PC based scintillator solvents were used. The safety issue is one of the main restrictions in large scale neutrino experiments. Therefore it would be preferable to use a less harmful solvent with a higher flashpoint such as PXE. To improve the chemical compatibility with acrylic, which is often used in such experiments due to its transparency and radiopurity, PXE could be mixed with dodecane. Dodecane is known to have a long attenuation length above 400 nm. Furthermore it has the positive side effect of a higher number of free protons which is the target nuclei for the antineutrino detection. In one liter of PXE ($C_{16}H_{18}$) there are 86 mol hydrogen atoms, instead one liter dodecane ($C_{12}H_{26}$) contains 114 mol of hydrogen. The disadvantage of the non-fluorescent dodecane is the reduction in light yield at increasing dodecane concentrations. The chemical compatibility of pure PXE and PXE/dodecane mixtures and the light yield at increasing dodecane fractions in the scintillator is presented next.

Chemical compatibility with acrylic

To test the chemical compatibility of possible scintillator solvents with acrylic that is typically used as detector material, acrylic samples (Roehm Plexiglas GS) were immersed in pure PXE and a PXE/dodecane (ratio 50:50) mixture. To quantify the effect on the material, numbers were scratched on the acrylic blocks. Fine cracks were found on the surface for both samples after 6 weeks. However, these cracks were found in each case on one side only. The effect was stronger for the sample in pure PXE. In Fig. 6.4 pictures of the acrylic blocks are shown before the test, and after 10 weeks in the liquid. No effect was observed at the edges of the blocks. They were still sharp as before. Two pieces were glued together and immersed in PXE. The liquid also caused cracks in the glue. The weight of each acrylic sample was measured before and after the test. No significant weight loss could be observed. These tests have shown that it is preferable to use more than 50 % dodecane in case that acrylic is used as detector containment material.

In a second 'stress' test acrylic tubes were immersed in pure PXE, a PXE/dodecane mixture (50:50) and pure dodecane. The tubes were compressed in a defined way while they were sitting in the solutions. At the chosen tension the sample in PXE cracked in several pieces within a few seconds. The sample in the PXE/dodecane mixture broke in two pieces after approximately 50 min. The tube sitting in pure dodecane stayed alive until the end of

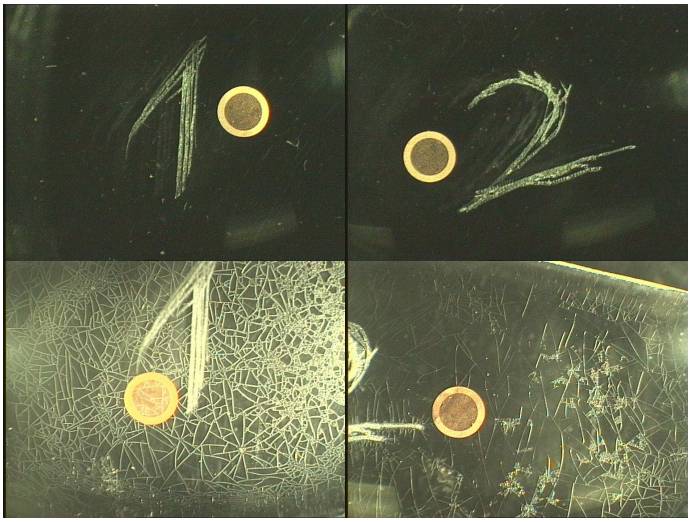

Figure 6.4: *The pictures show acrylic samples before (top) and 10 weeks after (bottom) they were immersed in PXE (left) and PXE/dodecane at a ratio of 50:50 (right). A round metal grid of 1 cm diameter was put on top of the block as a scale.*

the test period which was two weeks, but fine cracks were found in this sample already after the first day. However, these cracks were also observed within the same time period on a tube being in no liquid under the same tension. So the stress on the tubes was probably too high. A 'non-stress' test was also performed using the same tubes in the same solvents without any additional tension. These tubes were unchanged until the end of the two months test period.

Light yield of PXE/dodecane mixtures

In Fig. 6.5 the light yield of a PXE based scintillator is shown at varying dodecane concentrations. The PPO-concentration is kept constant at 6 g/l for all the samples. There is no light emission of dodecane in the visible or in the UV-region where the PXE and the fluor absorb. Therefore insignificant energy transfer from the dodecane to the PXE or the fluor and a lower light yield at a higher dodecane concentration is expected. This decrease in the light intensity is observed, however the light yields compared to the pure PXE version are far above the aromatic fraction in the scintillator. At a PXE/dodecane ratio of 50:50 the light yield is still above 90 % relative to pure PXE and even at a dodecane concentration of 90 % a light yield of more than 70 % was found. From these measurements a dodecane concentration of 50 % or more can be justified.

6.2.3 A Gd carboxylate system

The carboxylate system is a promising alternative to the acac-system also for Gd-loaded scintillators. The chemistry of Gd is comparable to the chemistry of the rare earth element Yb. Therefore the behavior of the Gd-carboxylate system is expected to be similar to the pH-controlled heavily Yb-loaded system described at the end of chapter 3. A main issue for carboxylate scintillators is hydrolysis. The hydrolysis constants of the rare earths are at much higher pH-values as compared to indium. Hence the Gd-carboxylates should be more stable

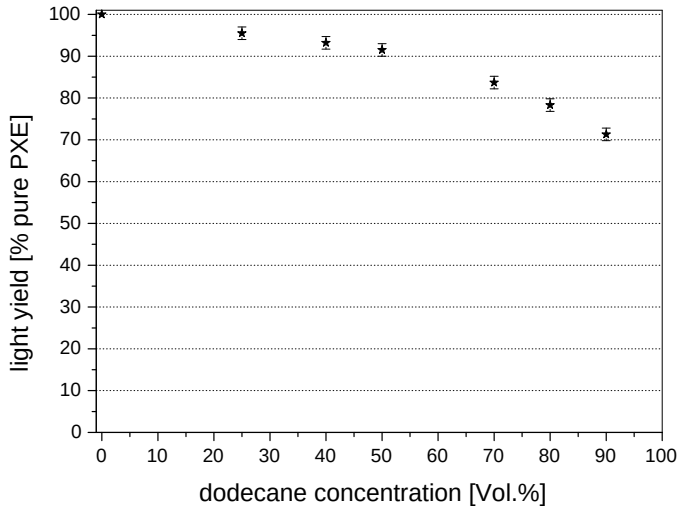

Figure 6.5: *Light yield of a PXE/dodecane mixture at varying dodecane concentrations at 6 g/l PPO.*

in contact with water than the In-carboxylate system.

Different solvents as PC and PXE were used to produce Gd-carboxylate systems. A stock solution was prepared by F.X. Hartmann in a pH-stabilized solution of an organic phase with 1 wt.% Gd-loading above an aqueous phase. After separation of the two phases the Gd-loaded organic solution can then be diluted to get the required Gd-concentration of around 0.1%. In the synthesis the HA concentration (TMHA, 9 carbons) in the organic phase was chosen to be 0.6 M. The $pH_{1/2}$ was found to be around 4.8 which is slightly above the value for Yb and well below the region where hydrolysis occurs.

The light yield of a 0.1 wt.% Gd-loaded scintillator with a PC/dodecane mixture (ratio 50:50 by volume) as solvent was tested. The PPO-concentration was 6 g/l and the light yield was found to be 87 % relative to a PXE/dodecane mixture containing PPO and dodecane at the same concentrations. In general PC based systems tend to have higher light yields than PXE based systems. The light yield relative to BC505 for the same Gd-loaded scintillator is 66 %. This number will increase if the wavelength shifter bis-MSB is added to the solution. The attenuation length of the 1 % metal loaded stock solution was determined to be in the 2 m range at 430 nm. This number improves upon dilution with the solvent. The final value depends on the purity of the solvent and the Gd-concentration. The attenuation lengths and light yields of the system using $Gd(acac)_3$ are presented next.

6.2.4 Attenuation lengths

The attenuation lengths of solutions containing hydrated $Gd(acac)_3$ were determined using the photospectrometer. In Fig. 6.6 the results are plotted for two samples with different purity levels. The transparency in the wavelength region of the scintillator emission is above 10 m for the purified material at a Gd-concentration of 1 g/l which is sufficient for the requirements of a reactor antineutrino experiment whereas the attenuation length of the unpurified material

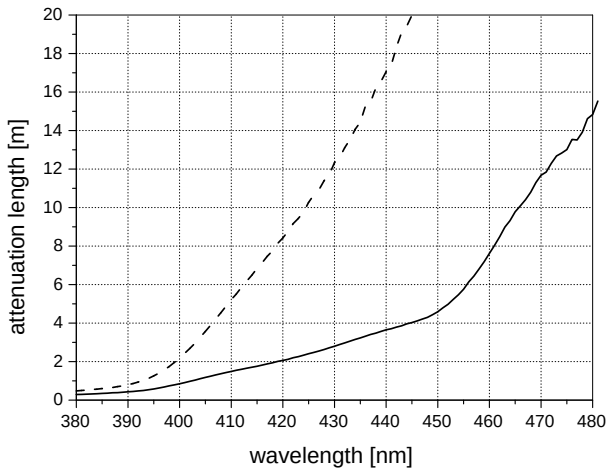

Figure 6.6: *The attenuation length for commercial $Gd(acac)_3 nH_2O$ from Aldrich (solid line) and self-produced purified $Gd(acac)_3 nH_2O$ (dashed line) at 1 g/l Gd is compared.*

is much shorter at a similar Gd-loading.

The curve having lower transparency at a given wavelength was obtained by dissolving $Gd(acac)_3 \cdot nH_2O$ (mainly monohydrate) bought from Aldrich in PXE at a concentration of 0.1 % Gd. The contribution of the PXE to the attenuation length of the solution was removed by subtracting the absorption spectrum of the pure solvent measured in a 10 cm cell from the spectrum of the Gd-loaded solution measured in the identical cell.

For the determination of the second curve in Fig. 6.6 a different procedure was applied. The hydrated $Gd(acac)_3$ was produced using the first of the two methods described in section 6.2.1. After the synthesis the material was purified as described above and dried in a desiccator to convert the material into the monohydrate. Then the material was dissolved in ethanol at 10 g/l Gd. The absorbance of the solution was measured in the photospectrometer in a 1 cm cuvette relative to pure ethanol in the reference beam. Following Lambert-Beer's Law the absorbance is proportional to the concentration, therefore the absorbance at a Gd-concentration of 1 g/l is obtained by dividing the result of the 10 g/l solution by 10.

Fig. 6.6 demonstrates a significant improvement of the optical clarity of the self-produced material compared to the commercial material. A further improvement of the transparency can be achieved by purifying the Hacac used in the synthesis. For the synthesis of the material used here the Hacac purification step was not applied.

6.2.5 Light yields of Gd-loaded scintillators

The light yield of several hydrated $Gd(acac)_3$-loaded scintillators was measured. As solvent PXE or PXE/dodecane mixtures were used. In Fig. 6.7 the light yield relative to the unloaded scintillator version is plotted for increasing PPO-concentrations. Pure PXE was used as solvent in this case. The Gd-concentration in this scan is about 0.5 g/l. As seen in the plot the saturation value for the light yield is already reached at approximately 6 g/l for these low Gd-concentrations. At higher fluor concentrations self-quenching of the fluor first seems to

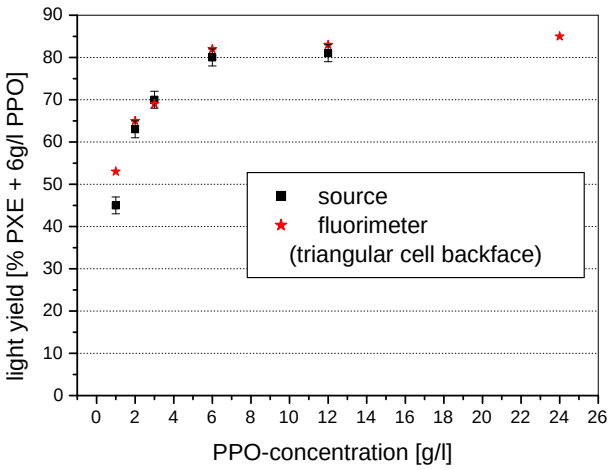

Figure 6.7: *The light yield of a $Gd(acac)_3 nH_2O$ loaded scintillator for varying fluor concentrations and a constant Gd-loading (0.05–0.1%) is shown. As solvent pure PXE was used. The light yield is given relative to an unloaded version at 6 g/l PPO.*

compensate and then to dominate the effect of an increased probability of energy transfer to the fluor.

Two different procedures were used to determine the light yields of the sample. In one method the scintillator samples were activated with a ^{137}Cs source and in the other method the light yields were determined using the fluorimeter. In the fluorimeter measurement the samples were excited in a triangular cell using the backface geometry. The scintillator was excited at the absorption maximum of anisole at 271 nm. The emission spectra were integrated and the values obtained were compared to the unloaded version at 6 g/l PPO. The results of both methods are plotted in the same diagram in Fig. 6.7. Except for the first data point at 1 g/l PPO which is slightly higher in the fluorimeter measurement, all the numbers are consistent within the errors. A higher light yield for a Gd-loaded scintillator at 6 g/l PPO relative to the unloaded version was found when measured in the fluorimeter using the front face geometry. The attenuation length of the $Gd(acac)_3$ at the used concentration is in the cm range at the wavelenghts of the PPO-emission. Therefore the better results when measured in front face geometry could be due to light absorption in the backface geometry since the light has to propagate a few mm through the triangular cell in this case.

Due to the incompatibility of pure PXE with acrylic it is preferable to have a PXE/dodecane mixture or something similar as solvent in a future reactor neutrino experiment. The light yield under irradiation with a ^{137}Cs-source was also measured at varying PPO-concentration for a scintillator mixture that is closer to the final composition which will be used in a reactor neutrino experiment. The PXE/dodecane ratio was chosen to be 20/80 by volume, the secondary wavelength shifter bis-MSB was added at 50 mg/l to avoid absorption due to the Gd-material and the Gd-loading was kept constant at 0.9 g/l. As a standard, an unloaded scintillator version was used at the same PXE/dodecane ratio with 6 g/l PPO and also 50 mg/l bis-MSB. This standard itself has a light yield of 78 % relative to the pure PXE version at the same fluor amounts. The results for the Gd-loaded scintillator samples are

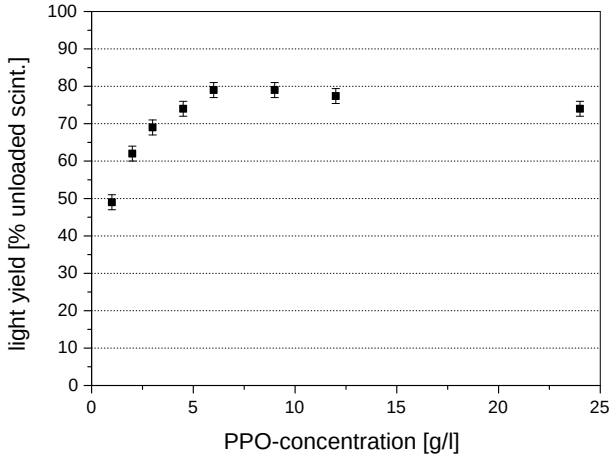

Figure 6.8: *The light yield of a Gd(acac)$_3$nH$_2$O loaded scintillator for varying fluor concentrations and a constant Gd-loading (0.9 g/l) is shown. As solvent a PXE/dodecane mixture is used in a volume ratio 20/80; the samples contained bis-MSB (50 mg/l). The light yield is given relative to an unloaded version at 6 g/l PPO.*

shown in Fig. 6.8. The light yield increases until a PPO-concentration of approximately 6 g/l is reached. There the plateau is reached at a light yield of approximately 80 % relative to the unloaded scintillator. At a PPO-concentration of 24 g/l self-quenching due to the high fluor amount is already observed.

6.2.6 Stability

As in most cases the stability of the scintillator transparency is expected to be the more severe issue than the light yield stability. Therefore the sample with Gd(acac)$_3$·nH$_2$O (Aldrich) dissolved in PXE used for the measurement of the attenuation length was stored in the 10 cm cuvette under nitrogen atmosphere and measured every two weeks. Some of the measured spectra are shown in Fig. 6.9. The minimum of the absorption spectra was set to 0. As baseline air was measured versus air. In a time period of 4 months no reduction in the attenuation length could be observed.

In summary both system, the carboxylate and the acac system, have high light yields and long attenuation lengths. The finally selected system will be the one which is more stable. This is expected to be the Gd(acac)$_3$ system, but this has to be confirmed. For a further characterization of the Gd-loaded scintillators the LLBF at Gran Sasso could be useful.

6.3 Nd-loaded scintillator for a $\beta\beta$-decay experiment

Although the chemistry of Nd and Gd is similar, there are essential differences between the behavior of Gd(acac)$_3$·nH$_2$O and Nd(acac)$_3$·nH$_2$O. First of all, the Nd(acac)$_3$·nH$_2$O absorbs also in the optical region. However, in the wavelength region of the scintillator emission between 400 nm and 500 nm only a small absorption is observed. There are little bumps in

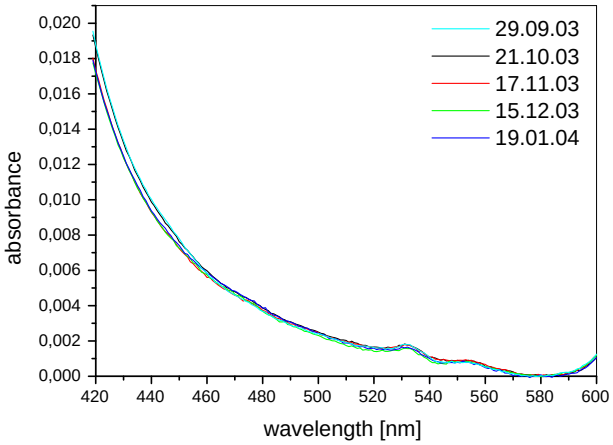

Figure 6.9: *The time stability of the absorption spectrum of a 0.1% Gd in PXE solution is shown.*

the spectrum e.g. around 470 nm. Whether they can be tolerated or not is one of the major questions that have to be addressed.

Solubility tests in similar solvents as investigated for the Gd-system were performed using $Nd(acac)_3 \cdot nH_2O$ from Aldrich. The results were an order of magnitude below the numbers obtained for the Gd. One reason for the lower solubility could be that the $Nd(acac)_3 \cdot nH_2O$ was found to be mainly a trihydrate. As for the hydrated $Gd(acac)_3$ it is possible to remove part of the water moleule by drying it in a desiccator. If Nd solubilities in the 0.2 % range can be achieved, and the transparent window in the absorption spectrum of $Nd(acac)_3$ is large enough, a $Nd(acac)_3$-loaded liquid scintillator would offer promising prospects for a detector to search for neutrinoless $\beta\beta$-decay detector.

Chapter 7

^{222}Rn background in solar neutrino experiments

7.1 ^{222}Rn emanation measurements in Borexino

The noble gas isotope ^{222}Rn ($T_{1/2}$ = 3.8 d) is fed by the α-decay of ^{226}Ra which itself is a member of the ^{238}U-decay chain. Radon can enter into the scintillator by emanation of detector materials. High ^{222}Rn concentrations in the scintillator solvent result in the accumulation of the long-lived isotope ^{210}Pb ($T_{1/2}$ = 22.3 a). Although the β-decay energy of that isotope (Q_β = 0.064 MeV) is below the energy window of the neutrino signal this isotope is one of the most critical background sources in Borexino due to the higher decay energies of its radioactive daughter nuclei ^{210}Bi (Q_β = 1.163 MeV) and ^{210}Po (Q_α = 5.407 MeV). Therefore all materials in contact with the scintillator as well as the liquid handling systems have to be checked for Rn-emanation.

7.1.1 Scintillator purification systems in Borexino

Several results on the ^{222}Rn emanation of detector materials, liquid handling systems and other Borexino subsystems can be found in the references [BUC01, FRE03, RAU99, RAU00, SIM00]. Within this thesis the ^{222}Rn emanation measurements of the scintillator purification systems in Borexino were completed. There are two such systems used in the Borexino experiment. The 'Modul Zero' [HAR97] was already used for the handling, purification and filling of the scintillator measured in the CTF prototype detector. For the liquid handling of the Borexino scintillator this system will operate in parallel with another purification system, the so-called 'Skids'. Several techniques can be applied to purify the scintillator in the Skids:

- **Filtration:** Teflon filters will be used to remove particles which are larger than 0.05 μm in diameter.
- **Distillation:** Distillation can be used to improve the optical transparency of the scintillator solvent. Another task of the distillation facility is the removal of the cosmogenically produced radioactive isotope ^{7}Be and other radioactive isotopes. The distillation column is 7 m high and operates at a pressure of 50 Torr and a temperature of 100°C.
- **Water extraction:** The approximately 6 m high water extraction column is approximately 0.25 m in diameter and filled with steel packages to increase the effective surface.

The counter flow principle is used to remove essentially ^{40}K that is dissolved in the scintillator.

- **N_2-stripping:** The N_2-stripping is done in a similar column than the water extraction column whereas this column has a smaller diameter. In this step gases as radon, argon, krypton or CO_2 will be removed. Furthermore, it removes oxygen that interferes with the scintillator performance. High purity nitrogen with a ^{222}Rn-activity of less than 1 μBq/m^3 (corresponding to an average number of 0.5 radon atoms/m^3) has to be used.

It is planned to operate the system at a flow rate of 1 m^3/h. The Skids are connected to the other scintillator purification system, the Modul Zero.

The Modul Zero is designed to store, mix and purify liquids. Like the Skids it is connected to the systems producing ultrapure water and nitrogen. The Modul Zero essentially consists of purification columns, various tanks and pumps. Solid column chromatography is used as purification method in this system. The surfaces of the scintillator purification systems are one of the last materials in contact with the scintillator before the detector filling. Therefore special care was taken in the selection and treatment of these materials.

7.1.2 Measurements and results

Measurement technique

The method applied to detect the radon atoms emanated by the investigated material is based on concentration, purification and low-background counting of gas samples. This technique allows the measurement of few radon atoms distributed in several m^3 of gas. For the Rn-detection special low background miniaturized proportional counters [WIN93] originally developed for the GALLEX-experiment are used. Only the α-decays in the Rn-decay chain are detected. The background of these counters in the relevant energy region (> 50 keV) is in the range of one count per day.

In the following the typical procedure for a measurement of the Rn emanation inside a closed volume (a tank or column) is described. First, the volume under study has to be carefully prepared since the ^{222}Rn-activity outside the volume is sometimes more than five orders of magnitudes higher than inside. To remove residual radon the volume is therefore flushed with pure nitrogen (^{222}Rn activity < 0.3 μBq/m^3). During the N_2-flushing also other gases that cause disturbing effects on the measurement as water vapor or CO_2 are removed. After the flushing the volume that is now filled with nitrogen is closed and remains untouched for at least one ^{222}Rn-halflife. In this time period the ^{222}Rn is allowed to emanate and to grow in the N_2 atmosphere. Then the N_2-gas containing the ^{222}Rn is pumped through a carbon trap cooled with liquid nitrogen (-196°C). The ^{222}Rn-activity in saturation is below 100 μBq for these traps [BUC01]. Next, the trap is warmed up to approximately -100°C. At that temperature the radon itself is still trapped whereas residual nitrogen in the trap is efficiently removed.

In the next step the gas sample has to be purified and filled into the miniaturized proportional counter. For this purpose the carbon trap can be connected to a vacuum counter filling line made out of glass. In this apparatus the sample is purified. Finally the radon is mixed with a counting gas and filled into the counter. With this method only ^{222}Rn can be detected since the other short-lived natural Rn-isotopes, ^{219}Rn and ^{220}Rn, decay during the counter filling process.

After the filling the counter is connected to the electronics and calibrated using a ^{55}Fe-source. Only events depositing more than 50 keV in the counter are recorded. This energy cut allows an efficient background reduction against β and γ-radiation since this kind of radiation cannot deposit more than 50 keV in the small volume of the counter ($\approx$ 1 ml). Approximately 50 % of the three α-decays in the ^{222}Rn-decay chain are detected in the counters. The measured activity in the counter allows to calculate the saturation activity in the tank or column under investigation.

Skids

First results on the Rn-emanation measurements of the Skids components were presented in [BUC01]. As part of this thesis the measurements were completed. A summary of the results obtained can be found in Table 7.1. Low emanation rates were found in the large surface columns for the water extraction and the Nitrogen stripping. These column are filled with steel packages with a total surface of several hundred m^2. The specific activity was similar for both columns and determined to be around 8 μBq/m^2. Such scaling of the surface activity typically does not work for vessels with small surfaces since in such cases the contribution of the gaskets and valves can start to dominate as can be seen in the measured value for the buffer tank. For the N_2 stripping and the H_2O extraction column blank runs were performed. This means that the columns were refilled with N_2 and the whole procedure was repeated immediately after the Radon extraction. The activity found was below 0.1 mBq showing that no significant amount of radon is introduced in the applied procedure.

Sample	Surface [m^2]	Activity [mBq]
Buffer tank	3	0.74 ± 0.09
N_2 stripping column	280	2.27 ± 0.14
H_2O extraction column	608	4.9 ± 0.3
heat exchanger E301		30.0 ± 1.0
heat exchanger E302		30.5 ± 1.5
heat exchanger reassembled		0.30 ± 0.07
Filter		0.27 ± 0.03
Trebor pump		0.39 ± 0.07

Table 7.1: *The ^{222}Rn activity in saturation of some components of the purification Skids is given along with the estimated inner surface of the investigated vessels.*

The volumes after the N_2-stripping column were studied in most detail since there is no radon removal after the N_2-stripping. In that part the components consist of a heat exchanger, piping, valves, a teflon filter and a pump. A first measurement of the whole volume including the heat exchanger and the filter showed an unexpected high result for the saturation activity A_{sat} of more than 30 mBq. The ^{222}Rn-activity in the PC (A_{PC}) from that source can be calculated by

$$A_{PC} = A_{sat} \cdot [1 - \exp(-\lambda t)] \tag{7.1}$$

with the Rn-decay constant λ. Assuming a flow rate of the PC of 1 m^3/h the ^{222}Rn-activity in 1 m^3 of the liquid after a contact time of 1 h can be calculated using the above equation.

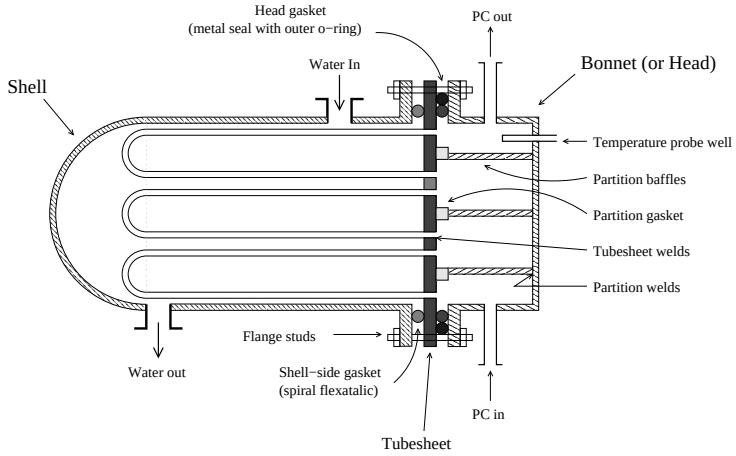

Figure 7.1: *This schematic diagram shows the components and assembly of a heat exchanger used in the Skids.*

Assuming now that all the ^{210}Pb accumulated from the Rn-decay remains homogeneously distributed in the scintillator the ^{210}Pb-activity A^{Pb} in the fiducial volume of the detector can be derived by

$$A^{Pb} = A^{Rn} \cdot \frac{T^{Rn}_{1/2}}{T^{Pb}_{1/2}} \tag{7.2}$$

From the above equation the estimated ^{210}Pb-activity is about one decay per day in the fiducial volume. This is above the limit of the tolerable background contribution of a single source.

Therefore, each component of the investigated volume was measured separately and the heat exchanger was found to be the main origin of the ^{222}Rn-activity. A diagram of the heat exchanger is shown in Fig. 7.1. The tubesheet and the bonnet are made of stainless steel and all the tubing was electropolished. Several emanation tests were performed to further isolate the emanation source. Some of the gaskets (Nylon) were measured and found to be radiopure. The head part and the tubing part of the heat exchanger were also measured separately from which it was found that the origin of the contamination is in the bonnet. After the bonnet was reassembled the emanation rate of the whole heat exchanger was measured to be 0.30 ± 0.07 mBq which is low enough for the requirements of the Borexino experiment. The ^{222}Rn emanation in the original heat exchanger was caused by contaminated welding rods used for the welded joints.

There are two more heat exchangers of the same type in the Skids. An emanation test of one of them showed a similar activity as the other one before the reassembling. However, it was decided not to reassemble the other two heat exchangers since they are located before

the N_2-column. Therefore their contamination is less criticial since most of the radon will be removed during the N_2-stripping.

Modul Zero

The central components in Modul Zero are the two purification columns filled with silica gel. The activity of the low ^{226}Ra silica gel[1] itself was determined to be < 1.2 Bq/kg [BUC01]. During operation approximately 30 kg of the silica gel will be used in each column. Emanation tests of one empty column resulted in an activity of (0.59 ± 0.05) mBq. The emanation of the silica gel filled columns were also tested and the activity was determined to be in the range of 5 mBq [FRE03]. Subtracting the activity of the empty column one can calculate a better upper limit for the silica gel activity than that given above of < 0.2 mBq/kg. More results about Rn-emanation measurements of Modul Zero components can be found in [FRE03, BUC01]. In conclusion, the measured Rn-purity levels of the Modul Zero and the Skids components are sufficient for the needs of Borexino.

7.2 ^{222}Rn background in LENS

Radon is a critical item in most neutrino experiments, especially when the energies to be detected are below 5 MeV. In an In-detector a background source would be the delayed coincidence between an indium β-decay and a β-γ-cascade from ^{214}Pb of the ^{222}Rn decay chain occurring in the same microcell. Assuming the size of the microcell is $(4 \times 4 \times 50)$ cm^3 (0.8 l) the In-activity at 8 %-loading would be 16 Bq/microcell. The pp-ν_e event rate would be approximately $2 \cdot 10^{-10}$ per sec. Under the conservative assumption that every ^{214}Pb-decay in the microcell and in the time window τ of 10 μs after an In-decay in the same cell mimics a ν_e-event one can calculate the allowed ^{214}Pb-activity in a microcell for a signal-to-noise ratio of 10:1:

$$10 \cdot A_{In} \cdot \tau \cdot A_{Pb} = 2 \cdot 10^{-10} \frac{B}{q} \Longrightarrow A_{Pb} = 0.125 \mu Bq \tag{7.3}$$

This corresponds to a ^{222}Rn-activity in the scintillator of 0.15 μBq/l.

Next the fraction of critical ^{214}Pb-decays (P_{bg}) is estimated. There is a 36 % probability [TOI96] for a $\beta - \gamma$-cascade with $E_\beta = 671$ keV and $E_\gamma = 352$ keV. Assuming realistic energy windows for the electrons and gammas of the delayed cascade (e/γ_2 and γ_3 in Fig. 1.4) in the neutrino signature along with a reasonable energy resolution the resulting probability for a fake event is 0.44 % in this branch. Furthermore, there is the possibility of a ^{214}Pb-decay into a higher excited state at 533 keV. The branching ratio of this mode is only 1.04 % [TOI96], but the sum of the emitted gammas is inside the energy window of γ_3. Also more electrons from the β-decay ($E^{\beta}_{max} = 490$ keV) are in the energy window of (e/γ_2). This results in a 0.25 % probability for critical background events. Therefore one obtains for $P_{bg} = 0.0025 + 0.0044 = 0.0069$. Contributions due to other branches are neglected. The calculated probability translates in a required radiopurity in terms of ^{222}Rn of $0.15/0.0069 \approx 20 \mu$Bq/l or $1.7 \cdot 10^{-12}$ g/g U. This corresponds to about 0.1 mBq per cell ($4 \times 4 \times 300$cm^3) or about 0.2 mBq/m^2 Rn-emanation of the surface material. There are huge variations in the emanation rates of different materials. It is therefore mandatory to test the Rn-emanation of the used cell materials in order to find a material with the required purity.

[1] Kromsail from the company Eka Nobel AB

Summary

The current interest in low energy neutrino physics is in the study of the mass properties of the neutrino. With novel metal loaded liquid scintillator systems future projects in the fields of solar neutrinos, reactor neutrinos and $\beta\beta$-decay become feasible. A limiting issue in past neutrino experiments was the long term stability of the metal loaded scintillators. The basic requirements on the scintillator are similar in all future experiments: long term stability, radiopurity, high light yield and long attenuation lengths in the wavelength region of the scintillator emission. A new method to produce metal loaded liquid scintillators that meet these requirements is described in this thesis.

A future solar neutrino experiment measuring the low energy neutrino spectrum in real-time via the charge current interaction could answer longstanding questions in particle and astrophysics. Several target isotopes were proposed in the last decades for such an experiment out of which ^{176}Yb and ^{115}In turned out to be the most promising candidates. The international LENS Collaboration studies the feasibility of a solar neutrino experiment using indium dissolved in a liquid scintillator as a target. In this thesis the development, purification, optical characterization, optimization and theoretical modeling of a novel highly In-loaded scintillator using β-diketone chemistry has been investigated. The metal β-diketone complex In(acetylacetone)$_3$ (In(acac)$_3$) can be dissolved in the scintillator solvent anisole up to an In-loading of 7.9 wt.%.

Metal β-diketone molecules like In(acac)$_3$ are known to be very stable even at high temperatures and to have high vapor pressures. This allows purification of the material by sublimation. With this purification method and a special synthesis procedure aiming at optical transparency of the final product, very pure In(acac)$_3$ could be produced. The measured attenuation length when dissolved in anisole at 5 wt.% In-loading was in the 3 m to 5 m range (without fluors).

This scintillator system needs high fluor amounts to obtain a sufficient light yield. Competing energy transfer processes occur, from the solvent molecules (excited by electromagnetic radiation) to the fluor, or alternatively to the In(acac)$_3$ molecules which absorb strongly in the UV-region of the solvent emission. Energy transferred to the In(acac)$_3$ is thus lost in terms of emission of scintillation light, since the In(acac)$_3$-molecule is non-fluorescent. Therefore, the energy transfer rate to the fluor has to be maximized whereas the energy flow to In(acac)$_3$ has to be minimized. This goal has been achieved by optimization of the fluor choice and concentration. This optimization process resulted in the use of the fluor BPO in high concentrations dominating the scintillator absorbance in the wavelength region of interest between approximately 420 nm to 450 nm.

From detailed measurements of the optical properties of the several components optimized scintillator compositions have been designed for a LENS prototype cell. The performance of two scintillator compositions was tested in a 5 cm $\times$ 5 cm $\times$ 100 cm quartz cell at an In-

loading of 2 wt.% and 4.1 wt.%, respectively. For the 2 wt.% (4.1 wt.%) scintillator the *effective* attenuation length (inclusive fluors) in the 1 m long cell was measured to be 1.58 m (1.28 m), the energy resolution at 477 keV was determined to be 10.2 % (11.6 %) and the spatial resolution in such a scintillator is 6 cm (7 cm). A (3×3) array consisting of the same kind of 1 m long quartz cells filled with In-loaded and unloaded scintillators was constructed, purified and loaded into an underground low radioactivity shielding (LLBF) at Gran Sasso for background studies. In this LENS prototype measurement a scintillator composition of 48 g/l In, 50 g/l BPO and 100 mg/l bis-MSB dissolved in anisole was chosen. The light yield of the In-loaded cell corresponds to approximately 30 % relative to the light yield of an In-free PXE based scintillator. No time variation of the scintillator performance was found in the four months since the start of the measurement (October 2003). A ^{7}Be-ν experiment is feasible with such a scintillator composition whereas for a pp-ν experiment a further tuning of the In-concentration is needed to further increase the light yield.

Future reactor neutrino experiments, e.g. Double Chooz, are planned to study the magnitude of the neutrino oscillations driven by the coupling of the electron antineutrino to the heaviest mass eigenstate characterized by the mixing angle Θ_{13}. To improve the current sensitivity on that mixing angle the systematic uncertainty in the experiment has to be minimized. Therefore, it is planned to operate identical detectors, one at far ($\approx$ 1 km) and one at a distance close to the reactor core, both filled with a Gd-loaded scintillator. The metal loading needed in this kind of experiment is more than one order of magnitude below the discussed metal loading in solar neutrino experiments, Gd-concentrations of 1 g/l are already sufficient.

The same approach as for the In-system was used to load the scintillator with Gd. The optical properties of $Gd(acac)_3$ and $In(acac)_3$ are similar whereas the chemistry of the molecules is rather different. For example, the rare earth acetylacetones form hydrates which could be a reason for the much lower solubility of Gd as compared to indium in some of the investigated organic solvents. A Gd-loading of 1 g/l is possible in a PXE/dodecane mixture which would be a favored scintillator solvent in the Double Chooz experiment. The production and characterization of such a scintillator resulted in light yields of 80 % compared to the unloaded scintillator version and transmission lengths in the 5 m range in the full scintillator mixture. Even longer attenuation lengths are expected after column purification of the solvent. It was found that organic solvents as PXE or anisole can be efficiently purified using a Al_2O_3 column. First tests on the long term stability which is the key point in the Gd-scintillator development showed so far no time variations in the optical properties.

A further application of metal β-diketone complexes dissolved in liquid scintillators could be in future $\beta\beta$-decay experiments. The isotope ^{150}Nd has a high Q-value (3.37 MeV) for $\beta\beta$-decay and is therefore a promising candidate in the search for neutrinoless $\beta\beta$-decay. First attempts were made to produce a $Nd(acac)_3$-loaded scintillator. The challenge in this system is the so far observed low solubility of the Nd-complex in the studied solvents, and the absorption bands of Nd in the optical region. However, there is a transparent window in the wavelength range between 400 nm and 500 nm which is the region of the scintillator emission.

All low-background neutrino experiments using liquid scintillators need systems for the handling and purification of the liquids. A common background source in these experiments is the omnipresent noble gas radon which is emanated from the detector materials into the scintillator. The ^{222}Rn emanation rate was measured for the liquid handling systems in Borexino and found to be sufficient low. Furthermore, an estimation of the required purity

level of ^{222}Rn in the scintillator of a LENS detector was made.

In conclusion, the new approach to develop stable metal loaded liquid scintillators presented in this thesis provides the basis for successful future experiments detecting neutrinos from different sources.

Bibliography

[BAH97] J.N. Bahcall, M.H. Pinsonneault, S. Basu, J. Christensen-Dalsgaard, Phys. Rev. Lett. 78 (1997) 171–174.

[BAH01] J.N. Bahcall, M.H. Pinsonneault, S. Basu, Astrophys. Journ. 555 (2001) 990.

[BEL03] E. Bellotti for the GNO Collaboration, GNO: Status report at TAUP 2003, Seattle, 5–9 September 2003.

[BER71] I.B. Berlman, Handbook of fluorescence spectra of aromatic molecules, Second edition, Academic Press, New York, 1971.

[BIL02] S.M. Bilenky, D. Nicolo, S.T. Petcov, Phys. Lett. B 538 (2002) 77–86.

[BOR02] BOREXINO-Collaboration, Astroparticle Physics, 16 (2002) 205–234.

[BU03] C. Buck, F.X. Hartmann, S. Schönert, U. Schwan, Presentation at Workshop on Future Low-Energy Neutrino Experiments, Munich, October 9–11, 2003.

[BUC01] C. Buck, Radonmessungen an Teilsystemen des Sonnenneutrinoexperiments Borexino, diploma thesis, Universität Heidelberg, 2001.

[BUC03] C. Buck, F.X. Hartmann, S. Schönert, U. Schwan, Journal of Radioanalytical and Nucl. Chem. 258, No. 2 (2003) 255–263.

[BUC04] C. Buck, F.X. Hartmann, T. Lasserre, D. Motta, S. Schönert, U. Schwan, Journal of Luminescence 106 (2004) 57–67.

[CAR23] Cario and Franck, Z. Physik, 17 (1923) 202.

[CHO99] Chooz-Collaboration, Phys. Lett. B 466 (1999) 415–430.

[CLE98] B.T. Cleveland, T. Daily, R. Davis, Jr., J.R. Distel, K. Lande, C.K. Lee, P.S. Wildenhain and J. Ullman, Astrophys. J. 496 (1998) 505.

[CRE03] O. Cremonesi, Nucl. Phys. B (Proc. Suppl.) 118 (2003) 287–296.

[DAN03] N.A. Danilov et al., Internal LENS report, Moscow, Assergi 2002–2003

[DAV68] R. Davis, D.S. Harmer, K.C. Hoffman, Phys. Rev. Lett. 20 (1968) 1205–1209.

[DES89] P. Destruel, M. Taufer, C. D'Ambrosio, C. Da Via, J.P. Fabre, J. Kirkby, H. Leutz, Nucl. Inst. and Meth. A 276 (1989) 69–77.

[DEX53] D.L. Dexter, J. Chem. Phys. 21 (1953) 836.

[FEI01] F. von Feilitzsch, Proceed. of the 5th Int. Top. Workshop at LNGS on Solar Neutrinos edited by V. Berezinsky and F. Vissani (03/2001) 388–409.

[FOR48] T. Förster, Ann. Phys. 2 (1948) 55.

[FOR59] T. Förster, Discussions Faraday Soc. 27 (1959) 7–17.

[FRE03] B. Freudiger, Untersuchungen zu den radioaktiven Edelgasnukliden als Untergrundquellen im Sonnenneutrinodetektor Borexino, dissertation, Universität Heidelberg, 2003.

[FXH03] F.X. Hartmann, private communication.

[GAL99] GALLEX Collaboration, Phys. Lett. B447 (1999) 127.

[GRA90] D.J.W. Grant, T. Higuchi, Techniques of Chemistry, Vol. XXI, Solubility behavior of organic compounds, Wiley-Interscience, New York, 1986.

[GNO00] GNO Collaboration, Phys. Lett. B490 (2000) 16.

[HAR91] F.X. Hartmann and S.R. Rotman, Chem. Phys. Letters 184 (1991) 537.

[HAR97] F.X. Hartmann, Proc. of the 4th Inter. Solar Neutrino Conference in Heidelberg edited by W. Hampel (1997) 202–209.

[HAR03] F.X. Hartmann, C. Buck, S. Schönert, U. Schwan, Presentation at Workshop on Future Low-Energy Neutrino Experiments, Munich, October 9–11, 2003.

[HEI02] B. Heisinger, private communication.

[HEU03] G. Heusser, M. Laubenstein, private communication.

[HIL50] J.H. Hildebrand and R.L. Scott, The solubility of nonelectrolytes, Reinhold, New York, 1950.

[HMO01] Heidelberg-Moscow Collaboration, Eur. Phys. J. A 12 (2001) 147–154.

[HMO02] Heidelberg-Moscow Collaboration, private communication.

[INO65] M. Inokuti and F. Hirayama, J. Chem. Phys. 43, No. 6 (1965) 1978–1989.

[JPM02] J.-P. Meyer, Simulation work done on the In target in an homogeneous detector, internal LENS report 03/09/2002.

[JPM03] J.-P. Meyer, Simulating solar neutrinos detection in an In loaded Hybrid detector, internal LENS report 07/01/2003.

[KAM96] Kamiokande Collaboration, Phys. Rev. Lett. 77 (1996) 1683.

[KAM03] KamLAND-Collaboration, Phys. Rev. Let. 90 (2003) 021802.

[KAL59] F.H. Brown, M. Furst and H. Kallmann, Discussions Faraday Soc. 27 (1959) 43–56.

[KLA01] H.V. Klapdor-Kleingrothaus, A. Dietz, H.V. Harney and I.V. Krivosheina, Modern Phys. Lett. A 16 (2001) 2409.

[KOE67] J.M. Koehler, W.G. Bos, J. Inorg. Nucl. Chem., Vol. 3 (1967) 545–548.

[LEN99] LENS-Collaboration: Letter of intent to the LNGS (01/1999).

[LIS77] I.B. Liss, W.G. Bos, J. Inorg. Nucl. Chem., Vol. 39 (1977) 443–447.

[LOW02] Borexino-Collaboration, Astroparticle Physics, 18 (2002) 1–25.

[MEH78] R.C. Mehrota, R. Bohr and D.P. Gaur, Metal Beta-Diketonates and Allied Derivatives, Academic Press, New York, 1978.

[MIK85] S.P. Mikheyev and A.Y. Smirnov, Sov. J. Nucl. Phys.42 (1985) 1441.

[MOO00] MOON-Collaboration, Phys. Rev. Lett. 85 (2000) 2917.

[MOT04] D. Motta, Feasibility analysis and prototype measurements of a novel approach for the real-time spectroscopy of low-energy solar neutrinos, dissertation, Universität Heidelberg, 2004.

[NED00] H. Neder, G. Heusser, M. Laubenstein, Applied Radiation and Isotopes 53 (2000) 191–195.

[PAL99] A.G. Piepke, S.W. Moser, V.M. Novikov, Nucl. Inst. and Meth. A 432 (1999) 392–398.

[PAL01] PALO VERDE-Collaboration, Phys. Rev. D 64 (2001) 112001.

[PAY90] A.G.D. Payne, N.E. Booth, Nucl. Inst. and Meth. A 288 (1990) 632.

[PER24] F. Perrin, Copt. Rend. 178 (1924) 1978.

[PFE78] L. Pfeiffer, A.P. Mills, R.S. Raghavan, E.A. Chandross, Phys. Rev. Lett. 41 (1978) 63.

[POP61] G.W. Pope, J.F. Steinbach, W.F. Wagner, J. Inorg. Nucl. Chem., Vol. 20 (1961) 304–313.

[PRE88] Press et al., Numerical recipes in C, The Art of Scientific Computing, Cambridge University Press, New York, 1988.

[PRZ71] J.K. Przystal, W.G. Bos, I.B. Liss, J. Inorg. Nucl. Chem., Vol. 33 (1971) 679–689.

[PXE04] Borexino Collaboration, A high-density and high-flashpoint organic liquid scintillator for applications in low-energy particle-astrophysics experiments, in preparation.

[RAG76] R.S. Raghavan, Phys. Rev. Lett. 37 (1976) 259.

[RAG97] R.S. Raghavan, Phys. Rev. Lett. 78 (1997) 3618.

[RAU99] W. Rau, Low-level-Radonmessungen für das Sonnenneutrinoexperiment Borexino, dissertation, Universität Heidelberg, 1999.

[RAU00] W. Rau, G. Heusser, Appl. Rad. & Isot. 53 (2000) 371–375.

[REI59] F. Reines, C.L. Cowan, Phys. Rev. (1959) 273.

[RIC68] M.F. Richardson, W.F. Wagner, D.E. Sands, Inorg. Chem. 7 (1968) 2495.

[RID86] J.A. Riddick, W.B. Bunger, T.K. Sakano, Techniques of Chemistry, Vol. II, Organic Solvents 4th edition, Wiley-Interscience, New York, 1986.

[ROT88] S.R. Rotman and F.X. Hartmann, Chem. Phys. Letters 152 (1988) 311.

[ROT89] S.R. Rotman and F.X. Hartmann, Chem. Phys. Letters 163 (1989) 437.

[SAG03] SAGE Collaboration, Nucl. Phys. B (Proc. Suppl.) 118 (2003) 39–46.

[SIM00] H. Simgen, Messung von ^{222}Rn and ^{226}Ra in Wasser im Rahmen des Sonnenneutrinoexperiments Borexino, diploma thesis, Universität Heidelberg, 2000.

[SNO03] SNO collaboration, Nucl. Phys. B (Proc. Suppl.) 118 (2003) 3–14.

[STA64] J. Stary, The Solvent Extraction of Metal Chelates, Pergamon Press, New York, 1964.

[STE19] O. Stern and M. Volmer, Physik. Z. 20 (1919) 183.

[STE53] J.F. Steinbach, H. Freiser, Anal. Chem., 25 (1953)881.

[STI48] J.G. Stites, C.N. McCarty, L.L. Quill, J. Amer. Chem. Soc. 70 (1948) 3142.

[SUP00] Super-Kamiokande Collaboration, Phys. Rev. Lett. 85 (2000) 3999.

[SUP01] Super-Kamiokande Collaboration, Phys. Rev. Lett. 86 (2001) 5651.

[SUP02] Super-Kamiokande Collaboration, Phys. Rev. Lett. B539 (2002) 179.

[SUZ90] Y. Suzuki, K. Inoue, Y. Nagashima, S. Hashimoto, T. Inagaki, Nucl. Inst. and Meth. A 293 (1990) 615.

[TOI96] R.B. Firestone, Table of Isotopes, 8th edition, Wiley-Interscience (1996).

[WAL88] B. Walter, Ann. Phys. 34 (1888) 502–533.

[WEI03] C. Weinheimer, Nuclear Physics B (Proc. Suppl.) 118 (2003) 279–286.

[WIN93] R. Wink, P. Anselmann, D. Dörflinger, W. Hampel, G. Heusser, T. Kirsten, P. Mögel, E. Pernicka, R. Plaga, C. Schlosser, Nucl. Instr. and Meth. A329 (1993) 541–550.

[WOL78] L. Wolfenstein, Phys. Rev. D 17 (1978) 2369.

Acknowledgements

This thesis was performed in the independent reserach group of Dr. S. Schönert at the MPIK Heidelberg. I would like to thank particularly

Dr. F.X. Hartmann for introducing me in the exciting world of chemistry and his brilliant ideas,

Dr. S. Schönert and Prof. W. Hampel for making it possible to work on this thesis,

U. Schwan for all her work and help in the chemistry lab,

the Graduiertenkolleg of the Ruperto-Carola University of Heidelberg for fellowship support,

LENS colleagues in Heidelberg, D. Motta and Dr. T. Lasserre for their help and useful discussions,

Dr. F. Dalnoki Veress, Dr. H. Simgen and Dr. G. Rugel for reading my thesis and their helpful comments,

my other friendly Heidelberg colleagues Dr. B. Freudiger, A. Germeroth, F. Kaether and Dr. G. Zuzel,

Dr. I. Barabanov, Dr. O. Besida, Dr. C. Cattadori and A. Di Vacri of the 'LLBF group' for their help at Gran Sasso,

my family, my friends and everybody I have forgotten here.